University of Stavanger

Faculty of Science and Technology

MASTER'S THESIS

Study program/ Specialization: Master of Science in Petroleum Technology, Drilling Specialization	Spring semester, 2013 Open
Writer: Tonje Immerstein	……

Faculty supervisor:

Bernt S. Aadnøy (University of Stavanger)

External supervisor:

Roar E. Flatebø (BP Norway)

Title of thesis:

"Wellbore Stability and Rock Mechanics Study on the Ula field"

Credits (ECTS): 30

Key words: Ula Drilling Wellbore stability Leak-off inversion technique	Pages: ……88…… + Appendix: …A-C (45 pages)…… Stavanger, …14.06.2013…….. Date/year

Acknowledgements

This Master thesis of Petroleum Engineering was prepared in the spring 2013 at BP Norway in collaboration with the University of Stavanger.

I would like to thank BP Norway for the opportunity to write this thesis and giving me access to all the data needed and making this thesis possible.

During the process of writing this thesis I got help from many people that I would like to thank. I would especially like to thank my to supervisors, Roar E. Flatebø (BP Norway) and Bernt S. Aadnøy (University of Stavanger), for all the support and good discussions during my work on the thesis.

I would also like to thank all the people in the Ula Tambar Subsurface team in BP that have helped me through my work and giving me support. Tor Jan Tjøstheim (BP Norway) has been a good support to give me a drilling point of view of the process of looking into the wellbore stability problems.

I also want to thank Mesfin Agonafir Belayneh (University of Stavanger) for his help on the simulation of the inversion technique and for letting me use his program to do this study on the leak-off tests. He also gave me good feedback on my thesis. Finally I would like to thank Rolf Tapper for reading through my thesis and giving me good constructive feedback.

Stavanger, Norway
June 2013

Tonje Immerstein

Abstract

In the years to come more challenging drilling conditions will occur when the last reserves need to be collected. More directional drilling will be used and good wellbore conditions will be necessary to make this possible. This means that good knowledge about the wellbore instability problems will be crucial.

To get a good background of the field to make a good as possible model a lot of data was collected to get a good understanding of the Ula field. A geological overview was made to see the geological perspective of it all. All the historical instability problems and mud weight was collected from previously drilled wells which was then put into a three-dimensional model. This three-dimensional model gave a good understanding of how the field was behaving, and look at the wells as an overall picture and not just one by one.

The objective of this study was to make a model that could be used to design a good mud program for the new injector wells that are going to be drilled on the Ula field in the near future. It is important that the mud program is designed such that the instability problems will be as low as possible and reduce non-productive time due to wellbore instability. From a calculated collapse curve it is possible to find the minimum recommended mud weight that could be used when drilling the new well.

This study also uses the leak-off inversion technique to find the orientation of the stress field on Ula. The horizontal stress orientation was then mapped on a geological map of the field showing a good overview of how the stress is acting. The result of this test can be used to find the leak-off values of a new well that can help to avoid instability problems in the well.

Table of Contents

List of Tables:

List of Figures:

Appendix

List of Abbreviations

DPZ	Distinct Permeable Zone
FBP	Formation Breakdown Pressure
FCP	Fracture Closure Pressure
FIT	Formation Integrity Test
FPP	Fracture Propagation Pressure
ISIP	Instantaneous Shut-In Pressure
LOT	Leak-Off Test
MD	Measured Depth
MW	Mud Weight
NPD	Norwegian Petroleum Directorate
PIT	Pressure Integrity Testing
PPFG	Pore Pressure Fracture Gradient
PVT	Pressure Volume Temperature
PZ	Permeable Zone
SCP	Substained Casing Pressure
SG	Spesific Gravity
TVD	True Vertical Depth
XLOT	Extended Leak-Off Test

Nomenclature

General rock mechanics

σ	Normal stress
τ	Shear stress
F	Force
A	Surface area
ε	Strain
E	Young's modulus
v	Poisson's ratio
σ_h	Minimum horizontal stress
σ_H	Maximum horizontal stress
σ_v	Overburden
P_p	Pore pressure
α	Biot-coefficient
S_0	Cohesion
φ	Angle of internal friction
μ	Coefficient of internal friction
C_0	Unconfined Compressive Strength
β	Orientation of the failure plane
T_0 / σ_t	Tensile strength
P_w	Well pressure
P_{wc}	Well collapse pressure
P_0	Formation pore pressure
P_{wf}	Fracture pressure
τ_0	Cohesive strength

Inversion technique

σ_v	Overburden stress
σ_H, σ_h	Horizontal in-situ stresses
P_{wf}	Borehole pressure at fracture
P_w	Borehole pressure
P_{fm}	Pore pressure
σ_x, σ_y	Normal in-situ stresses in x and y directions, respectively
$\sigma_{tensile}$	Tensile strength of the rock
γ	Borehole inclination
φ	Azimuth of the borehole from the X-axis
β	Auxillary angle to find the direction σ_H from the X-axis
θ	Polar angle on the borehole wall from the x-axis
X, Y, Z	Arbitrary coordinate system for the field, for example: Z points vertically, X points North, Y points West.
x, y, z	Coordinate system for the wellbore
$[A]$	Transformation matrix
a, b	Elements of matrix A
e	Error for each data set
D	True vertical depth

1. Introduction

The primary objective of this report is to look at the drilling history and the Ula field to see if there is some connection between the mud weights that were used while drilling and the instability problems that occurred. To do this a large amount of work has to be done to go through the final well reports of all the wells drilled to see if we can find a correlation of the mud weight that has been used and the drilling problems that has been experienced during the field life of Ula. From this we can make a 3D-model of the field to see if there is some areas of the field that have experienced more problems and which types of problems that have occurred in the different areas. This model will make it easier to get a good overview of the field to get a better understanding of how it all fits together. From this we can easily pick which wells we want to use for further work.

All the mud weights for the field are going to be collected from the final well reports so it could be used to show which mud weight that was used in the drilled wells. Since this is an old field, not much of the data will be electronic and the collection will therefore need to be done by hand. The actual mud weight used will then be compared to a calculated collapse curve that will be calculated from the rock properties and from the well properties of the wells that were picked. From this we can estimate the minimum mud weight that should have been used and also find the minimum mud weight that should be used when drilling new wells This model will be a good tool to use when designing a mud program for the injector wells that will be drilled on Ula in near future.

This study will also use the leak-off inversion technique which uses the leak-off test in previously drilled wells to calculate the leak-off value for a new well that is going to be drilled. This technique will show the stress orientation of the field which will then be mapped. This technique is good to use because it takes into account the direction of the wells, and can use historical data from old reports to do the calculations.

1.1. Background

Before a well is drilled the formation rock is in equilibrium. As soon as the drilling process starts this equilibrium is changed and the well needs a new barrier to withstand the forces around the well. The drilling fluid is therefore very important in order to withstand the normal stresses from the formation that occurs when some of the rock is removed while drilling. The drilling fluid can only partly support the normal stresses and cannot replace the original rock in place when it comes to shear stresses. Since the equilibrium of the stresses is changed when the well is drilled, the stresses and orientation around the borehole wall will be redistributed and modified to compensate for the rock that is removed. To have control of how these changes are occurring without resulting in any instability problems, it is important to have good knowledge about the strength of the rock in order to not damage the integrity of the rock during drilling.

Recently, it has been increasingly important for the petroleum industry to drill horizontal wells. They are more cost efficient as they makes it possible to drain more of the reservoir with fewer wells and thereby save time and money. Horizontal wells are however more complicated due to the in-situ stress field in the well. This makes it much more important to have good knowledge about the forces happening in the well while drilling to avoid that the well collapses and other instability problems.

From experience it has been seen that the instability problems of the wells that are drilled have a large connection between the mud weights that are used during drilling of the section. Therefore it is very important to have a good mud program for the well that is going to be drilled to avoid drilling problems.

1.2. Objective of the thesis

Literature study:

- General description of the Ula field.
- Geological description of the field.
- General rock mechanics descriptions.
- Theory behind the leak-off inversion technique.

Collection of data:

- Import drilling logs and well trajectories of all the wells into Gocad to get an overview of available data on the field.
- Read the final well reports to collect all the instability problems that have occurred in all the wells.
- Collect all the mud weights from the final well reports.
- Collect all the Leak-Off Test and Formation Integrity Tests.

Make a Pore Pressure Fracture Gradient (PPFG) plot:

- Plot the Pore Pressure and the Fracture Gradient of the field.
- Plot the leak-off data
- Pick some wells and make a plot for each with mud weight used, collapse curve (minimum mud weight) and the instability problem that occurred in that well.

Perform a leak-off inversion technique:

- Run the leak-off data through the inversion technique simulation.
- Map the result on a map of the Ula field to show the orientation of the horizontal stresses.

2. The Ula field well history

Ula is an oil field located in the south of the North Sea in block 7/12, 260 km South-West of Stavanger and is named after the famous Norwegian sea pilot called Ulabrand (Evans et al., 2003, Spencer et al., 1987). The field was discovered in September 1976 and the first discovery well was the well Nor 7/12-2 (Evans et al., 2003). The first well was drilled by Conoco, but British Petroleum later became operator of the field and drilled appraisal wells (Spencer et al., 1987). The Ula field is operated 80% by BP and 20% by DONG E&P Norway AS (NPD). The Ula basin is situated in the central part of the Ula Trend, and is a Jurassic hydrocarbon province with faulted margins northeast to the Central Graben (Spencer et al., 1986). The water depth in this area is approximately 70 m. The main reservoir is located at 3345 m TVDSS (10975 ft TVDSS) in the Upper Jurassic Ula formation. The Ula field has production, drilling and living quarters divided onto three conventional steel facilities.

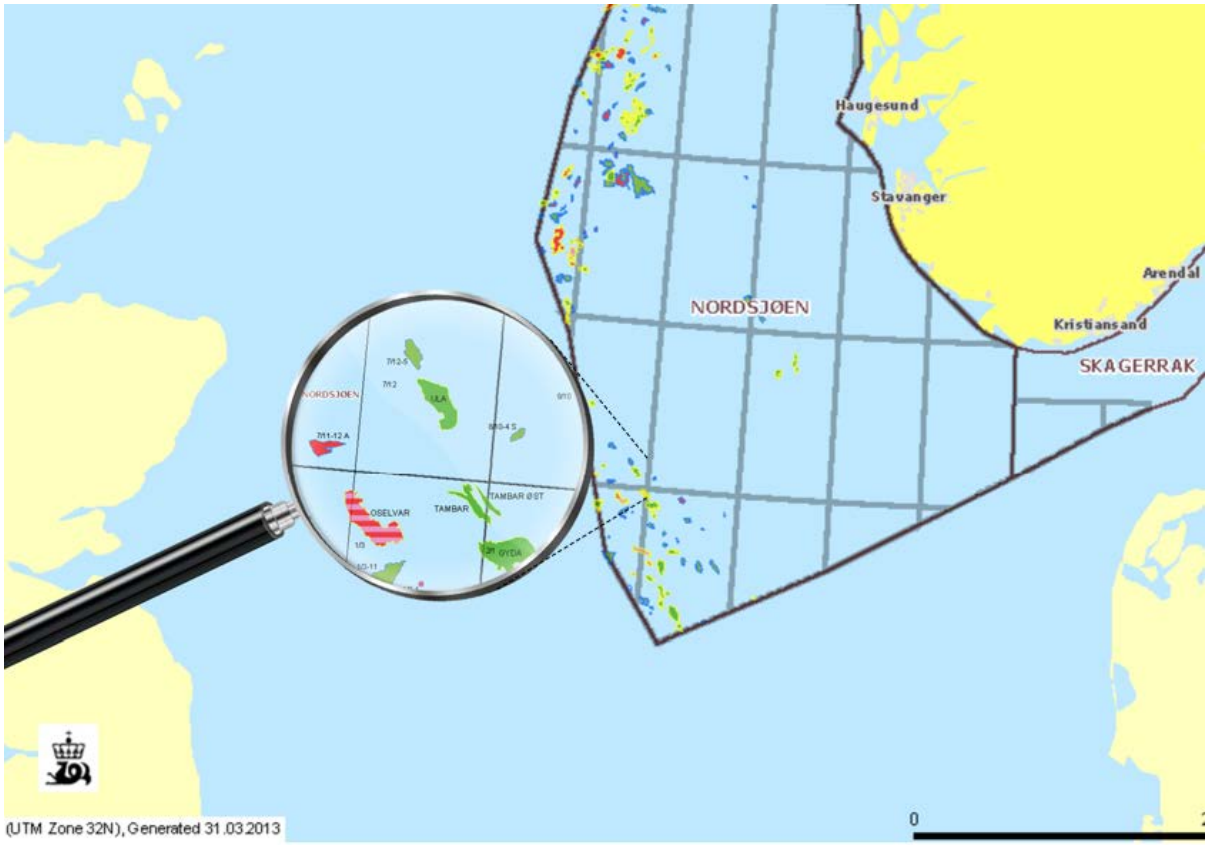

Figure 1: Ula field location

.

2.1. Ula well history

Table 1: Wells drilled on Ula

Wellboe - Exploration						
#	Wellbore name	Entry date	Completion date	Purpose	Status	Content
1	7/12-2	04.07.1976	24.09.1976	WILDCAT	SUSP.REENTERED LATER	OIL
2	7/12-2 R	24.03.1984	29.04.1984	WILDCAT	P&A	OIL
3	7/12-3	05.04.1977	03.06.1977	APPRAISAL	P&A	DRY
4	7/12-3 A	04.06.1977	06.09.1977	APPRAISAL	P&A	OIL SHOWS
5	7/12-4	11.09.1977	12.12.1977	APPRAISAL	SUSP.REENTERED LATER	OIL
6	7/12-4 R	16.03.1984	20.03.1984	APPRAISAL	P&A	OIL
7	7/12-6	10.04.1981	24.07.1981	APPRAISAL	P&A	OIL
8	7/12-7	20.06.1988	26.07.1988	APPRAISAL	SUSP.REENTERED LATER	OIL
9	7/12-7 R	14.05.1989	22.05.1989	APPRAISAL	P&A	OIL
10	7/12-8	03.10.1988	27.12.1988	APPRAISAL	SUSPENDED	OIL
11	7/12-9	18.03.1990	14.05.1990	APPRAISAL	SUSPENDED	OIL

Wellbore - Development						
#	Wellbore name	Entry date	Completion date	Purpose	Status	Content
1	7/12-A-1	27.02.1988	13.05.1988	PRODUCTION	PLUGGED	NOT AVAILABLE
2	7/12-A-1 A	03.10.1991	14.11.1991	PRODUCTION	PLUGGED	OIL
3	7/12-A-1 B	23.12.2000	12.02.2001	PRODUCTION	PRODUCING	OIL
4	7/12-A-2	29.10.1986	09.01.1987	PRODUCTION	PLUGGED	OIL
5	7/12-A-2 A	08.12.1995	20.12.1995	PRODUCTION	PLUGGED	NOT AVAILABLE
6	7/12-A-2 B	03.10.2005	14.12.2005	PRODUCTION	PRODUCING	OIL
7	7/12-A-3	15.11.1987	29.01.1988	INJECTION	PLUGGED	NOT AVAILABLE
8	7/12-A-3 A	28.01.1990	28.03.1990	INJECTION	PLUGGED	WATER
9	7/12-A-3 B	26.03.2010	29.05.2010	PRODUCTION	SUSP.AT TD	OIL
10	7/12-A-4	01.09.1988	11.11.1988	INJECTION	INJECTING	WATER
11	7/12-A-5	15.05.1988	03.02.1989	INJECTION	PLUGGED	WATER
12	7/12-A-5 A	23.03.1995	03.07.1995	PRODUCTION	PLUGGED	OIL
13	7/12-A-5 B	17.05.2005	10.08.2005	PRODUCTION	PRODUCING	OIL
14	7/12-A-6	05.10.1986	28.10.1986	PRODUCTION	PRODUCING	OIL
15	7/12-A-6 A					
16	7/12-A-7	19.04.1987	11.11.1987	PRODUCTION	PLUGGED	OIL
17	7/12-A-7 A	11.10.1996	23.10.1996	PRODUCTION	PLUGGED	NOT AVAILABLE
18	7/12-A-7 B	25.08.2000	22.11.2000	PRODUCTION	PLUGGED	OIL
19	7/12-A-7 C	30.01.2002	18.03.2002	INJECTION	INJECTING	GAS
20	7/12-A-8	09.02.1989	02.04.1989	INJECTION	PLUGGED	NOT AVAILABLE
21	7/12-A-8 A	13.04.1994	24.06.1994	INJECTION	INJECTING	WATER
22	7/12-A-9	30.08.1989	15.10.1989	PRODUCTION	PLUGGED	OIL
23	7/12-A-9 A	13.01.2006	30.08.2006	OBSERVATION	PLUGGED	
24	7/12-A-9 B			INJECTION		
25	7/12-A-10	09.07.1986	04.10.1986	PRODUCTION	PLUGGED	NOT AVAILABLE
26	7/12-A-10 A	21.02.1997	04.05.1997	PRODUCTION	PRODUCING	OIL
27	7/12-A-11	02.06.1993	13.11.1993	INJECTION	INJECTING	WATER
28	7/12-A-12	21.05.1988	24.07.1988	PRODUCTION	PLUGGED	NOT AVAILABLE
29	7/12-A-12 A	15.04.1990	14.06.1990	PRODUCTION	PRODUCING	OIL
30	7/12-A-13	08.04.1989	02.07.1989	INJECTION	PLUGGED	NOT AVAILABLE
31	7/12-A-13 A	04.11.1989	19.12.1989	INJECTION	INJECTING	WATER
32	7/12-A-14	08.12.1992	28.02.1993	PRODUCTION	PLUGGED	OIL
33	7/12-A-14 A	04.07.2001	10.08.2001	PRODUCTION	PRODUCING	OIL
34	7/12-A-15	02.07.1989	29.08.1989	PRODUCTION	PLUGGED	OIL
35	7/12-A-15 A	12.09.2009	19.10.2009	PRODUCTION	PRODUCING	OIL
36	7/12-A-16	01.03.1993	20.05.1993	PRODUCTION	PLUGGED	NOT AVAILABLE
37	7/12-A-16 A	16.08.1995	01.10.1995	PRODUCTION	PRODUCING	OIL
38	7/12-A-16 B			PRODUCTION		
39	7/12-A-17	05.04.1991	02.10.1991	PRODUCTION	PLUGGED	OIL
40	7/12-A-17 A	16.06.2003	12.10.2003	PRODUCTION	PLUGGED	OIL
41	7/12-A-17 B	08.12.2009	04.03.2010	INJECTION	INJECTING	WATER/GAS
42	7/12-A-18	11.01.1987	19.04.1987	PRODUCTION	PRODUCING	OIL

3. Geological settings

The Late Jurassic was very important for the evolution of the North Sea petroleum system for several reasons. It was at that time that the Kimmeridge Clay formation was deposited, which is a world-class oil source rock, equivalent to the Mandal formation found on Ula. The rifting of Pangea has resulted in the creating of many hydrocarbon bearing traps in the reservoir rocks, as an example the syn-rift in the Upper Jurassic and lowermost Cretaceous as well as the pre- and syn-rift in the reservoir rocks of Devonian to Middle Jurassic. All these rift traps contain almost as much as 80% of the discovered hydrocarbon reserves found in the North Atlantic Margin, including the North Sea. As much as 20% of the reserves are found in the Upper Jurassic reservoir rock, and this makes it the most important target for petroleum exploration (Evans et al., 2003).

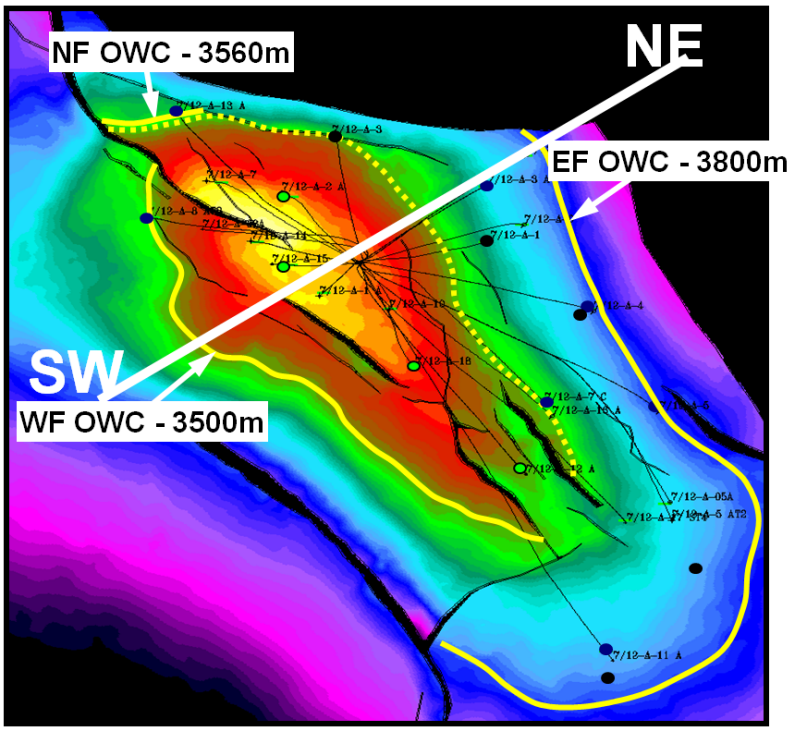

Figure 2: Overview of the structure of the Ula field (Ula Tambar Subsurface Team, 2013).

The structure of the Central Graben has a distinct trend going South-East, and it comprises two discrete troughs lysing east and west of the Forties-Montrose and Josephine highs which forms a spine between the two sub-basins. Although the most distinct trend is going south-east, some faults are formed and oriented north-south crossing the main trend. The structure of the Central Graben gets even more complicated when the presence of thick Zechstein[1] evaporites[2] detach the Triassic and the Jurassic reservoir rocks. This results in a reduction of

[1] Zechstein: A European series of geological time, Upper Permian

[2] Evaporite: Deposits of mineral salt from sea water or salt lakes due to evaporation of water.

the trap size of the faults, compared to reservoirs found in the northern North Sea (Evans et al., 2003).

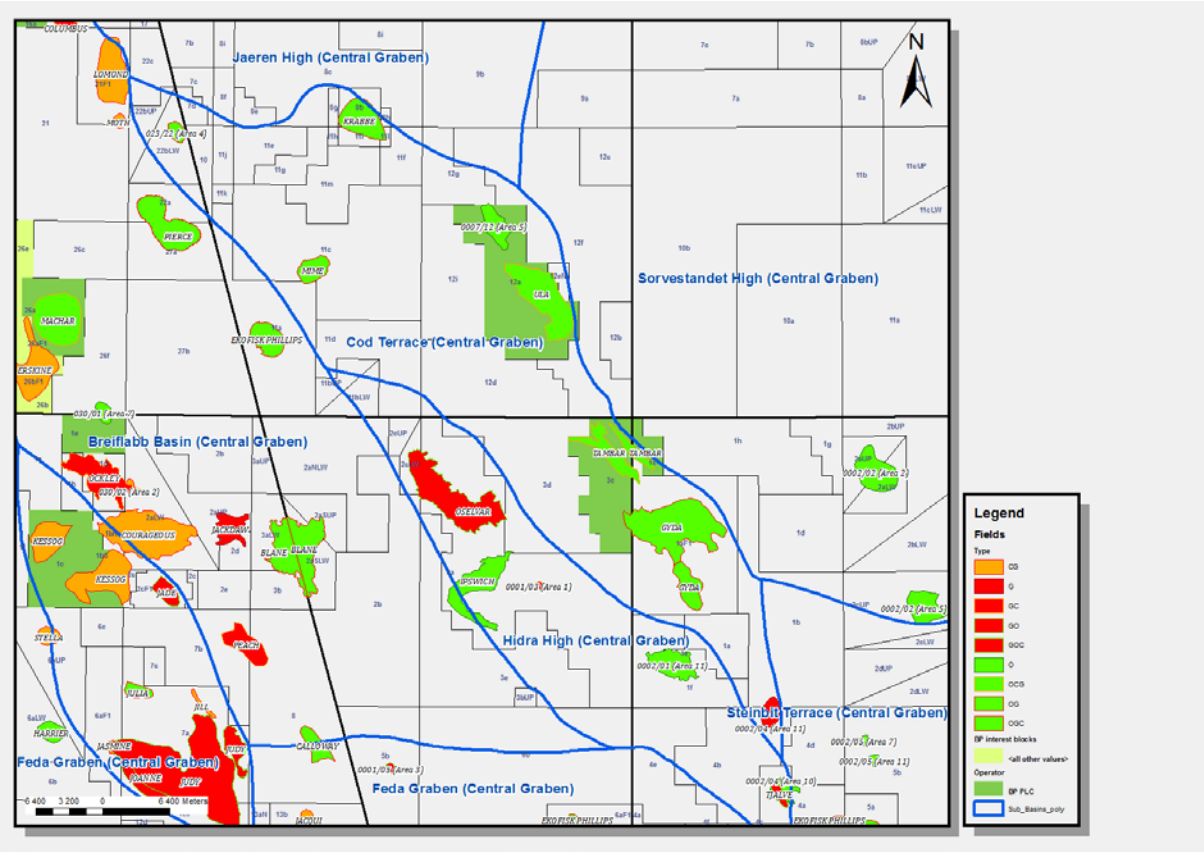

Figure 3: Regional map of the Central Graben

3.1. Lithology

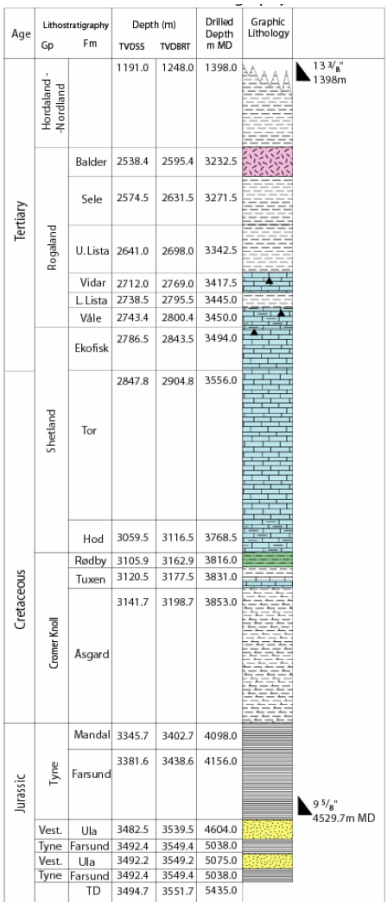

Figure 4: General lithostragraphy for Ula (Hordaland/Nordland continues up to seabed).

Formation descriptions are quoted from the NPD fact pages (NPD, 2013):
Nordland Group: Dominated by marine claystone, which are grey, sometimes greenish-grey and grey-brown, soft, locally silty and micaceous.

Hordaland Group: Consist of marine claystones with minor sandstones. The claystones are normally light grey to brown, fissile and fossiliferous. Red and green claystones sometimes occur at the base. Thin limestones and streaks of dolomite are present. Sandstones are developed at various levels in the group. These are generally very fine to medium grained, and are often interbedded with claystones.

Rogaland Group:

- *Balder formation*: composed of laminated varicoloured, fissile shales with interbedded grey, green and buff, often pyritic, sandy tuffs and occasional stringers of limestone, dolomite and siderite. Sandstones are locally present.
- *Sele formation*: consists of tuffaceous montmorillonite-rich shales and siltstones which are medium to dark grey or greenish-grey. They are finely laminated and carbonaceous, with minor interbeds of laminated sandstone which is frequently glauconitic.

- *Upper Lista*: consists of brown to grey-brown shales, which are generally non-tuffaceous and poorly laminated. Occasionally it contains stringers of limestone, dolomite and pyrite. Thin sandstone layers are locally developed. They are less than 5 m thick, and are most common in the lower part of the formation.
- *Vidar formation*: Homogenous limestone is the dominant lithology, but streaks of skeletal detritus and clasts of sandstone occur.
- *Lower Lista formation*: see description Upper Lista.
- *Våle formation*: typically consists of marls and claystones interbedded with limestone beds and stringers of sandstone and siltstone. In the Central Trough, the formation is developed as a light grey marl, but locally has chalk and limestone interbeds probably eroded from rising diapirs.

Shetland Group:

- *Ekofisk formation*: The formation usually consists of white to light grey, beige to brownish, mudstones or wackestones with occasional packstones/grainstones and pisolitic horizons, often alternating with argillaceous chalks, chalky limestones or limestones. Thin beds of grey, calcareous, often pyritic shales or clays are most common in the lower part while brownish-grey cherts occur rarely to abundantly throughout the formation.
- *Tor formation*: Generally homogenous, or consists of alternating white, grey or beige, moderately hard to very hard, rarely soft, mudstones or wackestones, rarely packstones, chalks, chalky limestones or limestones. Occasional fine layers of soft grey-green or brown marl occur and also rare stringers of grey to green calcareous shales.
- *Hod formation*: White, light grey to light brown, soft to hard chalk facies may dominate the formation or alternate with limestones. The limestones may be pink or pale orange. Thin, silty, white, light grey to green or brown, and soft, grey to black, calcareous clay/shale laminae are occasionally present. Pyrite and glauconite may occur throughout the formation and the latter may be common in the lower part.

Cromerknoll Group:

- *Rødby formation*: Mainly red-brown marlstones, but green and grey colours may occur. Glauconite and pyrite may be present. Sandstones and siltstones are known to be present locally.
- *Tuxen formation*: The formation is dominated by white to greyish-pink, calcareous claystones and marlstones. Along some of the structural highs the marlstones grade into purer limestones. Generally, the formation terminates vertically upwards with a chalk sequence containing subordinate marlstone layers. This chalk is white to pale orange or yellowish-grey, occasionally greenish and reddish. The marlstones are generally light grey to greenish-grey or olive-grey, but may be reddish-brown in some wells.

- *Åsgard formation*: The formation is dominated by light to dark grey, olive-grey, greenish and brownish, often calcareous claystones, and passes into light grey, light greenish-grey and light olive-grey marlstones and stringers of limestone. Mica, pyrite and glauconite are common. The claystones may be silty, and siltstones or very fine-grained sandstone layers or laminae are present. Where major sandstone layers occur they are regarded as belonging to the Ran sandstone units.

Tyne Group:

- *Mandal formation*: The formation consists of a dark grey-brown to black, slightly to non-calcareous, carbonaceous claystone becoming fissile in places. It is characterized by a very high level of radioactivity which is a function of organic carbon content. In addition it has an anomalously low velocity, a high resistivity and a low density. It may contain thin stringers of limestone/dolomite and, in some areas, sandstone.
- *Farsund formation*: The formation consists predominantly of medium to dark grey shale. The shale is often well laminated and contains frequent calcareous streaks. In the reference well 7/12-2, closer to the flank of the Southern Vestland Arch, a thinner Farsund formation is present as a clear "coarsening upward cycle", becoming consistently less radioactive towards the top of the unit.

Vestland Group:

- *Ula formation*: Generally massive, fine to medium grained, grey sandstone. A thin, dark grey siltstone is present in the basal part of the formation. The sandstones are arkosic to subarkosic, glauconitic and micaceous. Sorting and angularity vary between individual units of the formation. Bivalve shells and belemnite debris occur, often concentrated in thin lag deposits. Thin, nodular calcite-cemented bands are common.

Zechstein Group: Evaporates and carbonates with local clastic rocks. Halites dominate the basin-centre sequences, while limestones, dolomites and anhydrates prevail along the basin margins.

3.2. Reservoir rock

The main reservoir rock in the Ula formation is shallow marine sandstone from the Upper Jurassic which is accumulated on the terraces of the Ula-Gyda fault zone (Bjørnseth and Gluyas, 1995). The thickness of the reservoirs are determined by a combination of depositional processes, sediment supply and subsidence. The accommodation space of the Upper Jurassic sandstone is in some areas dominated by syndepositional rifting, but elsewhere dominated by salt movement and pre-existing topography. (Evans et al., 2003).

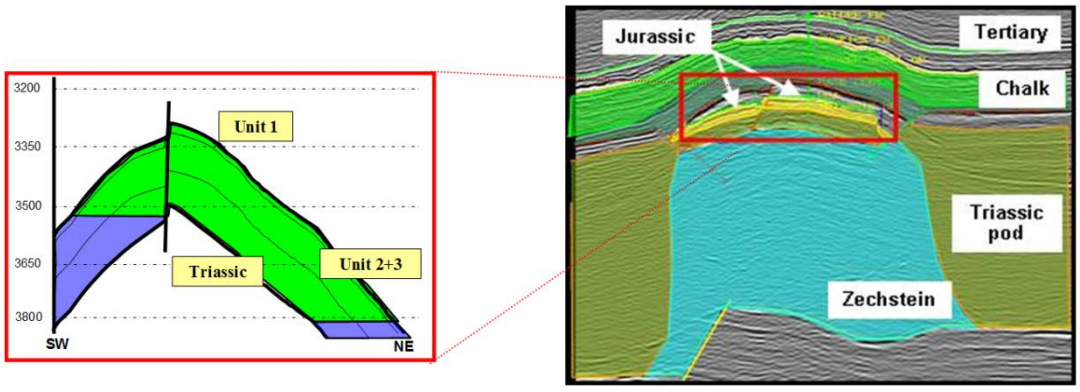

Figure 5: Overview of the reservoir with the trap made from the movement of the Zechstein salt (Ula Tambar Subsurface Team, 2013)

The Ula sandstone is characterized as an extensively bioturbated[3] dominantly fine-grained sand/silt package (Daae and Ula & Tambar Subsurface and Well Monitoring Team, 2011). The interpretations of the sandstone show that it was developed on a shallow marine shelf between storm and fairweather wavebase (Oxtoby et al., 1995). These sands are a result of the rapid rise in relative sea level happening in the Late Jurassic, creating sandstones with high reservoir quality as the sandstone found in the Ula formation (Evans et al., 2003). By using petrophysical and log studies of the reservoir, distinct differences in the reservoir can be found dividing the reservoir into five units, where unit 1 is the top unit and Unit 5 is the lowest one. The units are based on differences in grain size, bioturbation, mineralogy and log response (Spencer et al., 1987). The Ula producton and injection wells are located in Unit 1-3, where unit 2 and 3 have good reservoir quality and high net to gross sands. Unit 1 has poorer quality compared to Unit 2 as a result of a marine transgression leading to a retrogrational sequence. They are distal lower shoreface fine grained sands and silts. This has an effect on the permeability of the sandstone. The permeability of Unit 1 has an average of approximately 20mD, while Unit 2 and 3 has about 200mD (Thomas et al., 2008). This permeability is taken from a core plug scale of average permeability. The Unit 1 are separated from Unit 2 and Unit 3 by an distal marine shale barrier, and there is a similar but less effective barrier in the middle of the Unit (Paton, 2013).

[3] Bioturbation: The disruption of marine sedimentary structures by the activities of benthic organisms.

The description of the different units is quoted from the book Geology of the Norwegian Oil and Gas Fields (Spencer et al., 1987):

Unit 5 is a thin, fine grained grey sandstone with a sharp base and gradational top. The sands are poorly to moderately sorted, micaceous and glauconitic with some carbonaceouse debris. Mainly vertical burrows have obliterated any original sedimentary structures.

Unit 4 is a thoroughly bioturbated, dark grey siltstone with some grey, fine-grained sandstone. Occasional relics of a wispy lamination are discernible. Vertical burrows predominate, and belemnites, bivalves and sponge spicules occur.

Unit 3 consists of fine- to medium-grained, moderately to well-sorted, slightly micaceous and glauconitic sandstones. A general coarsening-up trend has been identified, but is superimposed on several smaller coarsening- and fining-up cycles. Details of sedimentary contacts are generally obscured by the pervasive horizontal bioturbation. Some zones do, however, occur, particularly in the lower half of Unit 3, in which parallel and low-angle inclined lamination are preserved. Also present are cosets of planar cross-beds with opposing dips.

Unit 2 is very similar to unit 3, though with less evidence of original sedimentary features. It is, in general, well sorted and apparently the best reservoir unit in the field. The sands have been homogenized by the pervasive horizontal bioturbation. Vertical burrows occur near its base.

Unit 1 contains finer-grained, less well-sorted sandstones with more vertical burrows than Unit 2. Belemnite debris also reappears. Sedimentary features are largely obscured by bioturbation, but thin (5-20 cm) fining-up sequences capped by siltstone can be found. Traces of low-angel cross-bedding, planar bedding and minor ripple structures are also noted.

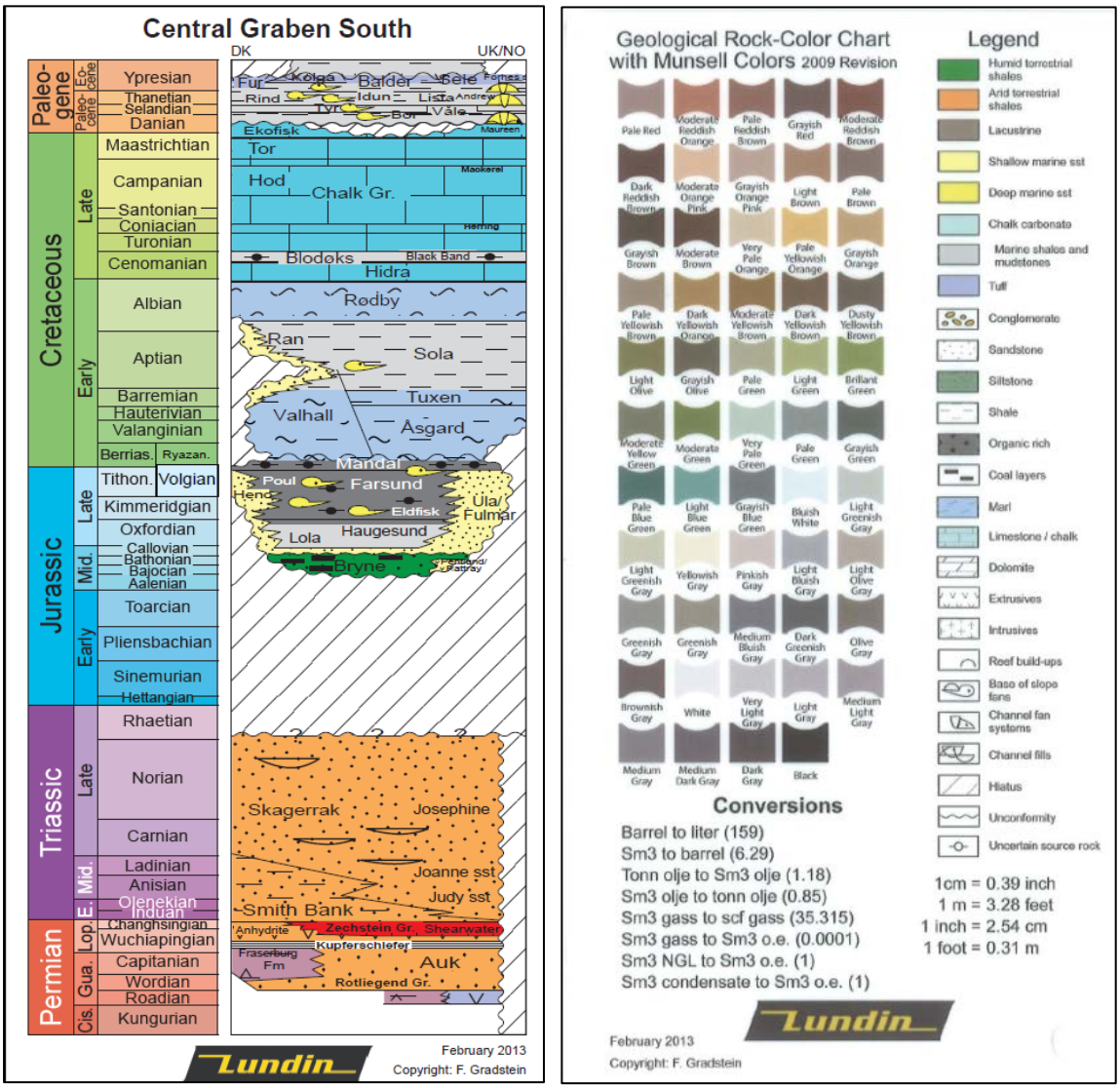

Figure 6: Stratigraphic table of the Central Graben South (Gradstein, 2013)(with permission from authors to use the model).

3.3. Source rock

The age of the source rock is from the Portlandian age, from the overlaying Mandal Formation (Oxtoby et al., 1995). “The overlaying Mandal formation is a “hot shale” and is the Kimmeridge clay equivalent” (Spencer et al., 1986). Geomechanical analysis on PVT (Pressure Volume Temperature) samples from Ula wells shows that the Mandal formation is the primary source rock responsible for charging the Ula reservoir. The Kimmeridge source is a world class deep marine clastic source rock and is the likely source for many of the producing fields in the Central Graben (Paton, 2013).

Looking at the permeable sandbodies of the Ula Trend it can be noticed that the trend tends to have a constant overpressure, while the overlying source rock become increasingly overpressured with depth. At a certain depth, the pressure in the source rock will exceed the pressure in the reservoir rock, and this will force the hydrocarbons downwards into the sandstone. Normally the hydrocarbons migrate upwards, but it will always seek the rock with the lowest pressure (Bjørnseth and Gluyas, 1995)

Research done on the Central Through (Central Graben) and the Sørvestlandet high (shown in Figure 3) show that the hydrocarbons from the Mandal formation should be present also in the traps on the Sørvestlandet High, but there is a belt of dry wells in this area. Hydrocarbons cannot be found in the Sørvestlandet High because major faults are separating the Sørvestlandet High from the basin (Bjørnseth and Gluyas, 1995). These faults are in the Jurassic level of the graben and are called the Hidra Fault Zone. The Hidra Fault Zone is believed to be Late Jurassic growth faults with throws of hundreds of meters (Spencer et al., 1987). The Mandal formation in the Sørvestlandet High has not the same conditions as in the Central Graben. The low permeability and thin sandstones in this area will tend to act as a pressure-isolated sandbodies, with slightly higher overpressure than the overlaying source rock. This pressure difference will therefore inhibit the migration of the hydrocarbons downwards as seen in the Central Graben. Another factor is that the Ula Trend is assigned a low charge risk, while the charge risk is considered to be high at the Sørvestladet High (Bjørnseth and Gluyas, 1995).

3.4. Trap

The Ula field has structural traps in the Late Jurassic part of the structure. The reservoir trap is a salt-cored, largely dip-closed pericline[4], which is stretching NW to SE (Oxtoby et al., 1995). The domal structure was foremed by the swelling of the underlying Zechstein salt which happened in the Tertiary times and is bounded to the north-east by the Hidra Fault Zone. The Zechstein salt is non-penetrive and has a gentle structural dipping at the Jurassic level which is less than six degrees (Spencer et al., 1987). The Ula structure has an

[4] Pericline: A fold characterized by central orientation of the dip of the beds.

approximately 500m long vertical closure which is dissected into two major and a number of minor blocks by normal faults (Oxtoby et al., 1995).

3.5. Glacial effect

Back in time much of the North Sea was covered by a large glacier. This has caused the top layers of the fields to be more compact than they normally would be. When the wells are drilled a conductor is first set and then a pilot hole is drilled. As a result there are no logs from these top layers and the logs will maybe start at a depth of 600-700m. The effect of the glacier will therefore not show in the logs (Flatebø, 2013).

Because of the compaction, the overburden of the layers will be much higher than it normally would be. This has an effect when plotting the overburden curve for the field when the normal trend of the overburden cannot be used (Flatebø, 2013).

Looking at the top layers of the Ula Trend and also much of the North Sea, the layers are more compact than they should be at that depth. This is because of the huge glaciers covering this area back in time. The weight of the glacier has therefore resulted in the compaction of the top layers. The densities of these layers are similar to much deeper layers (Olsen, 2013).

3.6. DPZ – Distinct Permeable Zones

There are two terms used when talking about permeable zones, which are PZ (Permeable Zone) and DPZ (Distinct Permeable Zone). PZ means a zone which has sufficient permeability such that a credible pressure differential would result in the movement of fluids (oil, water or gas) and/or development of sustained casing pressure (SCP). DPZ is a group of permeable zones in which intrazonal isolation is not required for operation or abandonment of the well (BP).

It is important to define the permeable zones in a field because isolation between two permeable zones is important. No isolation between two permeable zones can result in crossflow. While drilling there can occur crossflow when a lost returns event is followed by a well control event. This will cause the higher pressured reservoir fluid to flow into the wellbore, travel along the wellbore and flow into lower pressured formation. Crossflow can also be experienced during production. The formation fluid will then flow to a lower pressured zone instead of flowing up the production pipe. This can be prevented by closely controlling the production parameters (Flatebø, 2013).

Permeable zones can also cause influx into the well which makes the well pressure higher. This will flow up the wellbore and can damage the wellhead (Flatebø, 2013).

Limited work has been done on defining the DPZs on this field after the new requirements for these zones were defined. The work mentioned here should therefore be regarded as work in progress.

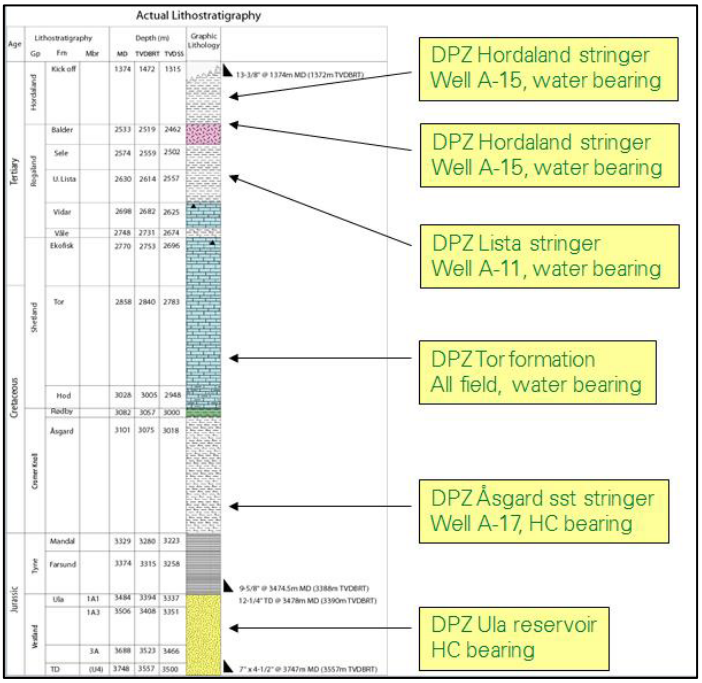

Figure 7: Example of the DPZs in overburden Ula

4. Rock Mechanics

When designing a well it is crucial to have good knowledge about rock mechanics. Not knowing what forces are influencing a well can result in well collapse and other problems. The design has to take into account the forces from the fluids in the well and the formation pressure. The overbearing loads when drilling a deep well also has to be considered. The design should also take into account a safety margin for other forces that can occur, like seismic shock, thermal expansions/contractions and many others.

Drilling equipment must be designed to drill through different types of rock materials, but the design should also be such that when drilling through the rock the rock formation integrity is not changed, thereby not affecting the stability of the drilled well (Aadnoy and Looyeh, 2011).

Solid mechanics is a concept where analytical methods are used to design solid engineering to ensure correct strength, stiffness, stability and integrity. This concept is used in all branches of engineering designs from building a car to designing a well. In well design, solid mechanics are used in all stages of the planning of the well, from exploration to production with drilling and completion in between. In these disciplines fundamental laws of Newtonian mechanics are used, which means that you look at the balance of forces and the mechanical properties of the material the object is made of (Aadnoy and Looyeh, 2011).

There are two key elements in solid mechanics, which is internal resistance and external forces. Internal resistance is the forces in the element that balance out the effect of the external forces around. This internal resistence is commonly represented by the term stress. The external forces are the forces that can change the shape and deform the object, and is called strain (Aadnoy and Looyeh, 2011).

In this chapter we will go through the basic principles of rock mechanics since this is essential for this study.

4.1. Stress

Looking at stress in detail can be quite confusing since a lot of algebraic calculations to find the stresses is needed. But the basic principles of stress are quite straight forward. To understand the principles of stress, some knowledge about forces and tractions are needed. The forces are commonly known as a push or a pull to a body of some material. The intensity of the force is significant in determining how the material will react to the force applied. The intensity of the force can be expressed as the force divided by the area of the surface of which the force is applied. This quantity is called traction, and has the unit force per unit area (Twiss and Moores, 2006).

At equilibrium equal and opposite forces are acting on each side of the surface area, hence the traction also must be equal and opposite on both sides. These types of equal and opposite tractions on a surface area are called surface stresses. The surface stresses therefore have a direct connection to the forces applied on the material on a given area (Twiss and Moores, 2006).

If only the surface stresses on two perpendicular surfaces that pass through a point are known, this can be used to calculate the stress acting on any surface of any orientation through that point. This will make you a two dimensional calculation. To make it three dimensional three surface stresses on three perpendicular surfaces through one point are needed. These surface stresses then define the state of stress at a point, or more simply stress. The equation for stress is shown beneath (Twiss and Moores, 2006):

$$\sigma = \frac{Force}{Area} = \frac{F_n}{A} \qquad 4.1.$$

$$\tau = \frac{F_p}{A} \qquad 4.2.$$

Where σ/τ is the stress (Pa or psi), F is the force (N or lbf) and A is the surface area (m^2 or in^2). The equation 4.1 is the normal stresses action on the surface. You then have the decomposed force as a normal vector to the plane. The shear stress is the equation 4.2 which is the stresses for the decomposed force going perpendicular to the plane. This is shown in Figure 8 and Figure 9 below. "The normal stress may result in tensile or compressive failure, and the shear stress in shear failure, where the material is sheared or slipped along a plane" (Aadnoy and Looyeh, 2011).

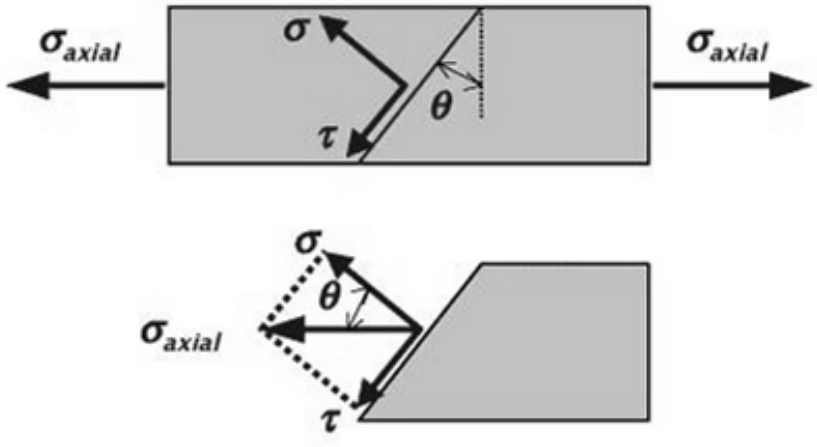

Figure 8: Stress components showing the normal and shear stress (Aadnoy and Looyeh, 2011).

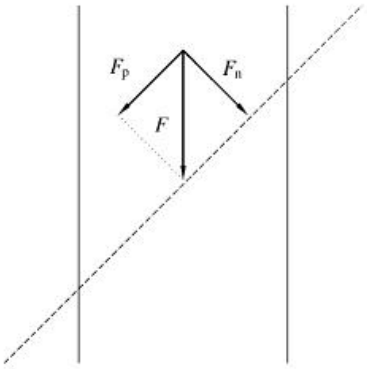

Figure 9: Decomposition of forces (Fjær et al., 2008)

4.2. Strain

When a mass is exposed to loading, the body will undergo displacement and/or deformation. This means that if you look at a point on or in this body you will see that the point has been shifted to another position as shown in Figure 10. When looking at stain you compare the deformation/ displacement to the original state of the body. You will then get a dimensionless parameter for the strain. The equation 4.3 shown below is the equation for strain, and it is defined as the deformed state divided by the original non-deformed body (Aadnoy and Looyeh, 2011):

$$\varepsilon = \frac{\Delta l}{l_0} \qquad 4.3.$$

where ε is the strain (dimensionless), Δl is the deformed dimension (measured in m or in) and l_0 is the original state of the body (m or in).

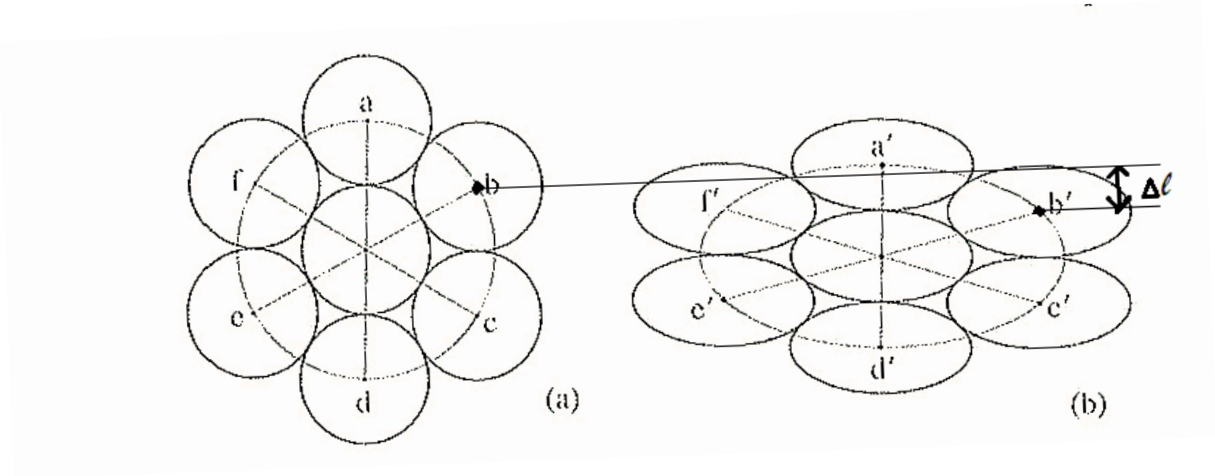

Figure 10: Center-to-center distances: (a) before strain; (b) after strain (Ragan, 2009).

Strain can be grouped it into two categories, engineering strain and scientific strain. Engineering strain use the initial/original dimension of the stress when performing the analysis, while the scientific definition of strain use the actual dimension of the strain which is changing by time. The equation 4.3 is no longer valid if the element/body you are working with have undergone to large deformations. There have been made two main equations for strain that has undergone large deformations. These two equations has been introduced by Almansi and Green and are expressed by (Aadnoy and Looyeh, 2011):

$$\varepsilon = \frac{l^2 - l_0^2}{2l^2} \qquad 4.4.$$

$$\varepsilon = \frac{l^2 - l_0^2}{2l_0^2} \qquad 4.5.$$

Equation 4.4 is called the Almansi strain formula, while equation 4.5 is Greens strain formula.

Strain components

When looking at a square (Figure 11) that is put under loading, it can be observed that the square has moved (translated) and has changed shape (deformed). Of the two it is only the deformation that causes changes in the stress on the square, and therefore this is looked at when doing a failure analysis.

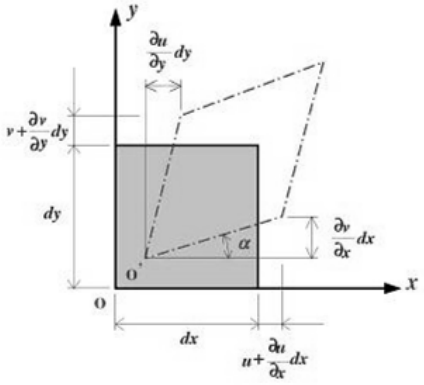

Figure 11: A square shape before and after loading (Aadnoy and Looyeh, 2011).

The deformation angle can be expressed by the equation:

$$\tan\alpha = \frac{\frac{\partial v}{\partial x}dx}{dx + \frac{\partial u}{\partial x}dx} \qquad 4.6.$$

This can be shortened by doing some approximation using the small deformation theory, and is then:

$$\tan\alpha \approx \frac{\partial v}{\partial x} \tag{4.7.}$$

When you look at the stress in x and y direction you can define the stress by:

$$\varepsilon_x = \frac{\frac{\partial u}{\partial x}dx}{dx} = \frac{\partial u}{\partial x} \qquad \varepsilon_y = \frac{\frac{\partial v}{\partial y}dy}{dy} = \frac{\partial v}{\partial y}$$
$$\varepsilon_{xy} = \frac{\frac{\partial v}{\partial x}dx}{dx} = \frac{\partial v}{\partial x} \qquad \varepsilon_{yx} = \frac{\frac{\partial u}{\partial y}dy}{dy} = \frac{\partial u}{\partial y} \tag{4.8.}$$

and

$$\varepsilon_{xy} + \varepsilon_{yx} = \frac{\partial v}{\partial x} + \frac{\partial u}{\partial y} = 2\varepsilon_{xy} = \gamma_{xy} \tag{4.9.}$$

where ε is the normal strain, and γ is the shear strain.

The three dimensional state of strain can be written as a matrix as done for the stress, as shown below:

$$[\varepsilon] = \begin{bmatrix} \varepsilon_x & \frac{1}{2}\gamma_{xy} & \frac{1}{2}\gamma_{xz} \\ \frac{1}{2}\gamma_{xy} & \varepsilon_y & \frac{1}{2}\gamma_{yz} \\ \frac{1}{2}\gamma_{xz} & \frac{1}{2}\gamma_{yz} & \varepsilon_z \end{bmatrix}$$
$$= \begin{bmatrix} \frac{\partial u}{\partial x} & \frac{1}{2}\left(\frac{\partial u}{\partial y} + \frac{\partial v}{\partial x}\right) & \frac{1}{2}\left(\frac{\partial u}{\partial z} + \frac{\partial w}{\partial x}\right) \\ \frac{1}{2}\left(\frac{\partial u}{\partial y} + \frac{\partial v}{\partial x}\right) & \frac{\partial v}{\partial y} & \frac{1}{2}\left(\frac{\partial v}{\partial z} + \frac{\partial w}{\partial y}\right) \\ \frac{1}{2}\left(\frac{\partial u}{\partial z} + \frac{\partial w}{\partial x}\right) & \frac{1}{2}\left(\frac{\partial v}{\partial z} + \frac{\partial w}{\partial y}\right) & \frac{\partial w}{\partial z} \end{bmatrix} \tag{4.10.}$$

The equations are valid for small deformations and can therefore be used for most of the engineering materials. If the deformations get too large the second-order terms becomes significant (Aadnoy and Looyeh, 2011).

4.3. Elasticity, In-situ stress and stress concentration around a wellbore

Elasticity is the linear relationship between the applied stresses and the resulting strains, of the materials which behave fully or partially elastically. There is a connection between the degree of deformation of a material (strain) and the magnitude of the stresses or loads the material has been exposed to. This makes the stresses very important for solids mechanics. The stresses cannot be measured, but are calculated from the strains that is measured in-situ or in a laboratory (Aadnoy and Looyeh, 2011).

Most rocks do not behave in a linear when subjected to large stresses, but their behaviour may normally be described linearly for sufficiently small changes in the stress (Fjær et al., 2008). Since not all the rocks parameters are known, it is usually assumed that the rocks are linear elastic, isotropic and homogeneous when modelling the rocks. If some of the rock parameters are know, this will make the calculations very complex and are highly dependent on the accuracy of your laboratory measurements and the subsequent analysis (Aadnoy and Looyeh, 2011).

4.3.1. Hook's law

There can in some cases exist a linear relationship between stress and strain, and this relationship is given by the following equation:

$$\sigma_x = E\varepsilon_x \qquad 4.11.$$

where ε_x is the engineering strain shown in equation 4.3 and σ_x is the stress as shown in equation 4.1. Equation 4.11 is known as Hook's law of deformation. The slope of the linear relationship is referred to as the Modulus of Elasticity or better known as Young's modulus, E (Aadnoy and Looyeh, 2011).

4.3.2. Poisson's ratio

The Poisson's ratio is almost the same as Hook's law. The difference is that Hook's law look at the linear relationship between the deformations of the lengths, while Poisson's looks at the linear relationship between deformation in the diameter and the applied stresses. The lateral elongation can then be shown by:

$$\varepsilon_y = \varepsilon_z = \frac{(D - D')}{D} \qquad 4.12.$$

In general the deformation makes D' larger than D, therefore you get a negative strain. The Poisson's ratio is then defined as:

$$v = -\frac{\varepsilon_y}{\varepsilon_x} \qquad 4.13.$$

Both equation 4.11 and equation 4.13 are defined by a specific state of stress where $\sigma_x \neq 0, \sigma_y = \sigma_z = 0$. Each component of strain is in general a linear function of all components of stress (Fjær et al., 2008).

4.3.3. Stress components

A general three dimensional state of stress can be looked at as a cube as shown in Figure 12, and the figure shows that the balance of forces show that each stress vector has an equal and opposite vector. In this case we only look at the stress acting on the surfaces of the cube. The stress vectors can be grouped into groups of normal and shear stresses. The normal stresses in a three dimensional case is σ_{xx}, σ_{yy} and σ_{zz}, and for the shear stresses you have τ_{xy}, τ_{yx}, τ_{xz}, τ_{zx}, τ_{yz} and τ_{zy}. The index letters refers to the Cartesian coordinate system. The first letter refers to the axis normal to the plane where the stress is acting; the second letter tells which direction the stress is acting. Normal stresses that have two identical index letters the expression are shortened so that $\sigma_{xx} \equiv \sigma_x$ (Aadnoy and Looyeh, 2011).

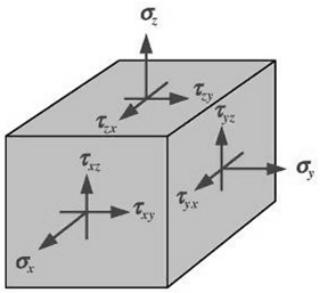

Figure 12: Three-dimensional stress state of a cube (Aadnoy and Looyeh, 2011).

When the cube is at rest, which means that the cube is not moving, you will have no net translational or rotational forces acting on the cube. While no translational forces is already ensured, no rotational forces requires that (Fjær et al., 2008):

$$\tau_{xy} = \tau_{yx}\,, \tau_{xz} = \tau_{zx}\ and\ \tau_{yz} = \tau_{zy} \qquad 4.14.$$

These stresses are easier seen in a two dimensional case as shown in Figure 13 below.

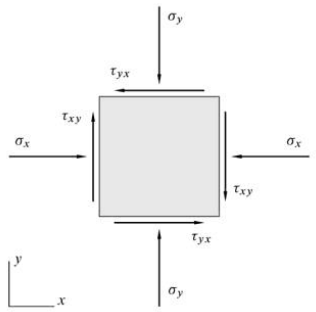

Figure 13: Stress components in two dimensions (Fjær et al., 2008).

The equation for three dimensional state of stress is then given by three normal stresses and three shear stresses as shown in Equation 4.15 below:

$$[\sigma] = \begin{bmatrix} \sigma_x & \tau_{xy} & \tau_{xz} \\ \tau_{xy} & \sigma_y & \tau_{yz} \\ \tau_{xz} & \tau_{yz} & \sigma_z \end{bmatrix} \qquad 4.15.$$

4.3.4. Principle stress

When the stresses in an element are acting in a direction such that there are only normal stresses and no shear stresses, they are called principle stresses. Similar if there are elements with only normal strains, these are referred to as principle strains. The principle stresses are required in any failure analysis because they say something about the maximum and minimum stresses, or the maximum differential stress value in the studied case (Aadnoy and Looyeh, 2011).

The principle stresses can be defined as:

$$[\sigma] = \begin{bmatrix} \sigma_x & \tau_{xy} & \tau_{xz} \\ \tau_{xy} & \sigma_y & \tau_{yz} \\ \tau_{xz} & \tau_{yz} & \sigma_z \end{bmatrix} = \begin{bmatrix} \sigma_1 & 0 & 0 \\ 0 & \sigma_2 & 0 \\ 0 & 0 & \sigma_3 \end{bmatrix} \qquad 4.16.$$

Moving the matrix on the right-hand side over to the left and taking the determinant, you get a solution for the principal stresses shown in the following equation:

$$\begin{bmatrix} \sigma_x - \sigma & \tau_{xy} & \tau_{xz} \\ \tau_{xy} & \sigma_y - \sigma & \tau_{yz} \\ \tau_{xz} & \tau_{yz} & \sigma_z - \sigma \end{bmatrix} = 0 \qquad 4.17.$$

To use this matrix to find the principle stresses, it has to be expanded and solved. The result you get is a cubic equation:

$$\sigma^3 - I_1\sigma^2 - I_2\sigma - I_3 = 0 \qquad 4.18.$$

where

$$I_1 = \sigma_x + \sigma_y + \sigma_z$$
$$I_2 = {\tau_{xy}}^2 + {\tau_{xz}}^2 + {\tau_{yz}}^2 - \sigma_x\sigma_y - \sigma_x\sigma_z - \sigma_y\sigma_z \quad 4.19.$$
$$I_3 = \sigma_x\left(\sigma_y\sigma_z - {\tau_{yz}}^2\right) - \tau_{xy}\left(\tau_{xy}\sigma_z - \tau_{xz}\tau_{yz}\right) + \tau_{xz}(\tau_{xy}\tau_{yz} - \tau_{xz}\sigma_y)$$

These equations (4.19) always have three real roots, which are known as principle stresses ($\sigma_1, \sigma_2\ and\ \sigma_3$) where $\sigma_1 > \sigma_2 > \sigma_3$ (Aadnoy and Looyeh, 2011).

4.3.5. Regional stress – in-situ stress

When looking at sediments beneath the earth crust there will always exist three orthogonal in-situ stress states. The vertical stress is due to the overburden of the sediments above, and the two horizontal stresses are due to tectonics and geological depositional processes.

4.3.5.1. Vertical stresses

Looking at formations underground the vertical stress at this point will be the weight of the overlaying sediments. Overburden increase with depth because the amount of sediments above increase. When there is a homogeneous column of height z the vertical stresses will be given as $\sigma_v = \rho g z$. If the density of the formation is not homogeneous and varies with depth, the vertical stress at depth D is:

$$\sigma_v = \int_0^D \rho(z) g dz \quad 4.20.$$

ρ = density of the material, g is the acceleration of gravity, dz = thickness of the formation, σ_v = vertical stress.

4.3.5.2. Horizontal stresses

In an isotropic environment the horizontal stresses will be equal to each other. This means that the formation is not influenced by earthquake or tectonic movements of the continental plates. This is usually in the top layers because the older the formation is the longer time it will have had to experience these events. If assumed that the formation is in a stress relaxed environment there can be made an assumption which says that a uni-axial deformation in the axial direction can give the horizontal stresses as given by this equation (Fjær et al., 2008):

$$\sigma_h = \frac{v}{1-v}\left(\sigma_v - \alpha P_p\right) + \alpha P_p \quad 4.21.$$

where σ_h = minimum horizontal stress, σ_v = overburden, P_p = pore pressure, α = Biot – coefficient (set as 1.0 for unconsolidated sands, and 0.9 in shale and consolidated sands). Figure 14 illustrates the schematic in-situ stress and the associated fault systems.

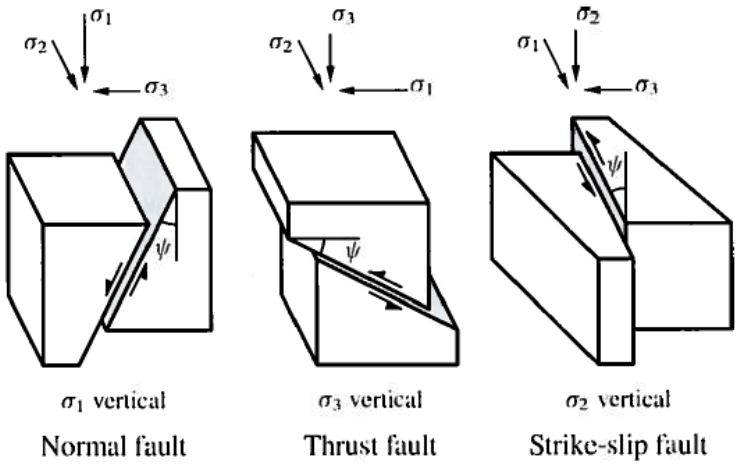

Figure 14: Schematic in-situ stress and the associated fault types (Fjær et al., 2008).

4.3.6. Stress around wellbore

By using Hook's law, equilibrium equations and compatibility equations, the stresses around the wellbore can be defined. In the inversion technique in chapter 8.1 the effective stresses for porous media is used. This is defined as the total stresses minus the pore pressure. Figure 15 illustrates the schematic stress states in radial coordinate

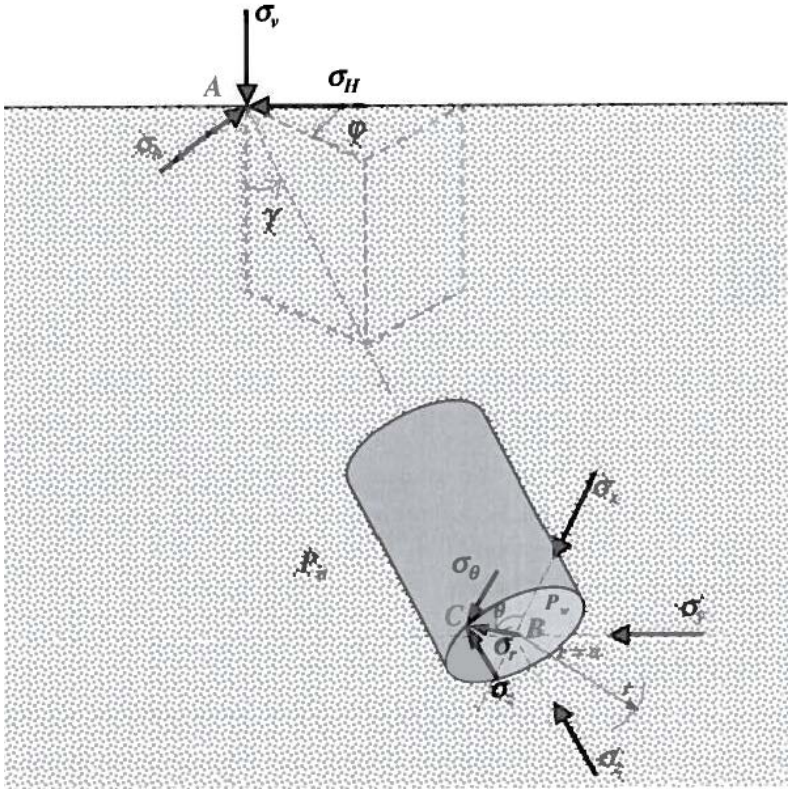

Figure 15: Schematic stress states in radial coordinate (Aadnoy and Looyeh, 2011).

During pressure loading the well will undergo a volumetric deformation. Ernst Gustav Kirsch managed to solve the stress concentration around a wellbore which was loaded with anisotropic maximum and minimum horizontal stresses, and with an vertical stress as the overload. The result of this was the well-known Kirsch equation which is given by:

$$\sigma_r = \frac{1}{2}(\sigma_x + \sigma_y)\left(1 - \frac{a^2}{r^2}\right) + \frac{1}{2}(\sigma_x - \sigma_y)\left(1 + 3\frac{a^4}{r^4} - 4\frac{a^2}{r^2}\right)cos2\theta + \tau_{xy}\left(1 + 3\frac{a^4}{r^4} - 4\frac{a^2}{r^2}\right)\sin 2\theta + \frac{a^2}{r^2}P_w$$

$$\sigma_\theta = \frac{1}{2}(\sigma_x + \sigma_y)\left(1 + \frac{a^2}{r^2}\right) - \frac{1}{2}(\sigma_x - \sigma_y)\left(1 + 3\frac{a^4}{r^4}\right)\cos 2\theta - \tau_{xy}\left(1 + 3\frac{a^4}{r^4}\right)\sin 2\theta - \frac{a^2}{r^2}P_w$$

$$\sigma_z = \sigma_{zz} - 2v(\sigma_x - \sigma_y)\frac{a^2}{r^2}cos2\theta - 4v\tau_{xy}\frac{a^2}{r^2}sin2\theta \rightarrow Plane\ strain \qquad 4.22.$$

$$\sigma_z = \sigma_{zz} \rightarrow Plane\ stress$$

$$\tau_{r\theta} = \left[\frac{1}{2}(\sigma_x - \sigma_y)sin2\theta + \tau_{xy}cos2\theta\right]\left(1 - 3\frac{a^4}{r^4} + 2\frac{a^2}{r^2}\right)$$

$$\tau_{rz} = (\tau_{xy}\cos\theta + \tau_{yz}sin\theta)\left(1 - \frac{a^2}{r^2}\right)$$

$$\tau_{\theta z} = \left(-\tau_{xz}sin\theta + \tau_{yz}cos\theta\right)\left(1 + \frac{a^2}{r^2}\right)$$

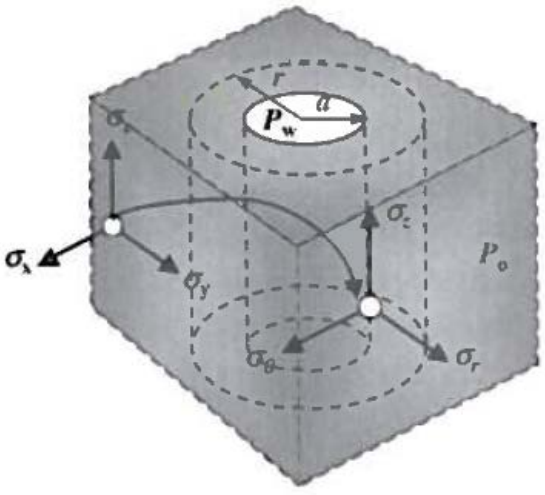

Figure 16: Position of stresses around a wellbore in the rock formation (Aadnoy and Looyeh, 2011)

In the case of anisotropic solutions at the wellbore wall, which means that r = a (see Figure 16), the Kirsch equation is reduced to:

$$\begin{aligned}
&\sigma_r = P_w \\
&\sigma_\theta = \sigma_x + \sigma_y - P_w - 2(\sigma_x - \sigma_y)cos2\theta - 4\tau_{xy}sin2\theta \\
&\sigma_z = \sigma_{zz} - 2v(\sigma_x - \sigma_y)cos2\theta - 4v\tau_{xy}sin2\theta \;\; \rightarrow \;\; Plane\ S\text{train} \\
&\sigma_z = \sigma_{zz} \\
&\tau_{r\theta} = 0 \\
&\tau_{rz} = 0 \\
&\tau_{\theta z} = 2(-\tau_{xz}sin\theta + \tau_{yz}cos\theta)
\end{aligned} \qquad 4.23.$$

4.3.7. Stress transformation

When working with wells the stress components should be transformed so they fit the inclination and azimuth of the wellbore. By using the principal in-situ stresses these can be transformed into the Cartesian coordinate system the stresses can be transformed so that they take into account the orientation of the wellbores. The direction of the new stresses is given by the inclination from vertical (γ), the geographical azimuth (φ), and the wellbore position from the x-axis (θ). This is shown in Figure 15 . In this transformation the y-axis is always parallel to the plane formed by σ_H and σ_h (Aadnoy and Looyeh, 2011).

The definition above and the figure will give these equations for the transformed stress components:

$$\begin{aligned}
\sigma_x &= (\sigma_H cos^2\varphi + \sigma_h sin^2\varphi)cos^2\gamma + \sigma_v sin^2\gamma \\
\sigma_y &= \sigma_H sin^2\varphi + \sigma_h cos^2\varphi \\
\sigma_{zz} &= (\sigma_H cos^2\varphi + \sigma_h sin^2\varphi)sin^2\gamma + \sigma_v cos^2\gamma \\
\tau_{xy} &= \frac{1}{2}(\sigma_h - \sigma_H)sin2\varphi cos\gamma \\
\tau_{xz} &= \frac{1}{2}(\sigma_H cos^2\varphi + \sigma_h sin^2\varphi - \sigma_v)sin2\gamma \\
\tau_{yz} &= \frac{1}{2}(\sigma_h - \sigma_H)sin2\varphi sin\gamma
\end{aligned} \qquad 4.24.$$

4.4. Rock strength properties

4.4.1. Cohesion, S_0

Cohesive strength is corresponding to the cohesive forces that are acting between atoms. This means that it is the ability of adhesive molecules to remain connected, and by this the ability of the material to resist tensile fracture without plastic deformation (Aadnoy and Looyeh,

2011). The Tresca criterion explains the cohesion which is also called the inherent shear strength as (Fjær et al., 2008):

$$S_0 = \tau_{max} = \frac{1}{2}(\sigma_1' - \sigma_3') \qquad 4.25.$$

where σ_1' is the maximum principle stress and σ_3' is the minimum principle stress. As seen in Figure 17 the Tresca criterion will appear as a straight line in a Mohr-Coulumb $\tau - \sigma'$ plot.

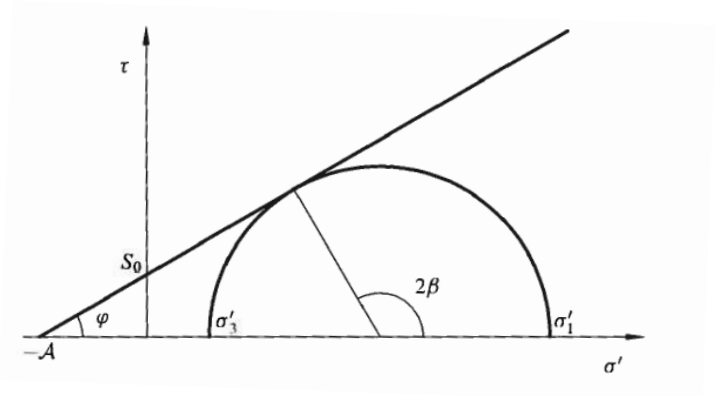

Figure 17: Mohr-Coulomb criterion showing the cohesion and the angle of internal friction (Fjær et al., 2008).

4.4.2. Internal friction angle

The angle of internal friction is defined as "a measure of the ability of a unit of rock or soil to withstand a shear stress. It is the angle (φ), measured between normal force (N) and resultant force (R), that is attained when failure just occurs in response to a shearing stress (τ). Its tangent (τ/N) is the coefficient of sliding friction. Its value is determined experimentally" (Allaby and Allaby, 1999a).

The angle that is shown in Figure 17 between the straight cohesion line and the mohr circle is called the angle of internal friction. This angle is defined as:

$$\tan\varphi = \mu \qquad 4.26.$$

where μ is the coefficient of internal friction defined as:

$$|\tau| = S_0 + \mu\sigma' \qquad 4.27.$$

There are many different empirical correlations that are used to calculate the internal friction angle. This is because when the friction angle is predicted from wireline data there is a great uncertainty due to lack of a significant database of reliable data. In this study the internal friction angle was calculated by three different methods, but just one of these were used to find the collapse curve in later chapter. The three different correlations are *(Chang and Zoback, 2003):*

$$\varphi = 18{,}532 V_P{}^{0{,}5148} \quad 4.28.$$

φ is in degrees and V_P is in km/sec (this is for all of the correlations).
Manohar Lal correlation (Lal et al., 1999):

$$\sin\varphi = \frac{V_P - 1}{V_P + 1} \quad 4.29.$$

Horsruds correlation (Horsrud et al., 2001):

$$\beta = 39{,}9° + 5{,}5 V_P$$
$$\varphi = 2(\beta - 45) \quad 4.30.$$

4.4.3. Unconfined compressive strength, UCS

The UCS is defined as "The strength of a rock or soil sample when crushed in one direction (uniaxial) without lateral restraint" (Allaby and Allaby, 1999b).

$$UCS = C_0 = 2S_0 \tan\beta \quad 4.31.$$

β is the orientation of the failure plane (Fjær et al., 2008).

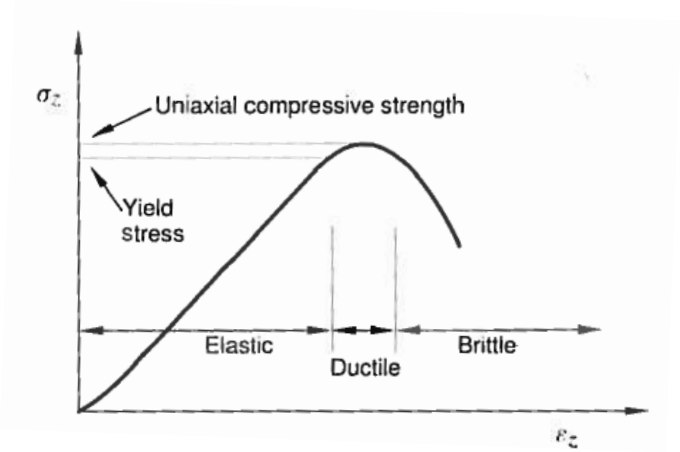

Figure 18: Principle sketch of stress vs. deformation in a uniaxial compression test (Fjær et al., 2008).

A key loading test that is performed on rocks is the uniaxial compression test. This test identifies the Unconfined Compressive Strength (UCS) of a rock. The test is performed by inserting a sample into a load frame and the axial load is increased with zero confining pressure. By monitoring the axial stress and the axial and radial deformation under drained conditions, one can measure the UCS, Young's modulus and the Poisson's ratio.

4.5. Failure modes

There are many reasons for a rock to fail, and it is important to know why the formation is failing, so precautions can be made to prevent it from happening. The wellbore logs are a good tool to use to see if the wellbore has experienced failure or not, and should therefore be

analysed. The image data from the wellbore should be analyzed to observe the stress-induced wellbore failure and determine the full stress tensor. This is extremely important because the stress tensor provide precise and reliable information about the failure mode (tensile, compressional or shear). Image logs can be used to identify both stress induced borehole breakouts and drilling-induced tensile wall fractures. These analyses can be used to reduce the drilling-induced fractures in the well. This chapter will go through some of the failure modes that can be experienced in a well.

4.5.1. Tensile failure

Tensile failure occurs when the tensile strength across a plain exceeds the critical limit of what the material/rock can handle. This limit is different from material to material and is called the tensile strength of the object. You can define the hydraulic fractures of rock material which is induced during drilling and operations as tensile strength. The tensile strength is given the symbol T_0, and has the same unit as stress. Since rocks have a lot of cracks, it has very low tensile strength, and it is a standard approximation for several applications to set the tensile strength of a rock to zero.

The equation below describe which stress conditions you need and which orientation the failure surface in principal stress space is located for tensile failure to occur (Fjær et al., 2008):

$$\sigma' = -T_0 \qquad 4.32.$$

4.5.2. Shear failure

Another word for shear strength is compressive strength, and it is measured for studying shear failure that is normally caused by high compressive loading (Aadnoy and Looyeh, 2011). The compressive loading will make the shear stress along the plane so high that the rock eventually will undergo shear failure. A fault is then created moving the two sides of the faultplane in each direction. The frictional force acting in the fault is acting against the relative movement of the two sides, and this frictional force is depending on the force that presses the bodies together. By reason it can be assumed that the critical shear stress (τ_{max}) which cause shear failure is depending on the normal stress (σ') acting on the fault plane. The equation is called the Mohr's hypothesis, and can be written as (Fjær et al., 2008):

$$|\tau_{max}| = f(\sigma') \qquad 4.33.$$

When the borehole collapse during drilling or in operations it is considered as shear failure. To analyse the collapse in a well, data is needed about the rock shear strength. This data can be obtained from a triaxial (shear) compression test (Aadnoy and Looyeh, 2011).

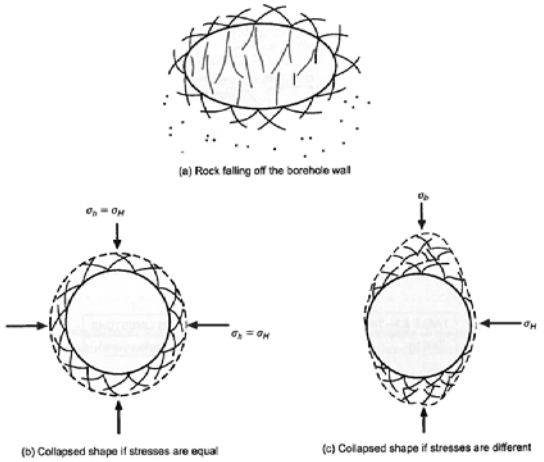

Figure 19: Collapse of borehole wall (Mitchell et al., 2011).

The stresses around the wellbore determine how the shape of the collapse will look like. If the stresses hare equal, the shape of the wellbore will remain circular in shape but will have a smaller diameter (as seen in Figure 19). When stresses are different, the shape will get more elongated after the collapse. In a vertical well the breakout of the wellbore wall will happen in the direction of the minimum in-situ stresses (Mitchell et al., 2011).

There are methods that can be used to calculate the "breakout width" (wBO), which is the angle that the borehole will break out, and predict at which proportion of the borehole circumference that will fail while drilling with a certain mud weight. It is assumed that the breakout or the angle of the breakout is symmetrical, and a breakout width of 180° describes a complete failure of the borehole wall (Zoback et al., 1985). This is shown in Figure 20 below:

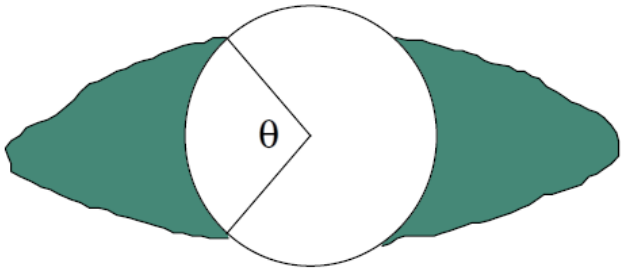

Figure 20: Schematic of a Borehole Breakout Defining the Breakout Width (wBO)

To calculate the predictions of the possible breakout, it is recommended to use a permissible breakout width equivalent to (Zoback et al., 1985):

$$90° - \frac{2}{3} \times well\ deviation \qquad 4.34.$$

where you use 90° in vertical wells and 30° in a horizontal well. In some extreme cases it can be advised to use 0° breakout width when you for instance are drilling a horizontal well that

are intersecting shale sections, you then will need good hole conditions when etc. the screens for the completion should be run.

This method is developed by Zoback et. al. (1985) and uses the Kirsch equation to calculate the breakout and the horizontal stresses. The problem with this is that the tangential stress equation from the Kirsch equation is only valid for a circular wellbore (Aadnoy et al., 2013). Lekhnitskii, Tsai and Cheron (1968) developed a method to find the tangential stress in a plate. Just recently Aadnøy et. al. (2013) presented a method that also could be used to calculate the breakout from elongated wellbore by modifying the work of Lekhnitskii, Tsai and Cheron (1968). The difference between the tangential stress in a plate and in a wellbore is that the formations are porous media that is always filled with fluid. When the pore pressure and the pressure in the wellbore is equal there will be no external loding in the formation. This means that the pressure difference between the wellbore pressure and the pore pressure will be equal to the external load that is exerted by the wellbore fluid. This resulted in an equation for the tangential stress in an elliptical borehole in compression, which is:

$$\sigma_A = (1 + 2c)\sigma_H - \sigma_h - \left(\frac{2}{c} - 1\right) P_w \qquad 4.35.$$

$$\sigma_B = \left(1 + \frac{2}{c}\right)\sigma_h - \sigma_H - (2c - 1)P_w \qquad 4.36.$$

where σ_H and σ_h represents the horizontal in-situ stresses in a vertical well (for an inclined well the bi-axial stress components are replaced by σ_x and σ_y), c = b/a and is the ratio between minor and major axes of the ellipse, P_w is the wellbore pressure, and σ_A and σ_B is the stress sin point A and B respectively.

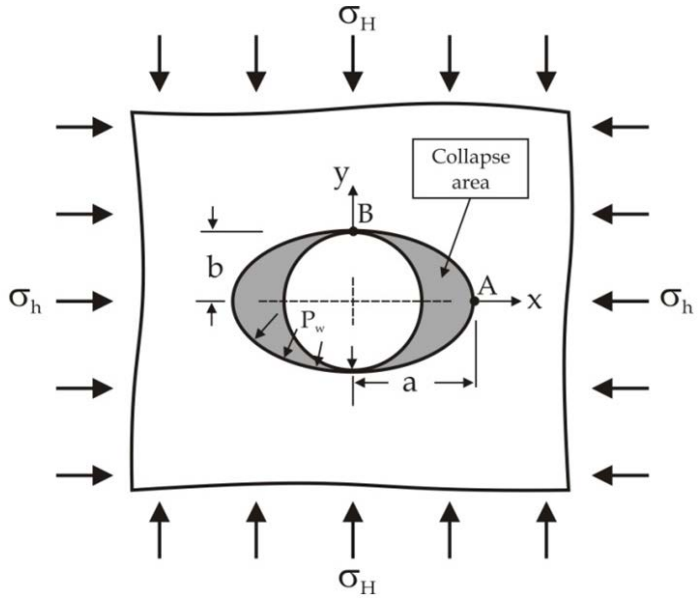

Figure 21: Initial circular hole and final elliptic hole (Aadnoy et al., 2013).

When the tangential stress in point A and B is equal, the borehole is considered sable and the tangential stress is uniform around the ellipse wellbore. By setting equation 4.32 equal to equation 4.36, this will give us:

$$c = \frac{b}{a} = \frac{\sigma_h + P_w}{\sigma_H + P_w} \qquad 4.37.$$

c is now defines the wllipse obtained when both the cohesion strength (τ_0) and the friction angle (φ) are equal to zero. This also shows that elliptical shape of the wellbore is not only dependent on the far field stresses but also on the wellbore pressure. This equation will only be valid for a wellbore with no strength, and is not the case for actual wellbores. Aadnøy et.al. (2013) then derived equations for different wellbore scenarios. For a well where $P_w \neq P_0$ you will get σ_H yilds:

$$\sigma_H = \frac{1}{1+2c}\left\{\sigma_h + 2\tau_0 \frac{\cos\varphi}{1-\sin\varphi} + (P_w - P_0)\frac{2\sin\varphi}{1-\sin\varphi} + \frac{2}{c}P_w\right\} \qquad 4.38.$$

and the wellbore collapse pressure yilds:

$$P_{wc} = \frac{c}{1-(1-c)\sin\varphi}\left\{\frac{1}{2}[(1+2c)\sigma_H - \sigma_h](1-\sin\varphi) - \tau_0\cos\varphi + P_0\sin\varphi\right\} \qquad 4.39.$$

These equations are valid for a well with two horizontal stresses and for all cases where the wellbore pressure and the pore pressure are different. To see the equation for the other scenarios and to see the derivation of the equations the reader should read the paper written by Aadnøy et. al. (2013) (IADC/SPE 163563).

4.5.3. Creep failure

Creep failure is when a material is deformed because it is under constant stress over time, and is dependant of the magnitude of the stress that is applied. There are three stages of creep failure, and the first stage is called transient creep. In this stage small fractures are formed, but if the stress that are forming the fractures are reduced to zero, the deformation will eventually also disappear over time. The next stage is called steady state creep. If the stress is reduced to zero after this stage is reached, the deformation will not vanish completely. This stage of derformation is constant over time. Afterwards the third stage is reached, which is called accelerating creep. Here the creep will accelerate over time and the deformation will quickly lead to failure of the material (Fjær et al., 2008).

4.5.4. Pore collapse or comprehensive failure

Pore collapse is a failure mode that is normally observed in materials with very high porosity. When the formation is compressed, some of the grains can lossen or break and then fall into the open pore spaces causing the material to be packed closer. This type of failure is called compaction. In sandstones the grain is of the same order or magnitude as the grain size, which mean that pore collapse typically consists in reorientation of the grains to better fill the void space. The pore collapse gets much more important in high porosity chalk where the grain size is smaller than the than the dimension of the pore spaces.

Pure hydrostatic loading may be the reason for the pore collapse, but if the rock is seen in a more microscopically manner it will show that the pore collapse is due to local excessive shear forces acting through grains and grain contacts. Pore collapse can in this matter be looked as shear failure within the material.

4.6. Well fracture model

3.1.1 Non-Penetrating-Fracture model

In a non-penetrating-fracture model it is assumed that the boundary condition of the wellbore is that there are no communication between the well and the formation pressure. The deformation that occurred is assumed to be linear elastic. By applying tensile fracture criteria to the equation for Kirsch hoop stress, one can obtain the fracture pressure as (Aadnoy and Chenevert, 1987):

$$P_{wf} = 3\sigma_h - \sigma_H - P_0 + \sigma_t \qquad 4.40.$$

Where σ_h and σ_H are the in-situ horizontal stresses, P_0 is the formation pore pressure and σ_t is the tensile strength of the rock.

A group of researchers argues in literature that the formation rock tensile strength is so low that it can be neglected for the analysis due to the natural fractures, cracks and flows.

3.1.2 Penetrating-Fracture model

The difference between a penetrating and a non-penetrating fracture model is that in a penetrating fracture model there is communication between the well and formation, which there is not in the non-penetrating. This meand that in the penetrating fracture model the formation is highly porous. This means that at the wellbore wall the well pressure is equal to the pore pressure.

The boundary conditions at the wellbore is such that the well and formation pressures are communicating. This means that physically, the formation is highly porous. Therefore, at the wellbore wall, the well pressure is equal to the pore pressure. With condition, from equation 4.40, the fracturing pressure is given as (Aadnoy and Ong, 2003):

$$P_{wf} = \frac{1}{2}(3\sigma_h - \sigma_H + \sigma_t) \qquad 4.41.$$

For isotropic stress field (i.e.$\sigma_h = \sigma_H$) and assuming a very low tensile strength, the fracture pressure that initiates the wellbore fracturing is given simply as:

$$P_{wf} = \sigma_h \qquad 4.42.$$

3.1.3 Complete History match fracture model

Based on volumetric strain, there could be derived a new fracture equation. The model takes into account the Poisson's ratio and temperature. The equation for the complete history match fracturing model for any well geometry is defined as (Aadnoy and Belayneh, 2008):

$$P_{wf} = \sigma_y + \frac{(1+v)(1-v^2)}{3v(1-2v)+(1+v)^2}\left(\sigma_x - \sigma_y - P_0\right) + P_0 + \frac{(1+v)^2}{3v(1-2v)+(1+v)^2} Ek(T - T_{init}) \quad 4.43.$$

where k is the coefficient of linear thermal expansion, E is the Young's modulus. Here σ_x is the least normal stress acting on the borehole. The transformed σ_x and σ_y and σ_z are given as equation 4.24.

Poisson's ratio (v) is an elastic constant that can improve lithology, porosity and pore fluid predictions. v is described as the ratio of fractional transverse contraction to the fractional longitudinal extension when a rod is stretched. v is generally low in stiff materials and higher in less rigid materials.

4.7. Well collapse models

When looking at the failure criteria on the material, knowledge is needed about if the material is brittle or ductile. This is because if the material is ductile, the stresses are compared to the yield strength since the permanent deformation would cause failure. If the material is brittle, there will be no yield poind and the stress is then compares to the ultimate strength of the material. This rule is applicable to almost all materials, but you will find exceptions (Aadnoy and Looyeh, 2011).

Different lithologies will also fail in different matters. Sandstone will fail in shear, while a claystone may fail due to plastic deformation. There are many different mechanisms that can cause failure in the wellbore or the area around, and will make the well instable. Some of the mechanisms are (Aadnoy and Looyeh, 2011):

- Tensile failure causing the formation to part
- Shear failure without appreciable plastic deformation
- Plastic deformation which may cause pore collapse
- Erosion or cohesive failure
- Creep failure which can cause a tight hole during drilling
- Pore collapse or comprehensive failure, which may happen during production

There are many failure criterions, but this thesis will present the five most important.

4.7.1. Von Mises failure criterion

The Von Mises failure criteria are the most reliable failure criteria for engineering materials. Von Mises uses the second deviatoric invariants and the effective average stress to do the analyses for the strength of the material. If you are assuming test conditions where $\sigma_1 > \sigma_2 = \sigma_3$, the equation for the deviatoric invariants will be:

$$\sqrt{J_2} = \frac{1}{\sqrt{3}}(\sigma_1 - \sigma_3) \qquad 4.44.$$

By using the same assumptions there can be made an expression for the effective average stress, which gives:

$$\sigma_m - P_0 = \frac{1}{3}(\sigma_1 + 2\sigma_3) - P_0 \qquad 4.45.$$

where P_0 is the formation pore pressure. In Figure 22 the second deviatoric invariant is plotted against the effective average stress for various axial loads σ_1 and confining pressures σ_3. This curve is known as the failure curve where you are safe when you are staying beneath the curve and that the material is unstable and will fail if you stay above the curve (Aadnoy and Looyeh, 2011).

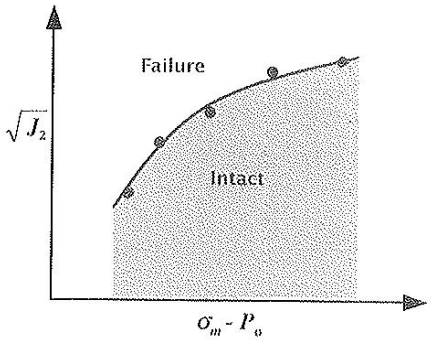

Figure 22: Von Mises failure model from triaxial test data (Aadnoy and Looyeh, 2011).

4.7.2. Mohr-Coulomb failure criterion

"This criterion relates the shearing resistance to the contact forces and friction, to the physical bonds that exist among the rock grains" (Aadnoy and Looyeh, 2011). The Mohr-Coulomb criterion is based on the assumption that $f(\sigma)$ is a linear function of σ. The equation for the linear approximation of the criterion is written as:

$$\tau = \tau_0 + \sigma \tan\phi \qquad 4.46.$$

where τ is the shear stress, τ_0 is the cohesive strength, ϕ is the angle of internal friction, and σ is the effective normal stress acting on the grain.

Since this criterion only is based on shear failure, you will get a deviation from the straight line when interpreting other failure mechanisms using Mohr-Coulomb. The criterion should therefore only be used in situations where it is valid. The failure envelope is determined by several Mohr's circles as you can see in the Figure 23 below, where each circle is one triaxial test (Aadnoy and Looyeh, 2011).

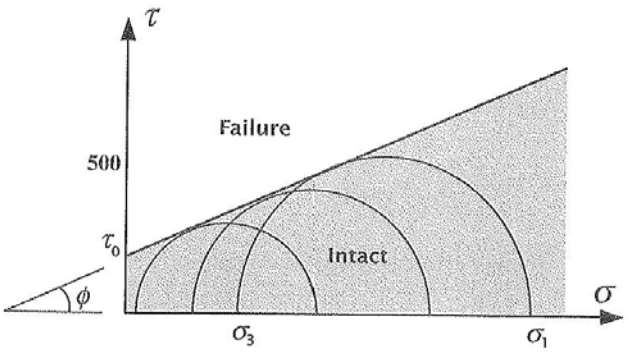

Figure 23: Mohr-Coulomb failure model from triaxial test data (Aadnoy and Looyeh, 2011).

4.7.3. Griffith failure criterion

While Mohr-Coulomb used Mohr's circles of shear stress to define their criterion, Griffith studied elliptical microcracks in a two dimensional model to develop his (Fjær et al., 2008). "The Griffith crack models can be used to derive different theoretical failure criteria for conditions of tensile and compressive stress" (Twiss and Moores, 2006).

If you put too much tensile stress on the tip of the small crack the crack will eventually start to grow and the failure process will start. There must be released a sufficient energy to provide the required surface energy that makes the crack grow. The strain energy that is released must be equal or greater than the necessary surface energy increase. If there is tensile failure where only the onset of cracking is considered the following equation applies (Aadnoy and Looyeh, 2011, Fjær et al., 2008):

$$\sigma_t = \sqrt{\frac{keE}{a}} \qquad 4.47.$$

where σ_t is the uniaxial tensile stress applied to the specimen at failure, k is a parameter that varied with the testing conditions, i.e. $k = 2/\pi$ for plane stress and $k = 2(1 - v^2)/\pi$ for plane strain, e is the unit crack surface energy, E is the Young's modulus, a is the one half of the initial crack length, and v is the Poisson's ratio.

From the Griffith criterion you can derive a relationship between the uniaxial tensile stress and the triaxial compressive stress, which gives:

$$(\sigma_1 - \sigma_3)^2 = -8\sigma_t(\sigma_1 + \sigma_3) \qquad 4.48.$$

$-\sigma_t$ is the same as T_0 in Figure 24.

In $\tau - \sigma'$ coordinates, Figure 24 b), the Griffith criterion is given by:

$$\tau^2 = 4T_0(\sigma' + T_0) \qquad 4.49.$$

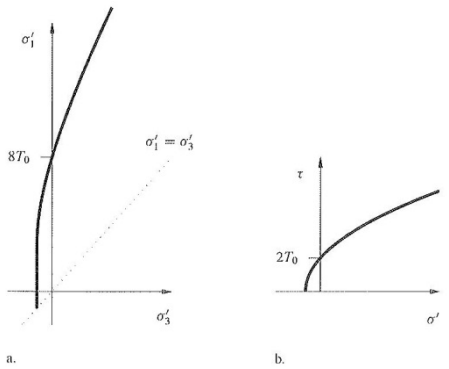

Figure 24: The Griffith criterion. a) Principle stress plot b) $\tau - \sigma'$-plot (Fjær et al., 2008).

4.7.4. Hoek-Brown failure criterion

When a rock is fractured the rock is much weaker than it was before the fracture occurred. This makes it important to look at the properties for both the fractured rock and for the intact rock. After the fracture has occurred the resistance in the rock against shear failure will be less (Fjær et al., 2008).

Numerical simulations methods are applied to the actual fracture system to understand and predict the behaviour of a fractured rock. Alternatively the rock can be assigned a much higher volume in the fractures (Fjær et al., 2008).

Hock and Brown manage to derive an empirical failure criterion which is normally used for naturally fractured reservoirs. The Hoek-Brown criterion can be written as:

$$\sigma_1 = \sigma_3 + \sqrt{I_f \sigma_c \sigma_3 + I_i \sigma_c^2} \qquad 4.50.$$

Where I_f is the frictional index, σ_c is the crack stress parameter, and I_i is the intact index. The indexes are properties that are dependent on the material. Because of this you can see that the criterions match brittle failure but gives bad results when dealing with ductile failure.

This is why the criterion is used on naturally fractured rocks. The value of I_f, I_i and σ_c are measured in the laboratory (Aadnoy and Looyeh, 2011).

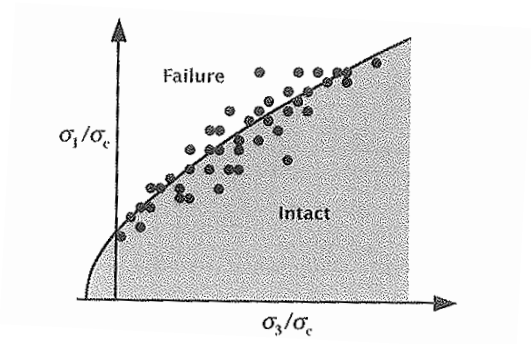

Figure 25: The Hoek-Brown empirical failure model using triaxial test data (Aadnoy and Looyeh, 2011).

4.7.5. Druker-Prager failure criterion

Druker and Prager derived an extended version of the Mohr-Coulomb failure criterion, where they assumed that the octahedral shearing stress reaches a critical value. The criterion is given by:

$$\alpha I_1 + \sqrt{J_2} - \beta = 0 \qquad 4.51.$$

α and β are material parameters and are related to the angle of internal friction ϕ and cohesion (cohesive strength) τ_0 for the linear condition. If you plot $\sqrt{J_2}$ and I_1 against each other at failure conditions, this will allow you to evaluate the given problem related to the rock formation failure. This criterion fits the high stress level (Aadnoy and Looyeh, 2011).

4.7.6. Mogi-Coulomb failure criterion

Al-Ajmi and Zimmerman was first out to introduce the Mogi-Coulomb failure criterion in 2006. They found some weaknesses in the criterions that already existed. When they were analysing their failure data they saw that the Drucker-Prager criterion overestimated rock strength, while the Mohr-Coulomb criterion underestimated it. They argued that the intermediat principle stress has an effect on the failure of the rock, and that the so called Mogi-Coulomb criterion would give the best fit. The criterion can be written much like the Mohr-Coulomb, as:

$$\tau_{oct} = k + m\sigma_{oct} \qquad 4.52.$$

where τ_{oct} and σ_{oct} are the octahedral shear and normal stresses, defined as:

$$\tau_{oct} = \frac{1}{3}\sqrt{(\sigma_1 - \sigma_2)^2 + (\sigma_1 - \sigma_3)^2 + (\sigma_2 - \sigma_3)^2} = \sqrt{\frac{2}{3}J_2} \qquad 4.53.$$

$$\sigma_{oct} = \frac{1}{3}(\sigma_1 + \sigma_2 + \sigma_3) \qquad 4.54.$$

and k and m are rock material constants that can be evaluated from the intercepted and the slope of the failure envelope that results from plotting τ_{oct} vs. σ_{oct}. This is shown in the Figure 26 below.

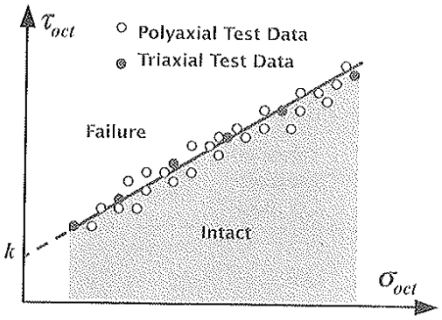

Figure 26: Mogi-Coulomb failure criterion for triaxial and polyaxial test data (Aadnoy and Looyeh, 2011).

It can be shown that the Mogi-Coulomb is reduced to Mohr-Coulomb for a triaxial stress state where $\sigma_1 = \sigma_2$ or $\sigma_2 = \sigma_3$. You can therefore be considering Mogi-Coulomb as an extension of Mohr-Coulomb in the cases where $\sigma_1 \neq \sigma_2 \neq \sigma_3$. This criterion is currently the most accurate failure model for hard sedimentary rock formations.

4.7.7. Ewy Modified Lade criterion

The Lade failure criterion is developed for cohesion material. The model reads:

$$\left(\frac{I_1^3}{I_3} - 27\right)\left(\frac{I_1}{P_a}\right)^m - \eta_1 = 0 \qquad 4.55.$$

I_1 and I_3 are the first and the second invariant stresses tensors, m and η_1 are material constants and P_a is the atmospheric pressure.

$$I_1 = \sigma_1 + \sigma_2 + \sigma_3$$

and 4.56.

$$I_3 = \sigma_1\sigma_2\sigma_3$$

Modified version

The modification is on the first and the second invariant stresses tensors. These are given as (Ewy et al., 1998):

$$I'_1 = (\sigma_1 + S - P_0) + (\sigma_2 + S - P_0) + (\sigma_3 + S - P_0)$$
$$I'_3 = (\sigma_1 + S - P_0)(\sigma_2 + S - P_0)(\sigma_3 + S - P_0)$$

The material constants *S* and η are related to the Coulomb strength parameters by:

$$S = \frac{c}{tan\phi}$$
$$\eta = 4tan^2\phi(9 - 7sin\phi)(1 - sin\phi)$$

Applying the modified Lade criterion, the critical mud pressure to avoid borehole instability is given by (Ewy et al., 1998) as:

$$P_w = \frac{B - \sqrt{C}}{2A} \qquad 4.57.$$

Where

$$A = \sigma_z + S - P_0$$

$$B = A\sigma_\theta - \tau_{\theta z}^2$$

$$C = B^2 - 4A\{D - (S - P_0)[A(\sigma_\theta + S - P_0) - \tau_{\theta z}^2]\}$$

$$D = \frac{(\sigma_\theta + \sigma_{zz} + 3S - 3P_0)^3}{(27 + \eta)}$$

$$\sigma_\theta = 3\sigma_x - \sigma_y$$
$$\sigma_{zz} = \sigma_z + 2v(\sigma_x - \sigma_y)$$
$$\tau_{\theta z} = -2\tau_{xz}$$

5. Formation pressure integrity testing (PIT)

The most common test done to test the formation pressure integrity is the FIT (Formation Integrity Test) and the LOT (Leak-Off Test). It is common practise when drilling a well to perform a PIT after each hole section has been drilled to test that the cement job is good enough for further drilling (Mitchell et al., 2011). A common problem with these tests is that it is difficult for the driller offshore to determine if the leak of pressure is reached or not. This is commonly done by using a ruler to look for deviations from the normal trend, and is really inaccurate. Therefore analysis need to be done of the test afterwards to verify which test has been done. In this chapter it will be explained the difference between these types of tests, but after reading through a lot of literature about these test it has been found that different authors have some variations on how to define the different tests.

5.1. Formation Integrity Test (FIT)

A FIT is often used instead of a LOT or a XLOT. A FIT is when you pump up the pressure in the well but stop before you reach the leak-off pressure. The trend of the test will therefore show a near linear trend when plotted as pressure against volume pumped. A disadvantage when using FIT is that it will not give any information about the principle stresses in the formation around the wellbore. The test will only verify that the casing shoe can withstand the pressure that is required to drill the next section according to the drilling program. One advantage of using the FIT is that it do not create a fracture in the formation, and the integrity of the well will therefore be intact. An induced fracture will cause loss of any tensile strength in the rocks where the fracture has started.

5.2. Leak-off test (LOT)

When more information about the strength of the formation is needed you perform a LOT. As for FIT a LOT is also used to check that the quality of the cement job that is done is good enough, and to check that the zonal isolation around the casing shoe has met its objective (Wang et al., 2011). To perform a LOT you first need to drill 4-6 m into new formation below the shoe (Mitchell et al., 2011). Afterwards you close the BOP (Blowout Preventer) and pump up the needed pressure in the well with a low pump rate. The leak-off pressure is identified when the pressure starts to deviate from the trend line, and there has occurred a fracture in the formation. Then the pump stops and you got a pressure the formation can withstand before leaking off to the formation. Usually the pumps are stopped before you reach the top of the curve, which is the formation-breakdown pressure. This is because it the test reaches this point, it will induce a large fracture in the formation. If you continue to pump past this point you will make a fracture that reaches far into the formation away from the wellbore. This can weaken the formation and cause problems while drilling the rest of the well (Wang et al., 2011).

There are numerous operational issues that have to be addressed to perform a successful LOT. Because of many factors revolving the LOT, it is difficult to interpret the tests. The LOT performed offshore has to be analysed afterwards to check if it actually is a LOT and not just a FIT. If you do manage to perform a well-designed and –executed LOT, this can be used to verify the fracture gradient predictions in the area. This gradient is important because if the mud weight is incorrect in comparison to this gradient, the wellbore can collapse (Wang et al., 2011).

Many have realized that the results of a simple LOT may be misleading when looking at the fracture gradient and other properties of the formations in the field. This is because when a LOT is performed, the fractures are made just near the wellbore and not deep into the formation. It is therefore not possible to predict the stresses that are actually represented out in the far-field. To get the right predictions for these stresses there should be done an extended leak-off (XLOT) (Wang et al., 2011).

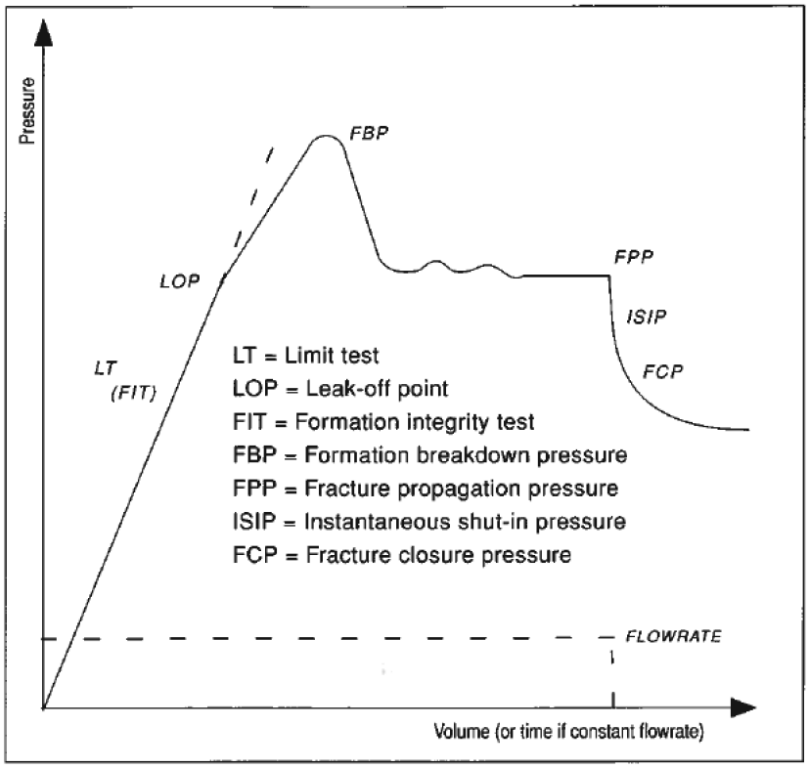

Figure 27: Extended leak-off test showing pressure as a function of volume (Heger and Spoerker, 2011)

5.3. Extended Leak-Off (ELOT/XLOT)

The difference between a XLOT and a LOT is that to pumping is continued after having reached the leak-off pressure. The pressure will then generally continue to increase, deviating from the near linear trend from the FIT, and will eventually reach a peak where the maximum pressure is reached which is known as the formation break down pressure (FBP) (see Figure 27) (Heger and Spoerker, 2011). The pumping should then be stopped when this peak is recognized to minimize the growth into the far-field stress regime. This peak is determined when pumping pressure decreases to a constant level which is called the Fracture Propagation Pressure (FPP). If it is seen that this pressure remains at a constant level the pumps should be shut down. The pressure that is read right after the pumps have been stopped, is called the initial shut in pressure (ISIP). The fracture that is induced during this test should have reached beyond the disturbed region around the wellbore, which allow the far field Fracture Closure Pressure (FCP) to be determined. The pressure that is read when the test have reached the FCP and the fracture closes, is assumed to be the best value for the least principle stresses (Heger and Spoerker, 2011).

Due to the massive volume of mud that is pumped to identify the stable FPP, the fracture induced may extend tens of feet away from the well as well as up and down the well. These fractures may reach faults and potential channels above the casing shoe which may result in the need for repair on casing shoe so it still meets the needed requirements.

To get good quality information about the minimum stresses in the field it should be conducted repeated XLOTS. If this is done it will usually remove all the influence from the near wellbore effects and represent the most accurate estimation of stresses from re-opening and shut-in pressure.

6. Overview of instability problems on the field

When analysing a field it is important to see how everything happening in the field is connected to each other. The more information obtained the better interpretations can be made from the models. The first thing that was needed to be done was to get an overview of the location of the wells relative to each other. Gocad was used because this is an easy tool to use when working with wells, logs and markers. This program had not been used on Ula ealier, therefore all the well paths and log files had to be exported from Openworks and imported to Gocad.

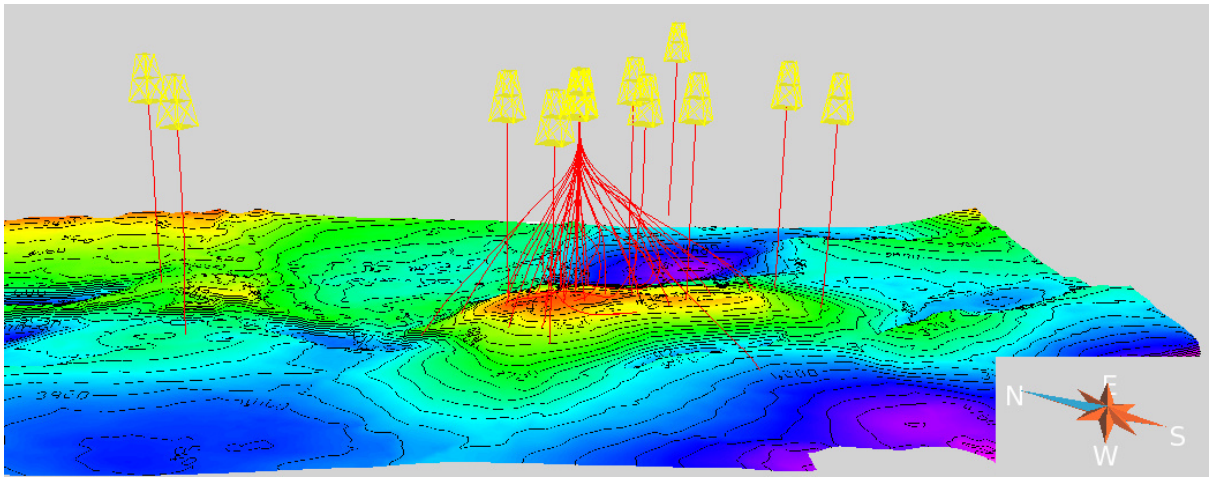

Figure 28: Overview of the wells on Ula from Gocad

The next step was to collect the data of which well that had experienced instability problems and on which depth it had happened. The data was found by reading through the “Final Well Reports” and the “Drilling and Completion Reports” for each well. Since Ula is an old field, most of these reports were hard copies that had to be found in BPs internal library. After collecting all this data into an excel file, this could be imported into Gocad as markers. Then the markers could be grouped into different types of instability problems, and some correlations of where the different problems occurred could be made.

6.1. Washouts

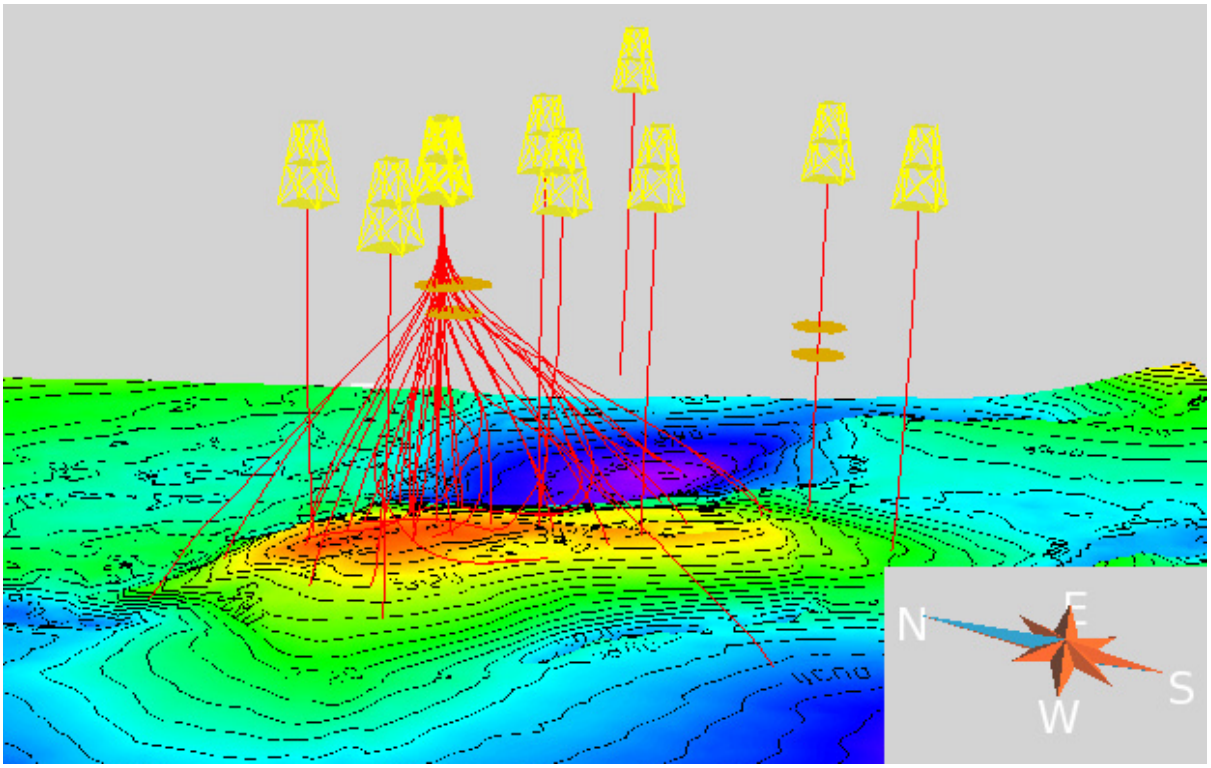

Figure 29: Occurred washouts on Ula

From this model it can be seen that the washouts have occurred in one of the upper sections in the wells. Washouts can occur when the bit is located at one depth at a long period of time. The drilling fluid that is flushing trough the nozzles are washing the wall of the wellbore and eventually carving into the formation.

6.2. Cavings

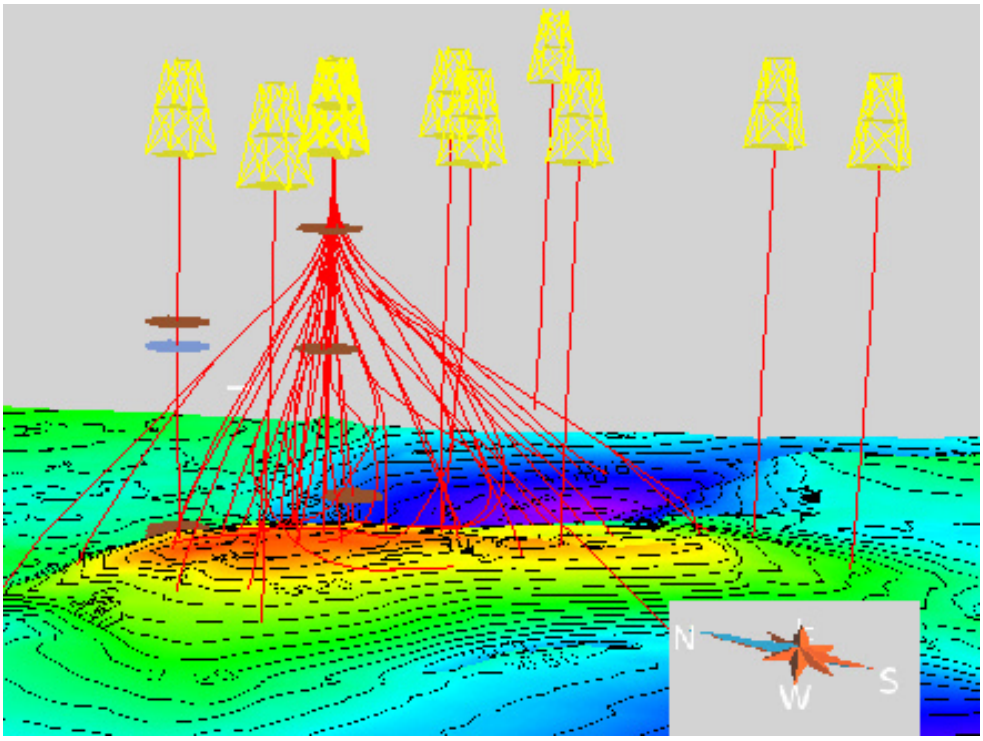

Figure 30: Cavings occurred on Ula

From this model it is difficult to see if there is a correlation between the locations of the different caving events. To find a correlation it would be useful to look at which formations the cavings has occurred and which lithology there is in this spot.

There are many different types of cavings, and the cavings can tell you much about what is happening in the well and why the problems are occurring. Some types of cavings you can experience are long and splintery, Tabular and angular cavings.

6.2.1. Splintery

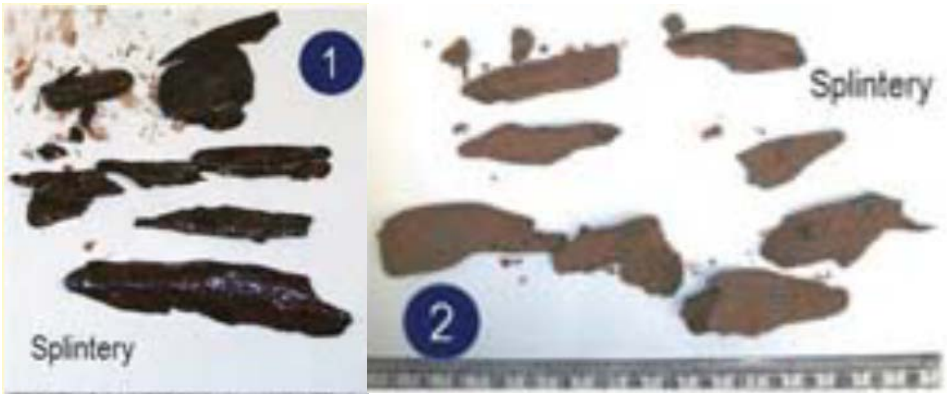

Figure 31: Splintery cavings (Kumar et al., 2012)

These types of cavings have a long and elongated shape, which may be splinters from a brittle rock or a hard formation. The cavings are formed due to tensile failure that are

occurring parallel to the wellbore wall and does commonly occur when drilling through an over-pressured zone (usually shale) with an underbalanced well. It can also happen when drilling to fast through a low permeability formation.

6.2.2. Tabular

Figure 32: Tabular cavings (Bradford et al., 2000)

Tabular cavings are a result of natural fractures or weak planes that have collapsed into the wellbore. If the tabular cavings are formed due to natural fractures, this means that the fluid pressure in the annulus has exceeded the minimum horizontal stress in the formation. This will result in mud intrusion into the fractures that are surrounding the wellbore, and can cause severe destabilization of the near-wellbore region. From this you can experience high rates of cavings, lost returns, stuck pipe and tools lost in hole. Since the blocks are surrounded by natural fractures the cavings will have flat, parallel faces (Bradford et al., 2000).

Another reason for getting tabular caving are due to weak planes. The caving that is formed due to weak planes occur because of a combination of low mud weight and a borehole axis that is within approximately 15° of the bedding direction. These factors will induce a massive failure along the planes of weakness, causing a lot of collapsing into the wellbore. Also these cavings are characterised by having flat, parallel faces (Bradford et al., 2000).

This type of cavings are characterised with a tabular shape that has a length that is greater than the thickness.

6.2.3. Angular

Figure 33: Angular cavings (Bradford et al., 2000)

Angular cavings are formed when the well is experiencing breakouts, which is explained in chapter 4.5. These cavings intersect at acute angels which are less than 90°, and are characterised by curved faces with a rough surface structure (Bradford et al., 2000). It has the shape of an arrow head or triangular, and there may be fresh fractures on the carving surface which has been formed when the breakout occurs.

6.3. Lost circulation/mud loss

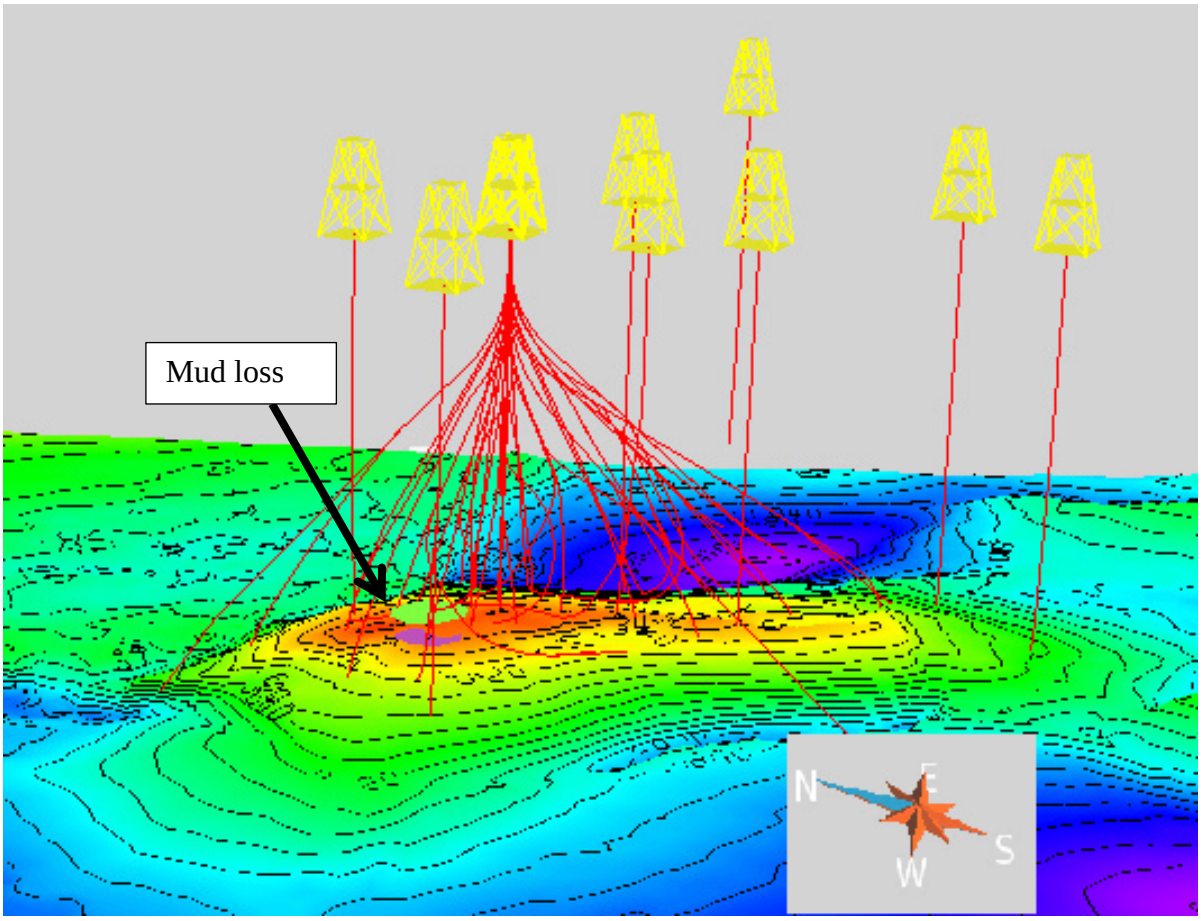

Figure 34: Green marker = mud loss, purple marker= lost circulation

There were not many episodes of mud losses and lost circulations on Ula, and as can be seen in this model, these events are located in the same area. There are many different reasons to why a well can experience lost circulation, and these are explained in chapter 7.

6.4. Stuck pipe

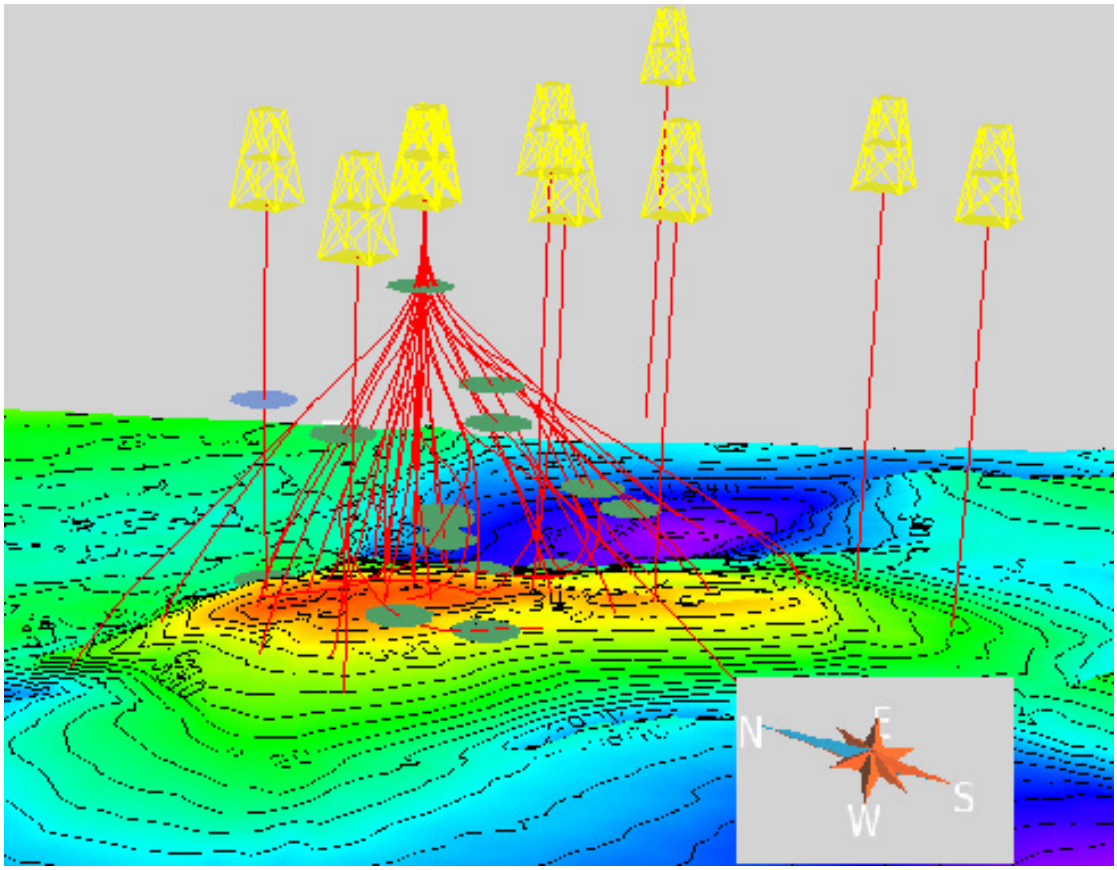

Figure 35: Stuck pipe

On Ula there have been many episodes of stuck pipe. All equipment that is put into the well can get stuck, and there are many reasons for this. The different reasons for a drilling equipment to get stuck are explained in chapter 7. Stuck pipe is often the reason for the need to drill an unplanned side-track after getting stuck and not getting loos again.

6.5. Tight spots

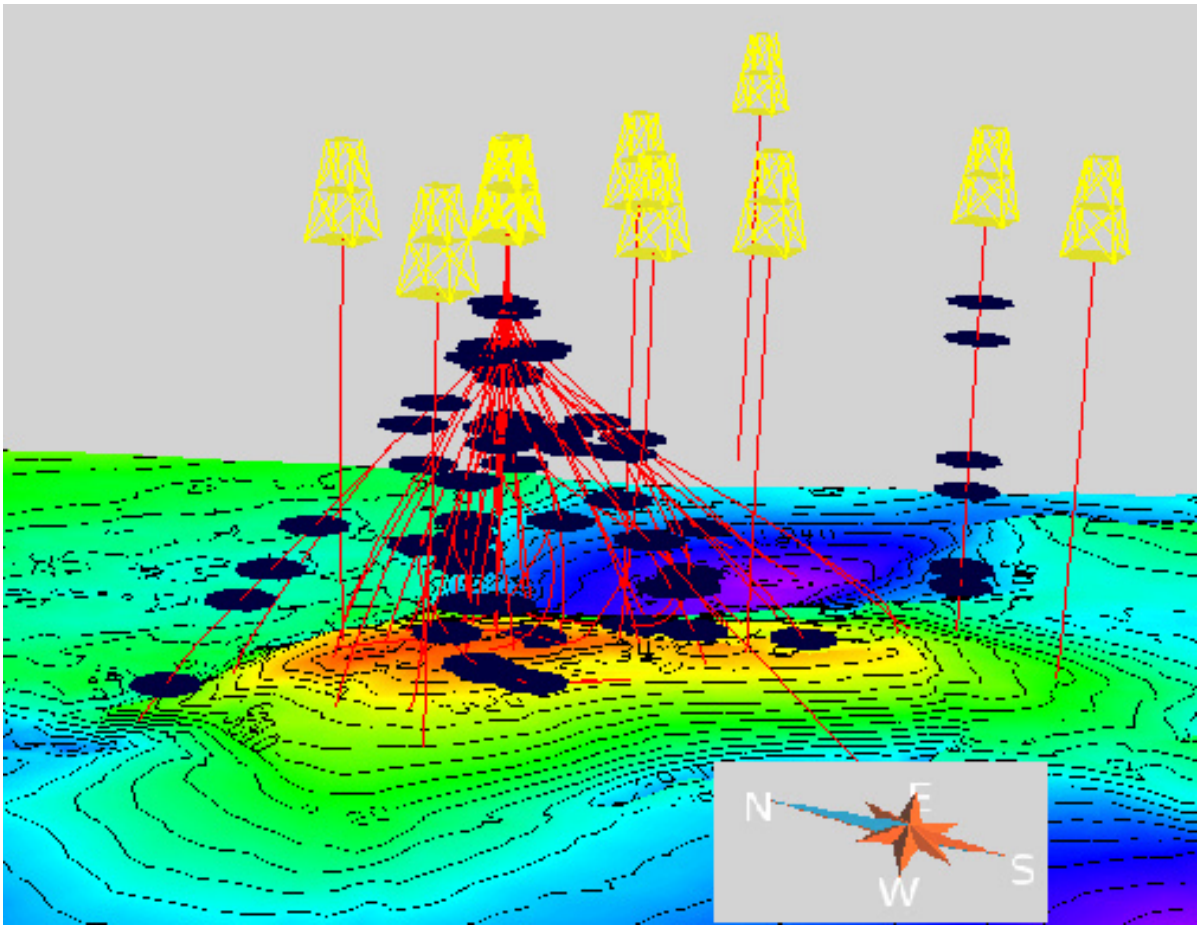

Figure 36: Tight spots at Ula

When drilling the Ula wells there have been experienced a lot of tight spots. In this model the marker marks the top of the section where there have been tight spots. In some cases it was large sections that had to be back reamed because of problems with tight spots. The definition “tight spots” can be a bit misleading because every time a driller experience that the drillsting experience some overpull, this is reported as a tight spot. Why the hole is tight you do not know before doing more analysis of what have happened. Tight spots can be caused by dogleg severity (high wellbore curvature, inward creep of the wellbore, etc. This is explained in more detail in chapter 7.

6.6. Gumbo

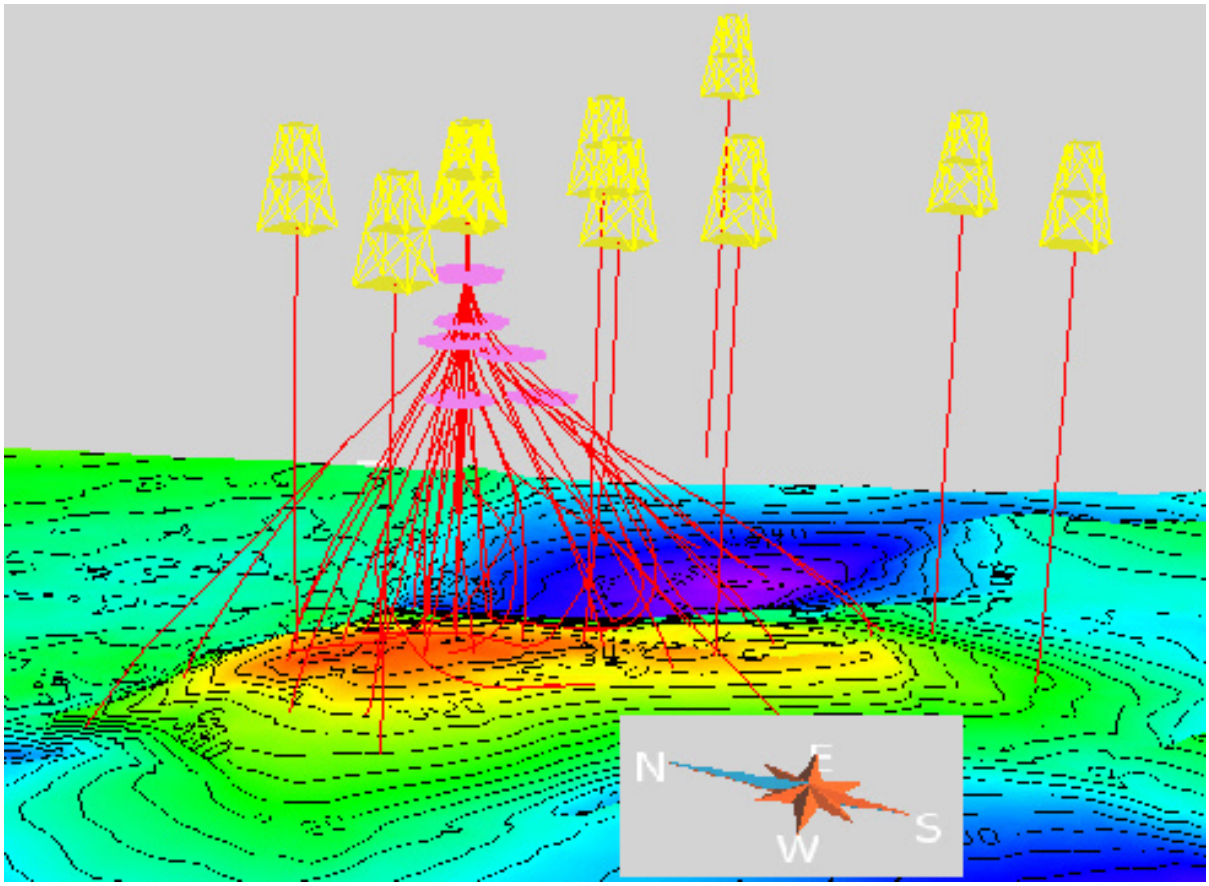

Figure 37: Gumbo events on Ula

Gumbo has occurred in the top of the wells on the main platform on Ula where the production wells and the injectors are drilled. Gumbo is when soil is chemically reacting to the water in the water based mud, making it swell and forming a soft and sticky mud. Gumbo shales typically comprise a high proportion of smectite-rich clays. Smectite-rich clays are usually found at depths shallower than 10000 ft (3048 m) below seabed (which you can see that match the result in the model), and where the temperature are less than 190°F (88°C).

7. Defining the right mud weight

When looking at instability problems in a well there is a large connection between the mud weight and the problems experienced in the well. If the mud weight is too low you can experience collapse and fill problems. A too high mud weight will on the other hand cause mud losses and stuck pipe (Aadnøy, 2010). When designing a mud program for a well the mud needs to have a density that makes the pressure in the well higher than the pore pressure gradient but lower than the fracture. This analysis is done by analysing the exploration wells and other wells in the area to find a correlation between the well to find out which properties the formation in the area where the well should be drilled.

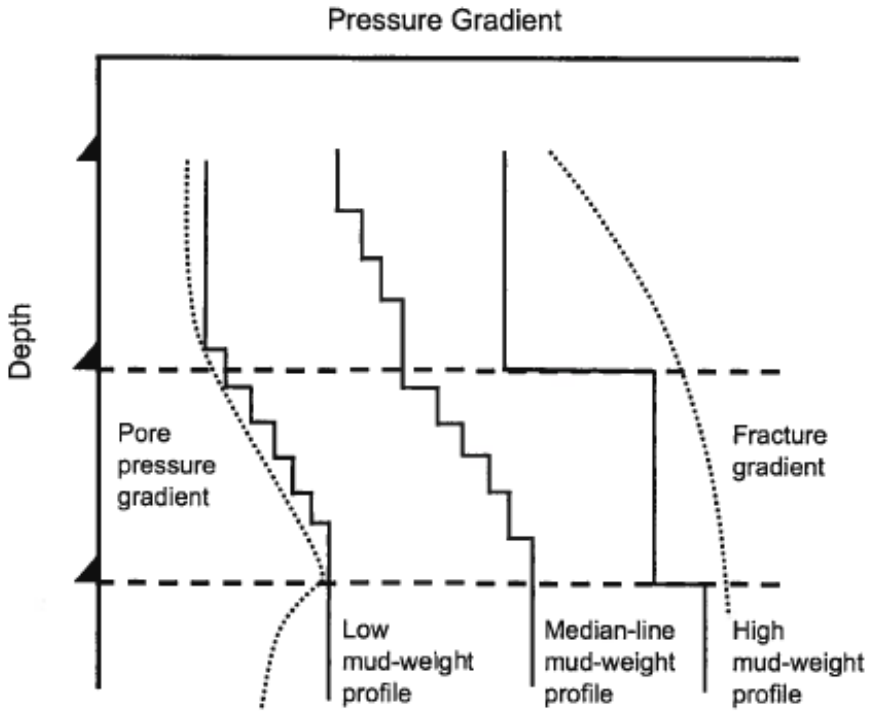

Figure 38: Example of a mud weight window (Mitchell et al., 2011)

During drilling all the equipment that goes into the well can get stuck, and there are many reasons for this happening. Some of the common reasons will be explained here, and is usually caused by using the wrong mud weight. One of the reasons for the drilling equipment to get stuck is that the borehole collapses. Borehole collapse is experienced when the mud weight is too low, which cause hoop stress around the borehole to be too high for the mud weight to hold the formation in place. Formation rocks will then collapse into the well and cause problems for further drilling. If the collapse of the well is too large, the drill sting may get stuck if the circulation in the well cannot transport the collapsed rock fragments. This filling may also accumulate in the lower part of the well, making it difficult to set the casing (Aadnøy, 2010, Mitchell et al., 2011).

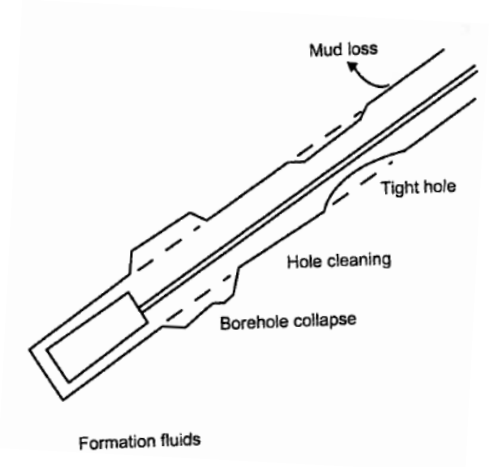

Figure 39: Typical borehole problems (Mitchell et al., 2011)

A high mud weight will balance the rock stresses around the borehole and keep the well more in-gauge, but you may experience tight hole anyway. The borehole can swell the first days after the well has been drilled, and decrease the diameter of the well. Tight hole can also be caused by borehole collapse that is packing up around the bottom-hole assembly (BHA) combined with doglegs (Aadnøy, 2010). When the driller experience high drag and torque, it is usually reported as a tight spot until other evaluations of the reason has been examined. To reduce the effect of the swelling of the formation it is often run wiper trips and/or back-reaming to maintain good borehole conditions.

Another reason to getting stuck is differentially sticking. Differentially sticking is caused by a large pressure difference between the borehole and the formation, and usually occurs across permeable zones such as sand. It is seen that the higher the permeability of the formation is, the higher the probability for going differentially stuck is. When the drilling fluid is moving across the permeable zones it tends to make a filter cake that can become very thick. Because of deviation in the wells the drillstring may lay against the mud cake, and since the mud cake has a high friction coefficient, the force that is required to pull the drillstring tangentially across this is very high. It is often the case that the rig is not powerful enough to pull the string, and that the string is not strong enough to handle the load. Differentially sticking is therefore the cause of many of the fishing operations offshore (Mitchell et al., 2011). For a collapse point of view you want a high mud weight, but this may increase the possibility of differential sticking. So this may cause a problem when designing the mud program. There should therefore be chosen a mud weight high enough to prevent collapse, but that is below the critical level for differential sticking (Aadnøy, 2010).

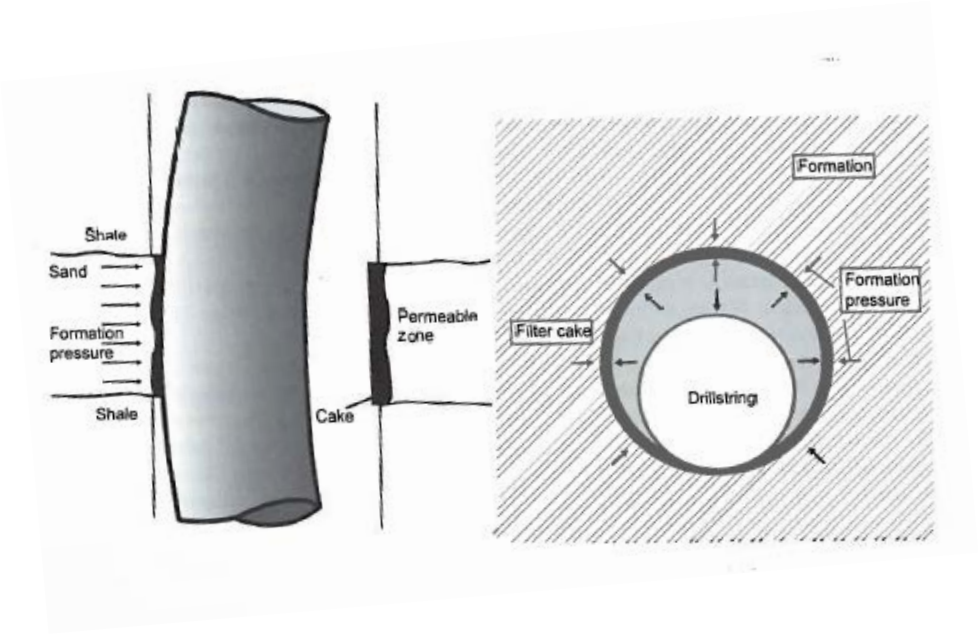

Figure 40: Differentially sticking (Mitchell et al., 2011).

During drilling you can also experience lost circulation, which occur when fluid penetrate into weak formations or fault etc. The most severe lost-circulation problems occur in cavernous or extremely vugular formations. These are typically limestone that has been leached by water. Figure 41 show some types of lost circulation you can experience.

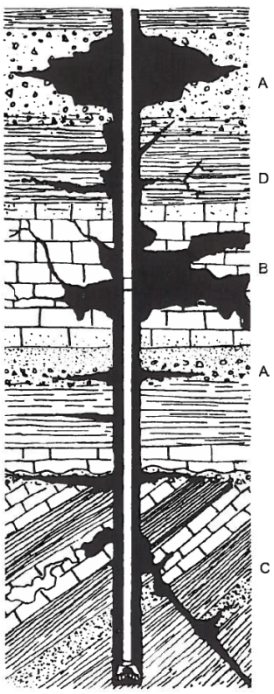

Figure 41: Types of lost circulation. A=Permeable zone, B=Caverns, C=Natural fractures and D=Induced fractures (Mitchell et al., 2011)

7.1. Experience from previously drilled Ula wells

To make a good pick of which wells that were going to be used to make a mud weight model for the Ula field, a lot of data gathering had to be done in advance. Logs, mudweights, instability problems, etc. had to be collected and imported into programs such as Techlog and Gocad. From this it was possible to choose wells that would be good for making these models. The wells that had experienced cavings and mud losses were therefore used, since these instability problems would give a good indication if the mud weight was the right one to use or not. A table with all the instability problems experienced can be found in Appendix A.

To run the data through GMI WellCheck there had to be made some templates with input data. A general rock data file had to be made from a sonic log in a vertical well. It was good to use one of the wells that had experienced instability problems and that also had a good sonic log for the whole well section. Well 7/12-6 is a vertical exploration well that had experienced lot of instability problems and had also a good sonic log. This well was picked as one of the wells that had experienced both mud loss and cavings and was therefore a good well to use to find the UCS and the Friction Angel for the field. By using this sonic log it was possible to calculate the UCS and the Friction angle which was needed to make a rock file that could be put into GMI WellCheck. An internal BP method was used to calculate the UCS, but in Chapter 4.4.3 there is explained one method to calculate the UCS. The Friction Angel was calculated by using the Chang and Zoback method which is explained in chapter 4.4.2. From this there could be made a rock file for the 7/12-6 well where the depth, Overburden, Minimum Horizontal stress, Pore Pressure, UCS, the Internal Friction Coefficient, Poisson's Ratio and Biot's Coefficient was put in. Then a well file was made for the five wells where the well trajectory had to be collected for each well.

When the rock file was run together with each of the well files in GMI WellCheck the result of the analysis was a collapse curve for each well. This could then be compared to the actual mud weight that was used for that well which is shown in chapter 7.1.1-7.1.5.

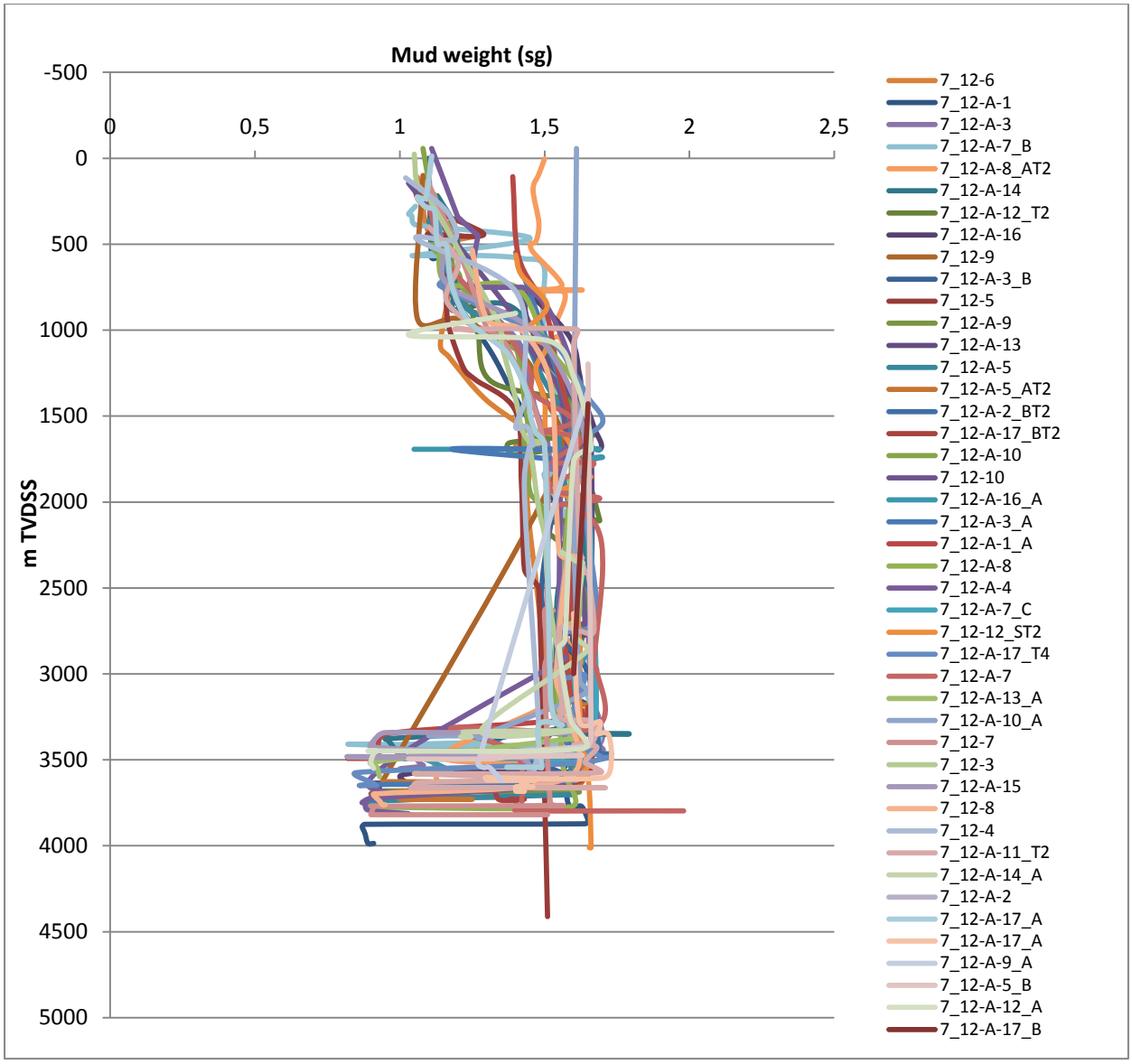

Figure 42: Mud weight vs. mTVDSS collected from the Ula field

7.1.1. Well 7/12-6

This well is a vertical exploration well, and this makes the TVD and the MD almost the same, with just a decimal in difference.

Figure 44 shows the mud weight used during drilling of the well and the calculated collapse curve for well 7/12-6. It also shows the general pore pressure curves and overburden for the Ula field together with the leak-off test done on Ula. The instability problems for this well are also plotted into the figure. From this it is possible to see if there is a connection between the mud weight that is used and the instability problems that occurred.

From the final well report it was found that there was mudstone cavings in the section 1480 mMD to 1520 mMD, which is in the 17 ½" hole section. The figure shows that the mud

weight that was used in this section is below the collapse curve and the expected pore pressure for this section. This confirms their assumption that the well was in underbalance when this occurred. This will also apply for the section from 1700 mMD where they had problems getting stuck and experienced large quantities of cavings. At 1818 mMD the rock bit was hung up and 60 bbls of mud were lost to the formation while the bit was packed off. The problems in the well occurred both when drilling and when pulling out from this section.

These problems are also seen when looking at the caliper log for the well, as plotted in Figure 45. Here it shows really well that the hole was much larger than the bit size in the 12 ¼ section and that large quantities of cavings had occurred.

They also had some problems with stuck pipe in the 8 ½" hole section when drilling and installing the 7" liner. After they had run a survey at 3700m a stabilizer became key-seated. This means that they probably did not get stuck because of the mud weight, but because of high dog leg in the well. Keyseat can also happen when soft formations between hard formations enlarge over time. Parts of the drillpipe as the stabilizers, drill collars or the bit can then get stuck in these channels made from washouts in the soft formation as Figure 43 shows.

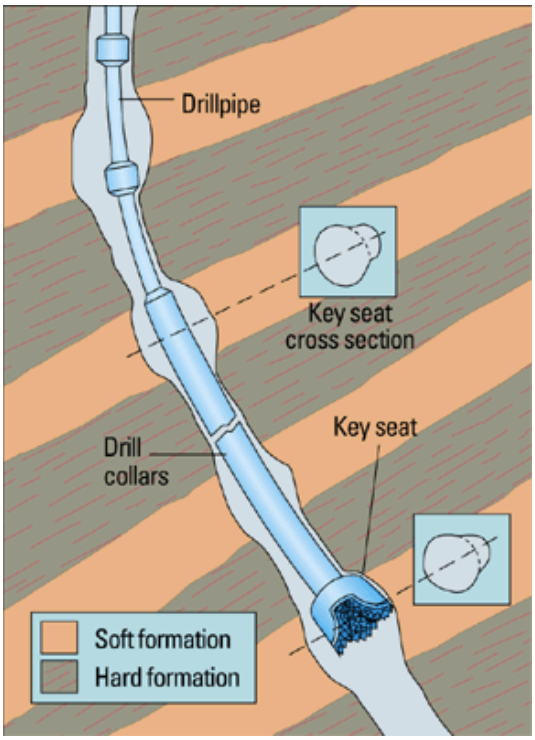

Figure 43: Key seats, often associated with hole deviation and variation in formation hardness (Schlumberger)

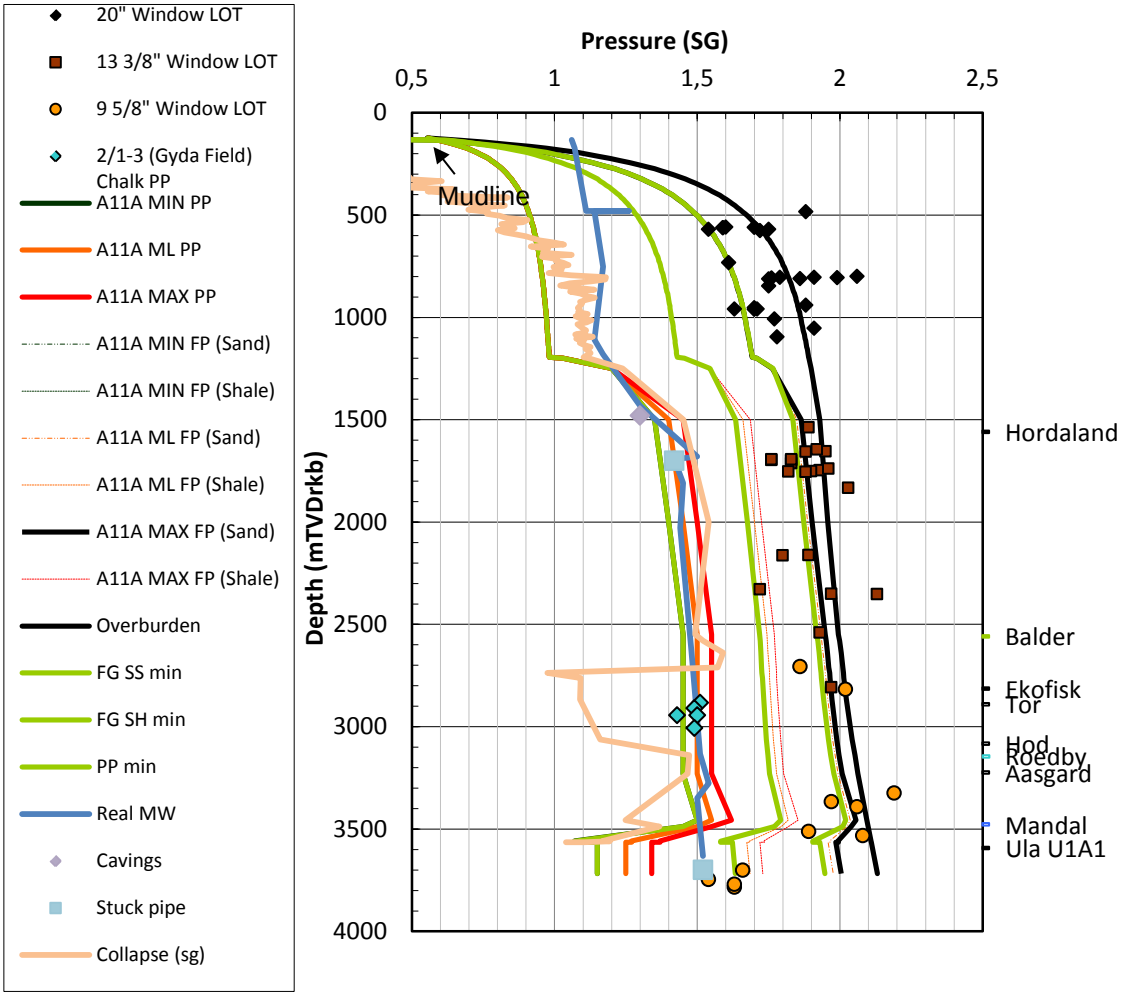

Figure 44: PPFG plot well 7/12-6.

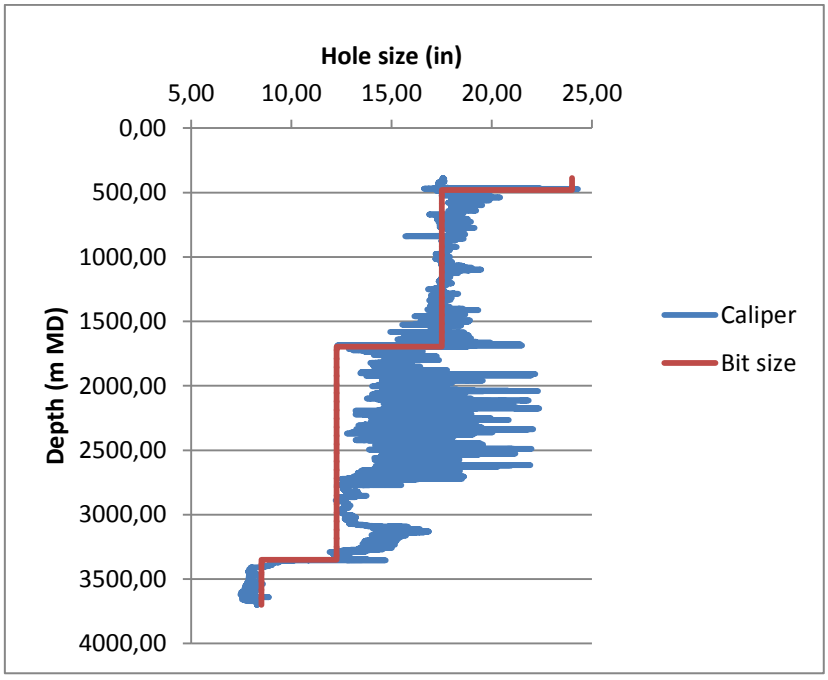

Figure 45: Caliper log showing problems in well 7/12-6.

7.1.2. Well 7/12-A-1

While drilling the 17 ½" hole section there were experienced tight hole at 2106 mMD (2035.97 mTVD) during a wiper trip. When pulling the drilling sting it was noticed that the BHA was balled up with dry, compact clay when it reached the surface. Also after they had drilled to TD at 2253 mMD (2167.28 mTVD) of this section they experienced tight spots during wiper trip. There are no indication why these tight spots occurred from Figure 47 so this may indicate that the tight spots was due to poor well cleaning.

While running the 13 3/8" casing they met some obstacles. The casing was run, circulated and worked down to 2248 mMD (2162.83 mTVD). Resistance was met at 1379, 1830 and 2230 mMD (1372.13, 1788.08 and 2146.91 mTVD) before the hole packed off and the string got stuck at 2233 mMD (2149.56 mTVD). In this section the actual mud weight was quite close to the collapse curve which could have caused the problems.

The string got stuck during connection at 3207 mMD (3029.53 mTVD) when drilling the 12 ¼" hole section. The string eventually came free after been differentially stuck in the limestone. Differentially sticking can occur in the limestone when high mud weight are used to help control of fluid loss and good drilling practice can overcome this problem. Further differentially sticking was avoided after this incident. Sticky hole and high drag developed while drilling from 3540 – 3561 mMD (3326.83-3345.49). Cavings were observed over the shakers when drilling from 3561 – 3567 mMD (3345.49-3350.83 mTVD), but was remedied by a slight increase of the mud weight. After reaching TD and logging of this section they experienced several stuck pipe incidences while running back into the hole.

The mud was displaced to 0.88 SG oil based mud when they were drilling the 8 ½" section. After reaching TD the logging tool got stuck during logging of the section.

In this well the caliper log shows little information about what has happened during drilling. This is because they have just logged the 8 ½" section, and the problems occurred higher up in the well.

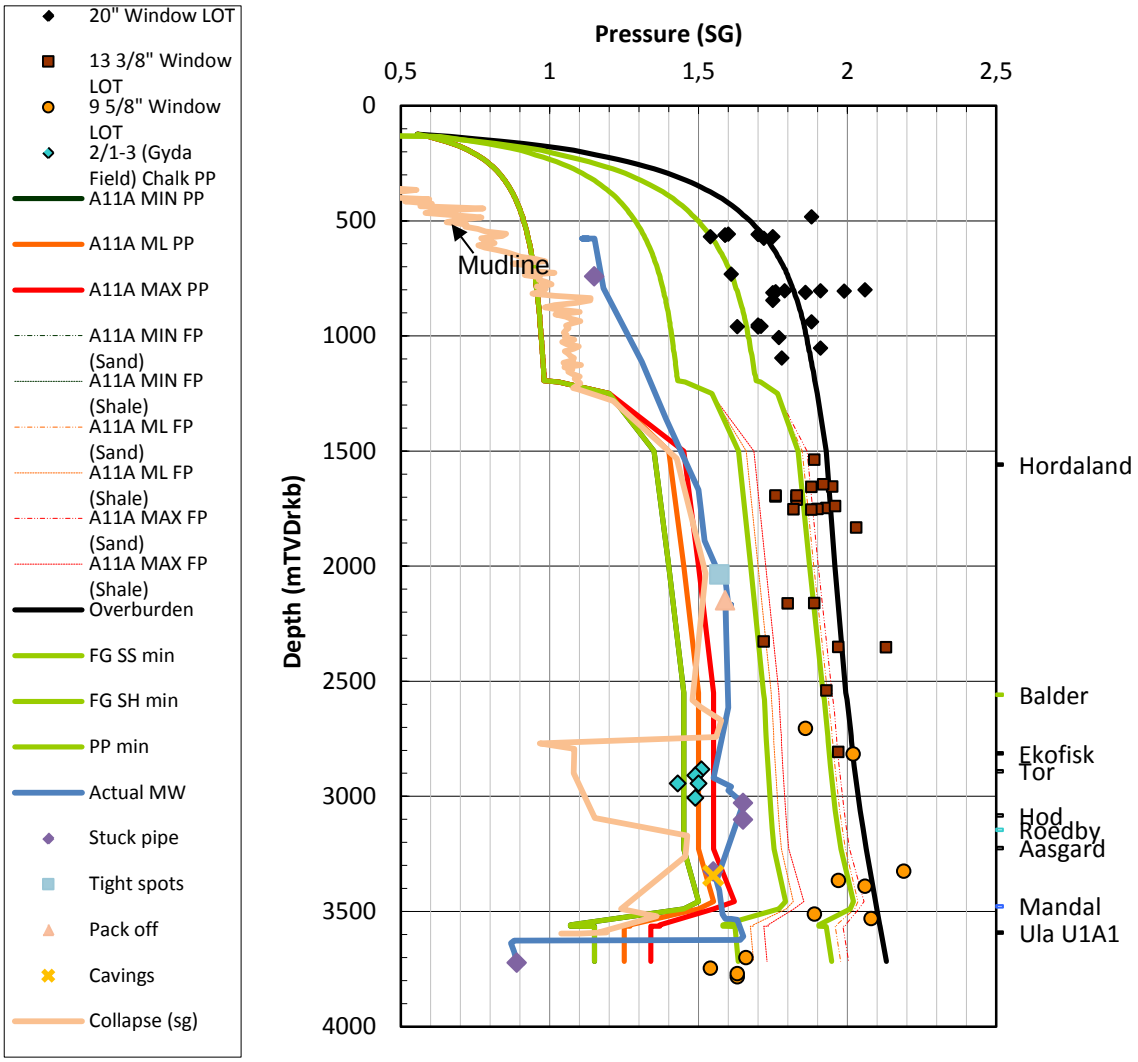

Figure 46: PPFG plot well 7/12-A-1.

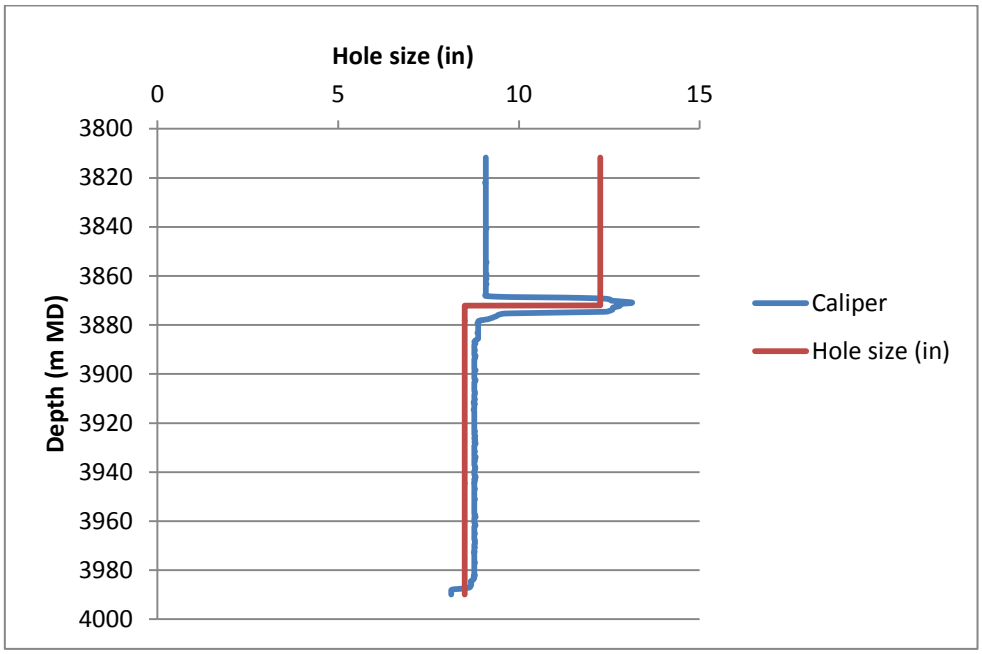

Figure 47: Caliper log vs. Bit size well 7/12-A-1.

7.1.3. Well 7/12-A-3

From Figure 48 it can be seen that there was experienced some tight spots at 970 m MD (952 mTVD) in the 17 ½" hole section. The figure shows that the calculated collapse curve, which should be the minimum MW allowed, is lower than the MW used in the well. The drilling report shows that the wellbore conditions were good but that they experienced an overpull of 80 klbs because of tight hole. They therefore increased the MW. There can be many reasons for tight spots to occur. In this point it looks like it may occur as a result of poor hole circulation and not because of wrong mud weight compared to the collapse curve.

At 2185 mMD (2026 mTVD), which is in the 12 ¼" hole section, there were encountered tight spots. By studying Figure 48 it is seen that this tight hole section is at the same place as where the actual mud weight used is almost the same as the collapse curve. This indicates that the MW was to low and that this could have cause the formation to cave into the wellbore and cause tight hole in this section. The mud weight was then increased from 1.64-1.67 sg to stabilize the upper section of the hole. It was recommended if possible for future wells to lower the 13 3/8" casing to seal off the troublesome section.

When drilling the 8 ½" hole section there were used a 1,04-1,07 SG KLC/Cal.Carb. mud due to the reservoir pressure depletion. At 3864 mMD (3545 mTVD) there were experienced considerable amounts of cavings which caused a few thight hole problems in the Ula sand section. When compared to the caliper log it looks like the caving has occurred as a washout beneath the casing shoe and it may be a reasonable assumption that it has occurred in the unstable shale that lies above the Ula sand. If they had thought that they had reached the Ula sand they had decreased the mud weight which would be much too low for the shale section and causing the cavings.

During logging the logging tool got differentially stuck at 3989 mMD (3578 mTVD). Because of the cavings that they had experienced beneath the casing shoe they may not have had as low mud weight as they should when drilling the Ula sand. This could be the reason for the logging tool getting differentially stuck.

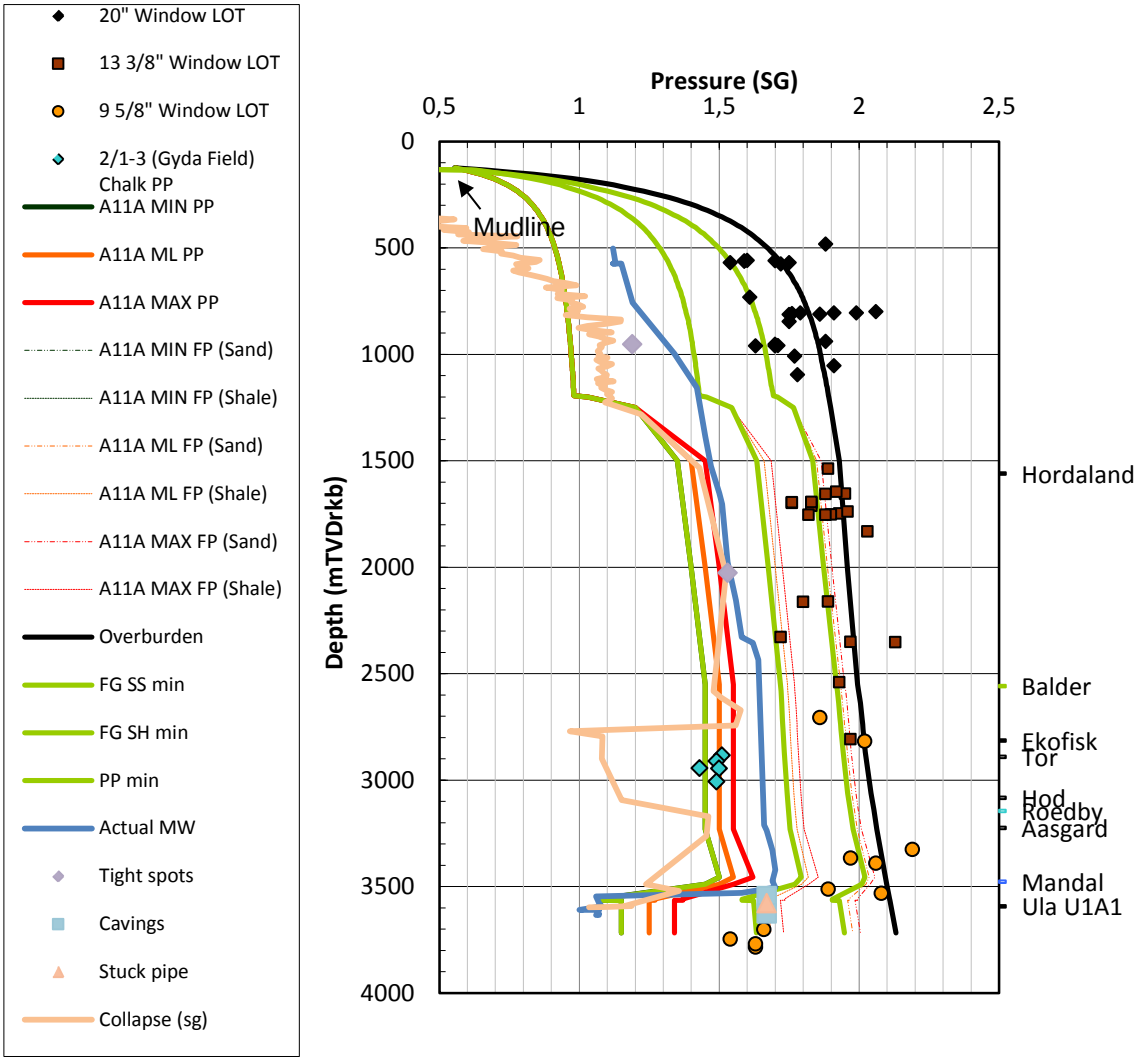

Figure 48: PPFG plot well 7/12-A-3.

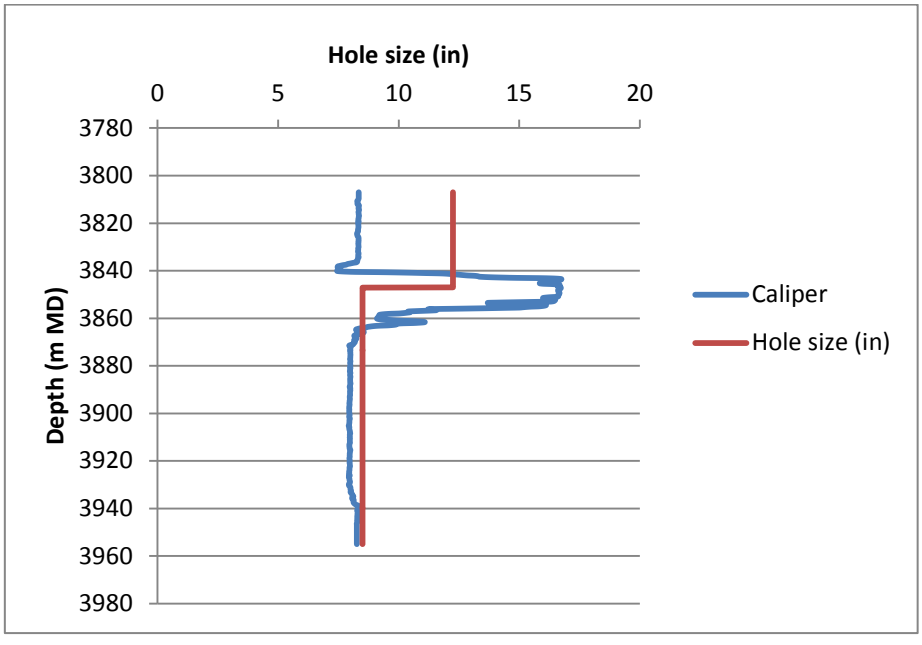

Figure 49: Caliper log vs. Bit size well 7/12-A-3.

7.1.4. Well 7/12-A-7B

In the 16” hole section there were experienced large amount of cavings over the shakers at 681 mMD (680 mTVD). The cavings was long, thin and splintery. Splintery cavings were also experienced at 719-748mMD (717.46-746.40 mTVD). Splintery cavings occur when the tensile strength of the formation is broken parallel to the wellbore wall. This usually happens when drilling through an over-pressured zone (usually shale) with an underbalanced well. This can indicate that the cavings occurred at the point where the mud weight was close to 1.0 SG and that it was registered later due to the time it takes to circulate the cavings up to surface.

This well did not experience many instability problems, and after these cavings they only experienced some tight spots at the end of the well. This indicates that the mud weight they used was correct for this well.

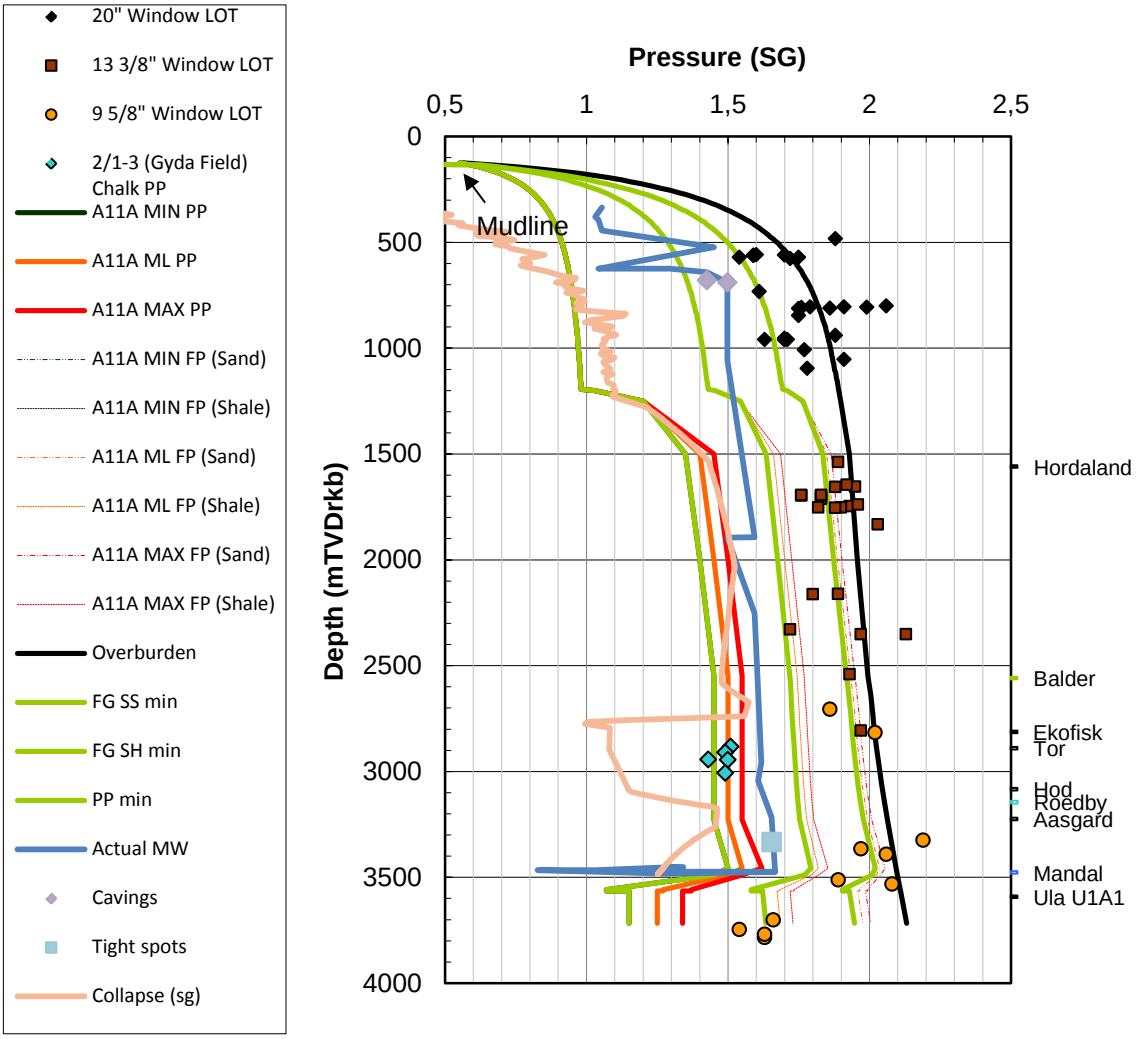

Figure 50: PPFG plot well 7/12-A-7B.

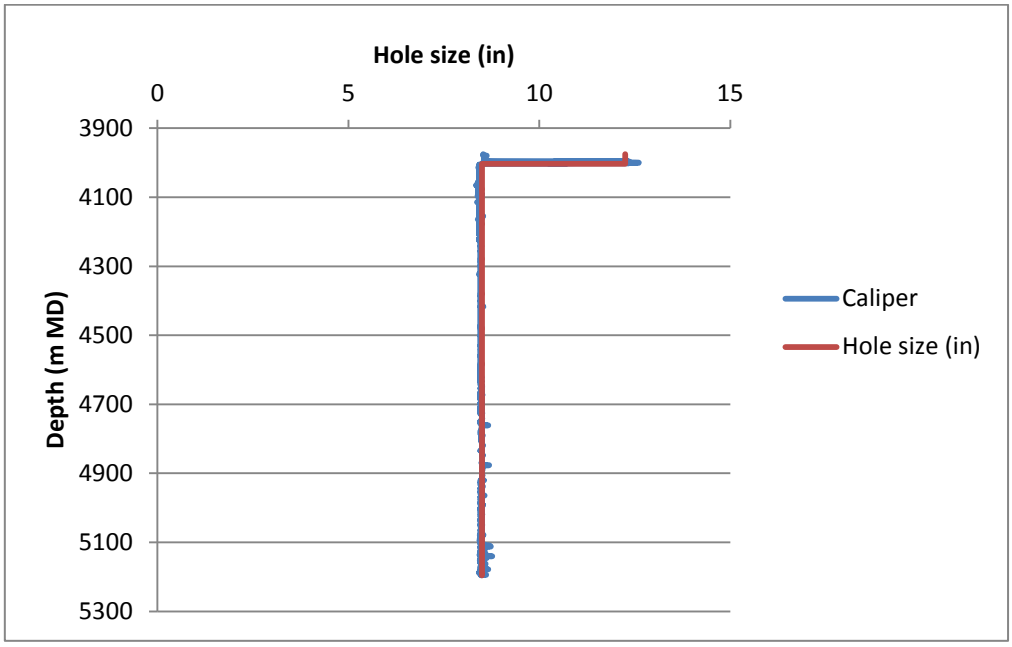

Figure 51: Caliper log vs. Bit size well 7/12-A-7B.

7.1.5. Well 7/12-A-8A T2

When drilling out the 13 3/8" casing window there were experienced lost circulation. The mud that was used was a 1.63 SG Petrofree mud. At 831 mMD (824.61 mTVD) the pipe got stuck and the hole packed-off. Figure 52 shows that the mud weight that was used in this section is too high and this could be the reason for the drillpipe getting stuck. Usually when the mud weight is so high and close to the fracture gradient, it is likely that the drillpipe has gone differentially stuck over a permeable zone. It is also possible that the drilling fluid has penetrated into the formation and can release faults that already exist. This can make the block drift into the wellbore and cut the wellbore. The result of this is that the drillpipe gets stuck between the fault block and the wellbore. It was observed that there were mud losses drilling from 831 – 836 mMD (824.61-829.39 mTVD) and that the losses continued while circulating the wellbore clean. It was noted that they had experienced mud losses also prior to the pack-off. These problems can indicate that a weak zone was taking fluid even before the pack-off.

Also during the running of the 9 5/8" casing they experienced that the mud return was lost, and several attempts to establish circulation with no luck. The high viscosity and gel strength of the cold Petrofree mud could have resulted in excessive surge pressure causing the formation to break down. The casing was pulled so that they could wash and ream the wellbore. Washed and reamed from 2475 mMD (2097.80 mTVD) to 2680 mMD (2234.57 mTVD), where they had indication of cuttings beds and hole packing off but full returns. Washed and reamed from 2888 mMD (2375.11 mTVD) to 3060 mMD (2498.72 mTVD) and they lost returns when the hole packed off.

Because of the problems experienced they decided to remove the 13 3/8" casing and run a new 13 3/8" casing with a deeper setting depth and the mud was displaced to a 1.55 SG Petrofree mud. The MW was then increased again from 1.55-1.63 SG during drilling of the 12 ¼" hole section. Because of the lower 13 3/8" casing isolated the weak zone this resulted in no instability problems during drilling of the new 12 ¼" section.

In the 8 ½" hole section there was experienced some tight hole problems from 3323 mMD (2707.10 mTVD), and they had to ream and backream several times. While cleaning the wellbore, heavy cuttings returns were observed. After circulating the hole clean, the mud weight was increased from 1.58 to 1.62 SG. As seen in Figure 52 the tight spot occurred at a place where the actual mud weight was the same as the collapse curve for this section. This could then cause the wellbore to cave in and pack around the wellbore making the hole feel tight. After this tight hole problems occurred they increased the mud weight which gave them good wellbore conditions for further drilling.

At the reservoir section the logging tool got stuck at 4412 mMD (3652.14 mTVD). It may look like that the logging tool got stuck because of the cavings that occurred higher up in the well which is seen on the caliper log at approximately 4310 mMD (3555.30 mTVD).

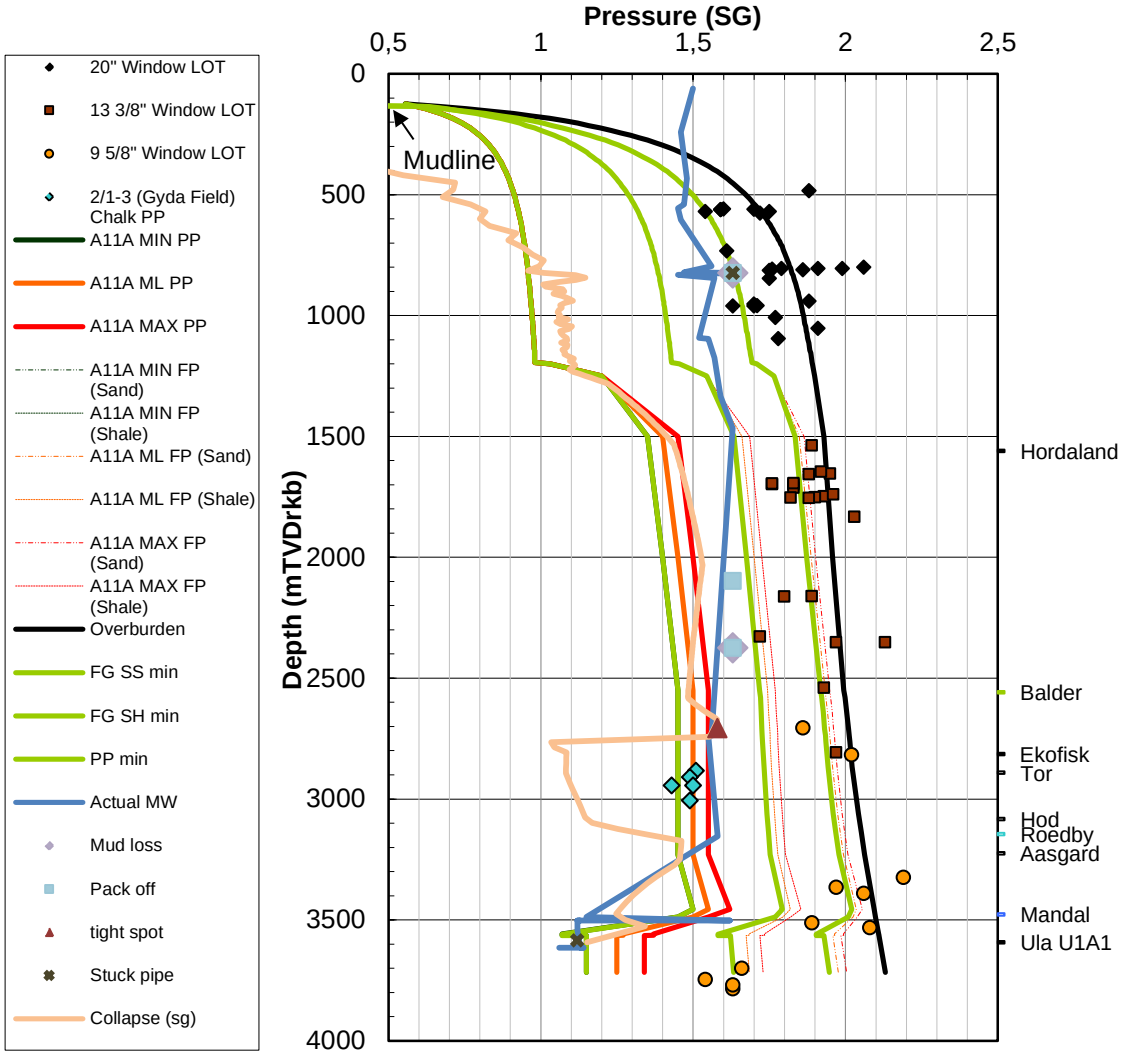

Figure 52: PPFG plot well 7/12-A-8 AT2.

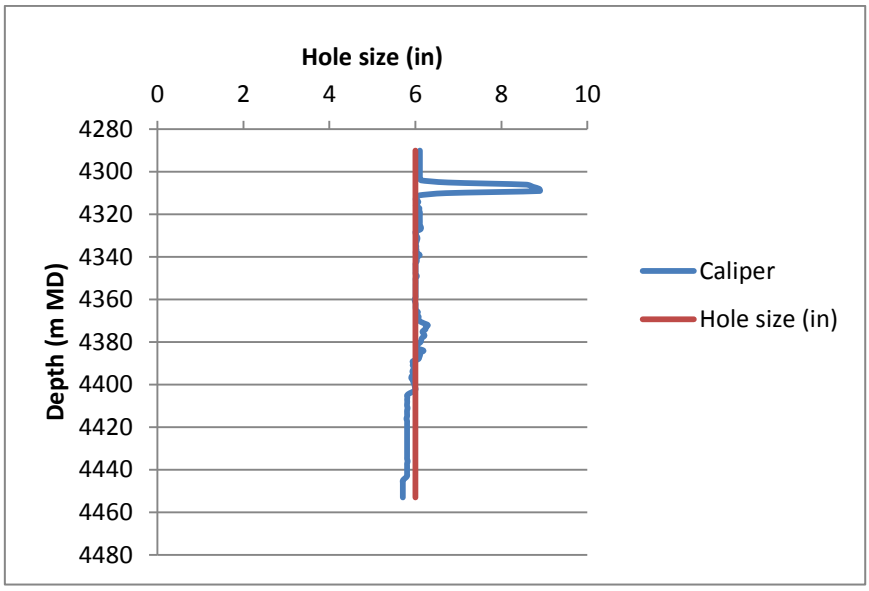

Figure 53: Caliper log vs. Hole size well 7/12-A-8 AT2.

7.2. Future work

Previosly when they were drilling wells on Ula, they had to rely on experience from drilling of older wells. This can be an expensive way of drilling since some of the instability problems could have been avoided. When a model which explain the strength of the formations is made this could be used to design the mud weight program for a new well.

If looking at well 7/12-A-8A T2 it is seen that the mud weight is too high for the upper sections and that it crosses the collapse curve in the end of the well as seen in Figure 54.

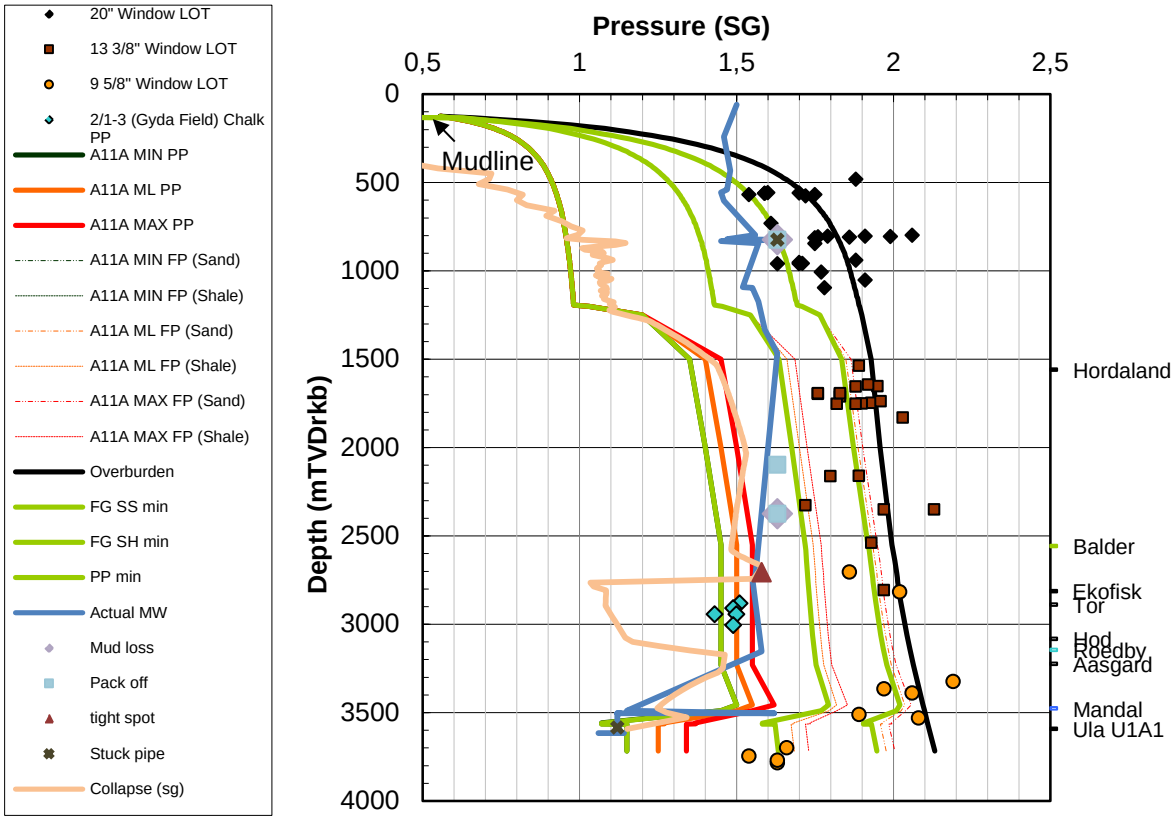

Figure 54: MW used in 7/12-A-8A T2

From this it is possible to create a model where a mud weight that should have been used could be drawn. The formation strength of the formations on Ula is so strong that as long as the well are in overbalance the well will not experience too much wellbore stability problems. Although, the mud weight program should also be made such that the mud weight do not reach to close to the fracture pressure of the formation. In Figure 55 there has been drawn a recommended mud weight that could be used in the future while drilling the new water injectors that are planned on Ula. As seen in the figure the collapse curve follows the pore pressure curve, but the two peaks that are marked in the circle should be taken into account when designing the mud program for the well.

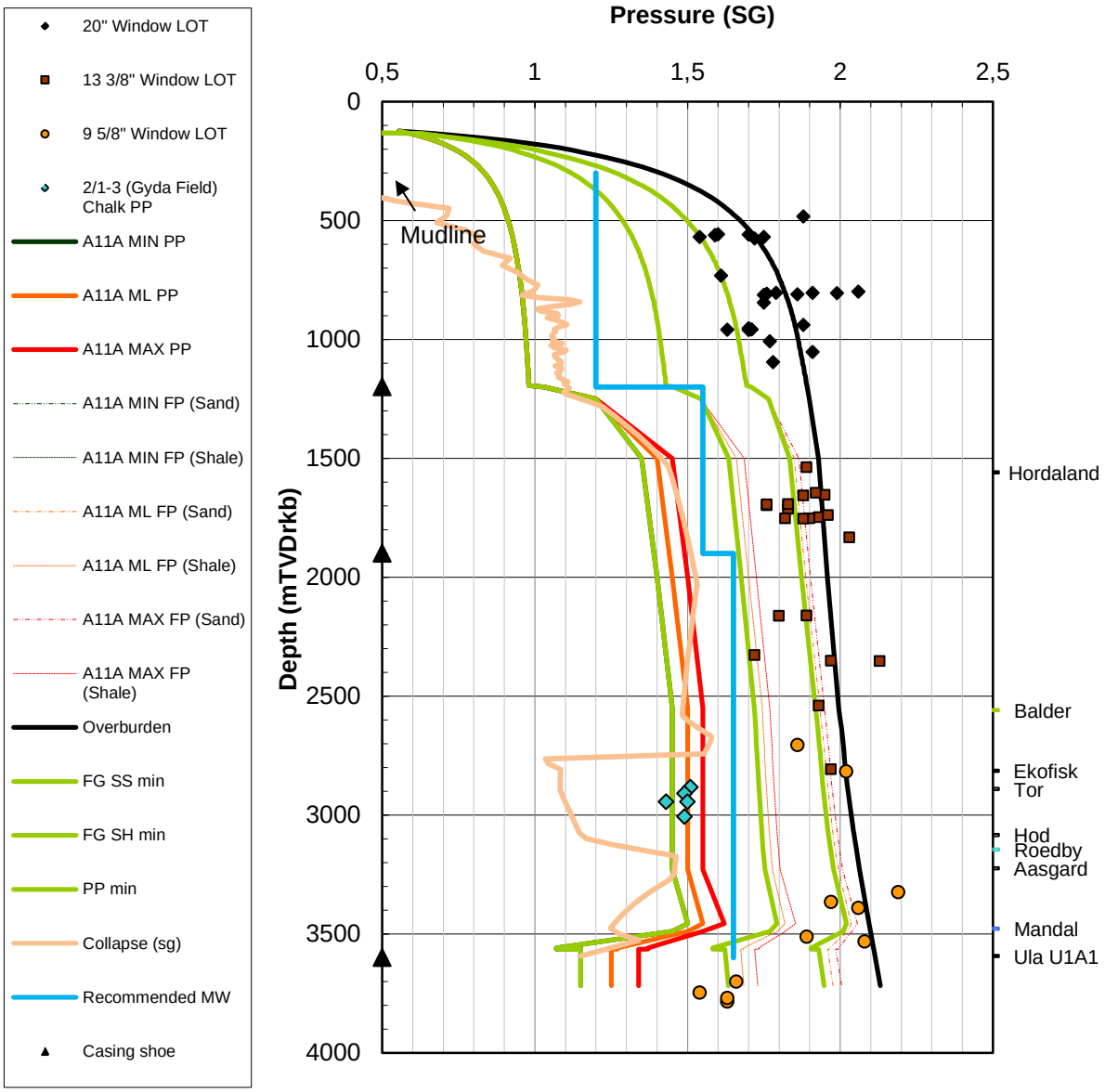

Figure 55: Recommended MW for well 7/12-A-8A T2

8. Geomechanical evaluations

There are many methods that can be used to determine the stresses in the depositional system that is analyzed, but many of these methods are neglecting the tectonic effect on the sediments. The reason these methods do this is because if they neglect this effect they can say that the horizontal in-situ stresses in a relaxed depositional environment are only dependent on the compaction This will make the horizontal stresses equal to each other and make the calculations much easier. The depositional environment will then be isotropic. From experience in geotechnical and mining engineering it is seen that this is usually not the case and that normally the depositional environment will be anisotropic and influenced by tectonic effects and salt domes etc. If the depositional system is isotropic or not is also dependent on the depth and it is seen that the top layers can be close to isotropic but will get more and more anisotropic with depth. The deeper layers have gone through many changes over time that have changed the stresses in the area.

Inversion technique is a method that is derived to model anisotropic stress fields and is based on the leak-off pressure, pore pressure, overburden stresses, borehole inclination and borehole azimuth. Here it is taking into account that the well can be deviated which will have an impact on how the leak-off is interpreted. This method was used on the datasets on Ula to find out the direction of the maximum horizontal stresses in the field. This will be shown in chapter 8.2.

8.1. Inversion technique

The inversion technique uses the fracturing pressure equation and the stress transformation equation to solve the two horizontal in-situ stresses in the studied area. When using these equations together with the azimuth and inclination there will be only two unknowns, which are the two horizontal stresses. The benefit of using the inversion method is that all the information that is needed is found in the final well report of all wells. This makes it possible to evaluate the stresses around old wells in the field, which are done for the Ula field in chapter 8.2.

The inversion technique needs two or more datasets to calculate the horizontal stress field that fits the dataset which is used. This means that the first thing that is done is to calculate the minimum and maximum horizontal stresses for the dataset. These data are then used to further analyze the rock mechanics in existing or new wells.

In an offshore field there are drilled many wells and all of them have different azimuth and inclination. It has therefore been challanging to find a method that can be used to look at a single well and measure its in-situ stress state. By using the advantage of the geometry of the

wells, by running many dataset a model is created that can find the in-situ stresses for one single well that will approximately satisfy all the measurements.

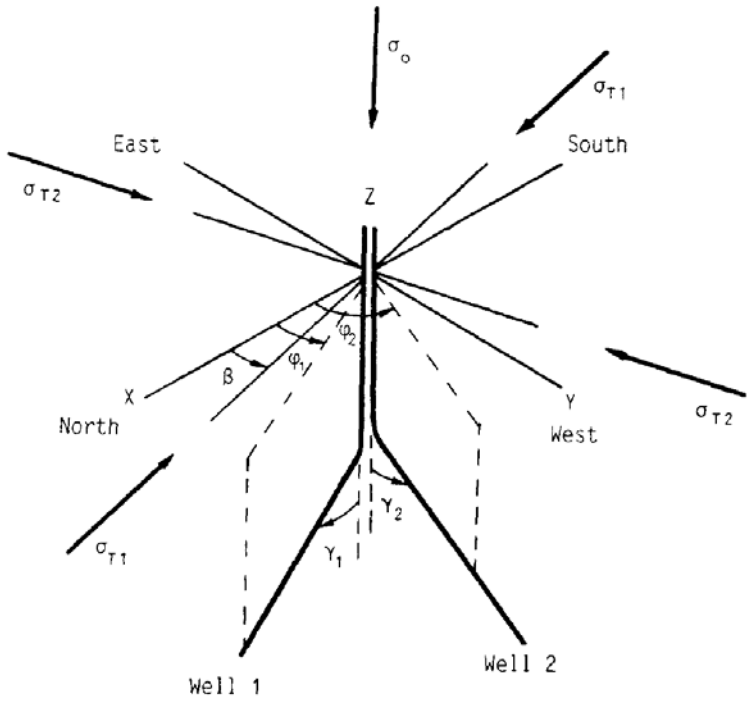

Figure 56: Geometry of the inversion technique (Aadnoy, 1989).

From the well-known Kirsch equation (equation 1 and 4.23) there can be derived a much used relationship for the fracture pressure of a borehole, which is (Aadnoy, 1989):

$$P_{wf} = 3\sigma_y - \sigma_x - P_{fm} + \sigma_{tensile} \qquad 8.1.$$

This equation can be used on any well and its unique orientation because the equation refers to the Cartesian coordinate system with x, y and z of the borehole (z = the direction along the axis of the hole). It is important to be aware that equation 8.1 assumes that $\sigma_x > \sigma_y, \theta = 0°$, and that the calculation has to be checked if this assumption is correct for the calculated case. If $\sigma_y > \sigma_x$ and $\theta = 90°$ the equation will be (Aadnoy and Looyeh, 2011):

$$P_{wf} = 3\sigma_x - \sigma_y - P_{fm} + \sigma_{tensile} \qquad 8.2.$$

By assuming that the fracturing process is governed by equation 8.1 the two normal stresses can be replaced by the transformed equivalents (shown in equation 4.24) which will turn equation 8.1 into (Aadnoy and Looyeh, 2011):

$$\frac{P_{wf} + P_{fm} - \sigma_{tensile}}{\sigma_v} + sin^2 = (3sin^2\varphi - cos^2\varphi cos^2\gamma)\frac{\sigma_H}{\sigma_h} \qquad 8.3.$$

$$+(3cos^2\varphi - sin^2\varphi cos^2\gamma)\frac{\sigma_h}{\sigma_v}$$

or

$$P' = a\frac{\sigma_H}{\sigma_v} + b\frac{\sigma_h}{\sigma_v} \qquad 8.4.$$

Where

$$P' = \frac{P_{wf} + P_{fm} - \sigma_{tensile}}{\sigma_v} + sin^2\gamma$$

$$a = (3sin^2\varphi - cos^2\varphi cos^2\gamma)$$

$$b = (3cos^2\varphi - sin^2\varphi cos^2\gamma)$$

in equation 8.4 there are two unknowns, which is the two horizontal stresses. It is also seen that since the two angles φ and γ are physical constants that are based in the orientation of the wellbore, the equation 8.3 is linear. The inversion technique used in this study is therefore linear elastic. If there are many datasets, the equation 8.4 can be written as a matrix, which makes it possible to capture all the data into one equation. The matrix is then written as (Aadnoy, 1989):

$$\begin{bmatrix} P'_1 \\ P'_2 \\ P'_3 \\ \vdots \\ P'_n \end{bmatrix} = \begin{bmatrix} a_1 & b_1 \\ a_2 & b_2 \\ a_3 & b_3 \\ \vdots & \vdots \\ a_n & b_n \end{bmatrix} \begin{bmatrix} \sigma_H/\sigma_v \\ \sigma_h/\sigma_v \end{bmatrix} \qquad 8.5.$$

or

$$[P'] = [A][\sigma]$$

This matrix can be used if there are two or more datasets available. When solving these types of equations there will always be a marginal error between the solved value and some of the datasets. This error is defined as (Aadnoy, 1989):

$$[e] = [A][\sigma] - [P'] \qquad 8.6.$$

To minimize the error of the calculations the least-squares method can be used. This square method is again minimized when:

$$\frac{\partial e^2}{\partial[\sigma]} = 0 \qquad 8.7.$$

where

$$e^2 = [e]^T[e] \tag{8.8.}$$

These equations result in an equation where it is possible to calculate the unknown horizontal in-situ stress, which is:

$$[\sigma] = \{[A]^T[A]\}^{-1}[A]^T[P'] \tag{8.9.}$$

This equation is a complex equation and a computerized numerical analysis method is needed to solve the equation (Aadnoy, 1989). The stresses and the unknown error will be computed from 0° to 360° which are used in the program for the inversion technique in chapter 8.2. The results are then repeated four times and it could therefore have been solved for 0° to 90°.

8.2. Field case using inversion technique on Ula

To do this field case on Ula, all the leak-off test from the field had to be collected from the different well-sections. The leak-off data was then run through a numerical analyzing program that was made by Mesfin Agonafir Belayneh at the University of Stavanger. The simulation was run for three groups and for the three sections 18 5/8", 13 3/8" and 9 5/8". After one simulation was run, one or two leak-off tests were removed to see if that made the error smaller.

To do the simulations it was important to have information about the location of the different wells in order to divide wells into groups by location. The wells were divided into three groups as shown in Figure 59. The data was also divided into groups by depth; this means that there were simulations run for each group for each casing depth. Then five wells (if possible) were picked from each group based on depth. When picking the wells it would be good to try and find wells that had leak-off tests in almost the same depth because this would make the result more accurate. From a geological perspective the formation will then have more the same properties in approximately the same depth. The simulation was then run for a direction of 0° to 360° from North to find the degree where the error was smallest. The graph will then repeat itself four times during the simulation. If looking at Figure 57 the yellow line represent the error. The location where the yellow line is smallest will give a result for the horizontal stresses. If the red line shows the minimum or the maximum horizontal stress will change throughout the simulation. It will be the same case for the green line. The line with the highest value at the point where the error is smallest will be the maximum horizontal stress given as σ_H, and the other will be the minimum horizontal stress (σ_h).

In this chapter one of the simulations will be shown as an example of how the analysis were done. The results of the other simulations will be found in Appendix C. Group II was chosen as an examples because of its good predictions in all sections. Three of the wells had data

simulated in all sections and these wells were therefore chosen for this example. The data in Table 2 was input data for the analytic numerical inversion model that was used. The model was made to make it possible to use two wells, three wells and up to five wells at a time. When running the simulations we started with five wells in the area we chose and then limited the simulation with fewer wells based on depth or location. The data in Table 2 to Table 4 are the input and the result from group II from the highest number of wells in this group for each section.

In this example the result shows that the horizontal stresses are almost isotropic in the two upper sections. This means that the depositional basin in this area is relaxed and not influenced by tectonic movement. In the 9 5/8" section the two horizontal stresses are more different, which show clear stress anisotropy at this depth.

This example also shows that the overburden stress is higher than the horizontal stresses, which means that there will be normal fault in this section. This means that the overburden loading pushes the fault block down, which is shown in Figure 14.

Table 2: Field data used in the inversion analysis.

Well pressure and survey data							
Well #	**Casing**	**Depth (m TVD)**	**Pwf (LOT) (s.g)**	**Po (s.g)**	**Overb (s.g)**	**Inc (deg)**	**Azim(deg)**
A 4	18 5/8" / 20"	813	1,75	0,9582	1,8208	26,9	103,73
	13 3/8"	1740	1,96	1,382	1,942	32,79	103,79
	9 5/8"	3785	1,63	1,15	2,14	35,4	110,9
A 9	18 5/8" / 20"	811	1,86	0,958	1,8205	26,47	71,1
	13 3/8"	1755	1,88	1,386	1,943	27,48	73,05
	9 5/8"	3747	1,54	1,15	2,135	12	102
A 03A	18 5/8" / 20"	846	1,75	0,96	1,83	15,89	66,04
	13 3/8"	1753	1,9	1,385	1,943	25,22	48,18
	9 5/8"	3701	1,66	1,15	2,129	25,84	54,74

Table 3: Prediction after linear elastic inversion.

Analysis- Linear elastic							
Well	**Casing**	**Depth (m TVD)**	**σx (sg)**	**σy (sg)**	**Predicted -LOP**	**Measured-LOP**	**Difference**
A 4	18 5/8" / 20"	813	1,4267484	1,3906792	1,787089258	1,75	-0,0370893
	13 3/8"	1740	1,7494803	1,67534	1,894539548	1,96	0,0654605
	9 5/8"	3785	1,9127717	1,5678123	1,640665074	1,63	-0,0106651
A 9	18 5/8" / 20"	811	1,4218297	1,3930228	1,799238545	1,86	0,0607615
	13 3/8"	1755	1,736948	1,6637542	1,868314551	1,88	0,0116854
	9 5/8"	3747	1,8608491	1,5175005	1,541652392	1,54	-0,0016524
A 03A	18 5/8" / 20"	846	1,3685313	1,3849498	1,826318032	1,75	-0,076318
	13 3/8"	1753	1,7226416	1,6712099	1,905988083	1,9	-0,0059881
	9 5/8"	3701	1,8692666	1,5575534	1,653393583	1,66	0,0066064

Table 4: Results inversion of group II.

Inversion result					Stress ratio		
Depth interval (m TVD)	σ1 (sg)	σ2 (sg)	Direction from North, β (deg)	Σerror²	Sigma1/Sigma2	Sigm1/Sigv	Sigm1/Sig v
811 - 846	1,3982	1,3178905	356	0,0039332	1,0609642	0,7696733	0,725447
1740 - 1755	1,6607	1,6843643	322	0,0011706	0,9859275	0,8527581	0,8649298
3701 - 3785	1,8989528	1,4670235	82	1,38E-05	1,294425647	0,8895782	0,6872377

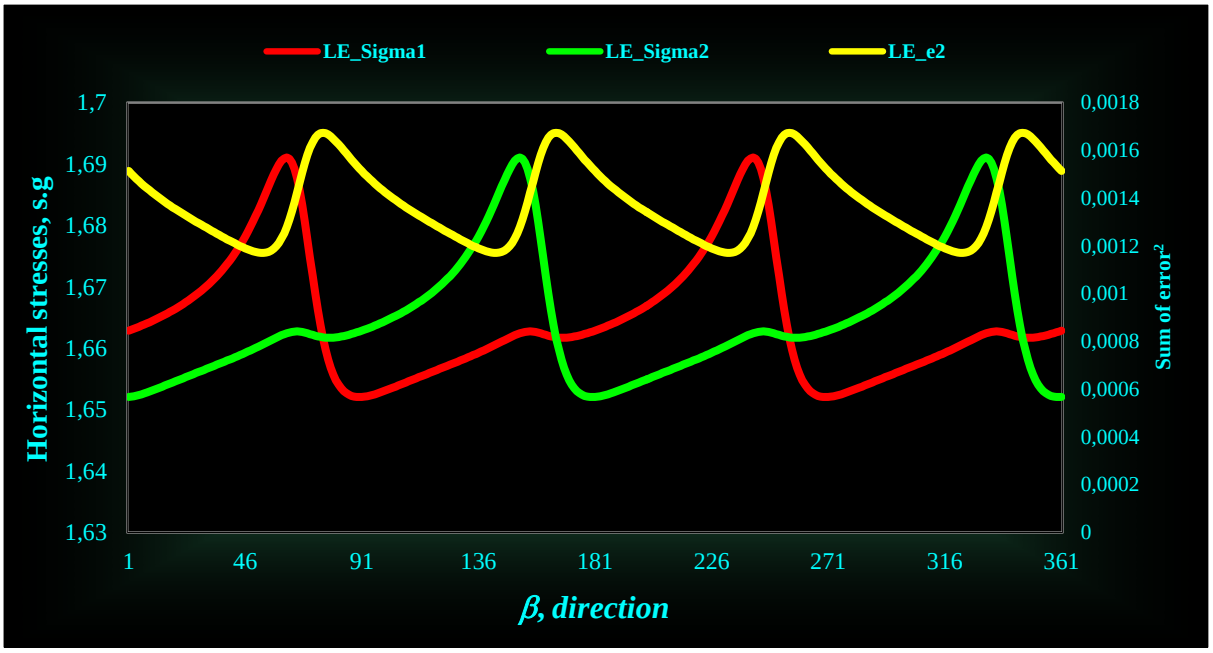

Figure 57: Example of the calculation done in 360° for the 18 5/8" section shown in Table 2.

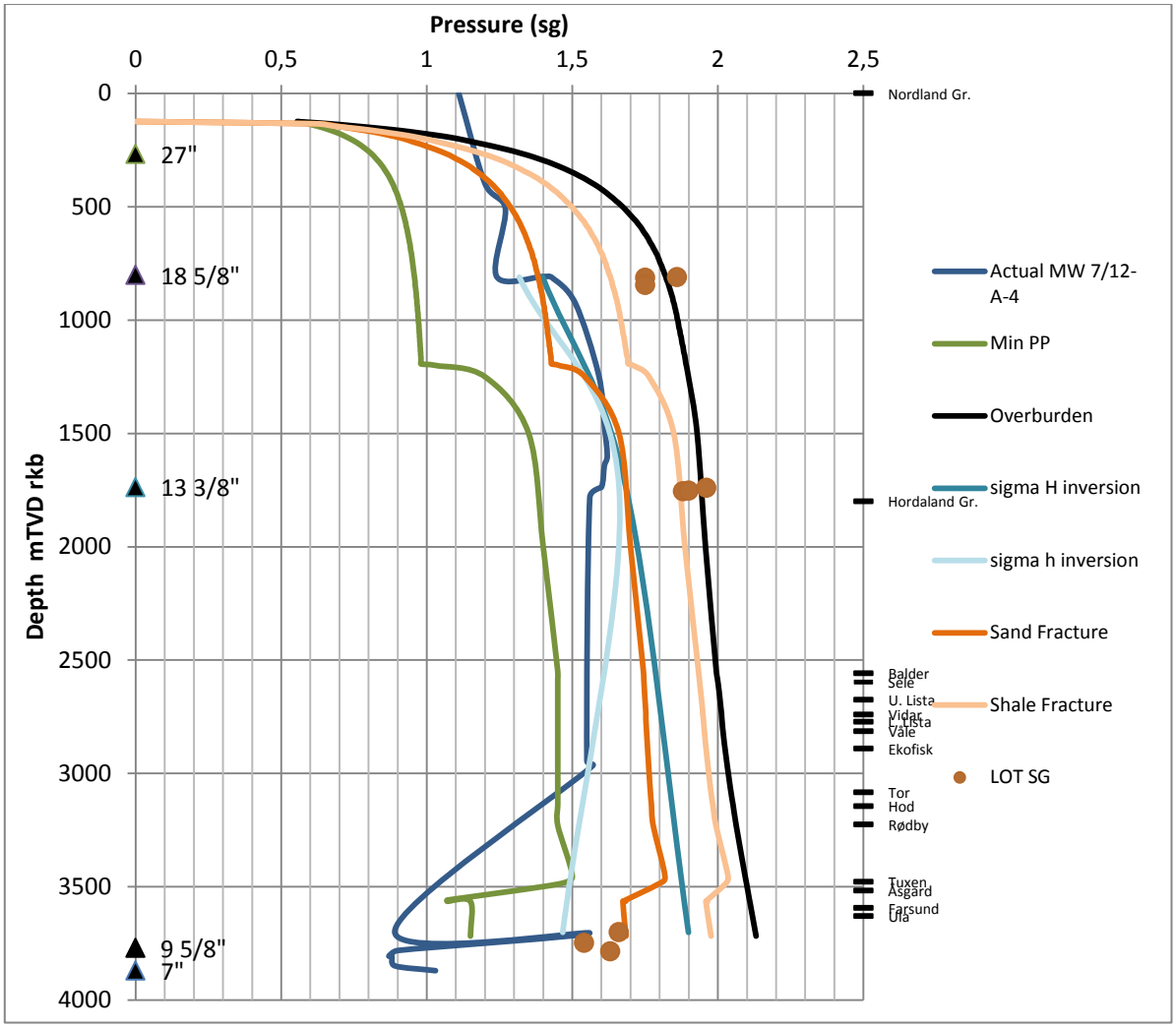

Figure 58: Example showing data used in wells and data from inversion technique

In Figure 58 the curves shows that the maximum horizontal stress almost follows the fracture curve for sand in this area, while the minimum horizontal stress deviates from this curve below 1500 mTVD. The leak-off tests done in the lower section of the well lie just above the minimum horizontal stress at this section. Higher up in the formations the leak-off values are higher than the maximum horizontal stress.

The map below (Figure 59) shows the direction of the maximum and the minimum horizontal stress. The longest line is the maximum stress and the short line is the minimum stress. As seen in Figure 59 the maximum stresses are mostly parallel to the mapped faults, and we can see a clear trend from North-West to South-East which confirm the geological interpretations done one the field. Although the main trend goes from North-West to South-East the figure shows that in group II there is a trend that goes North-East to South-West. These lines follow the fault that lies on the east edge of the field. In group I it is seen that the lines are split between the two directions. This may indicate that it is here the two stress fields are split and the fault direction changes. But maybe if there were leak-off data simulated higher up toward north in group II, the stress field would maybe be changed more toward a North-West to

South-East direction. The stress lines also indicate that they are directed such that the stress field goes around the anticline of the Ula field.

It is obvious that the structure of the field is affecting the horizontal stress direction it can be reasonable to infer that principal stress direction will not be completely horizontal and vertical at all locations. “This implies that on the crest, principle stress directions are likely to be vertical and horizontal, while they will become tilted on the flanks of the dome” (Fjær et al., 2008).

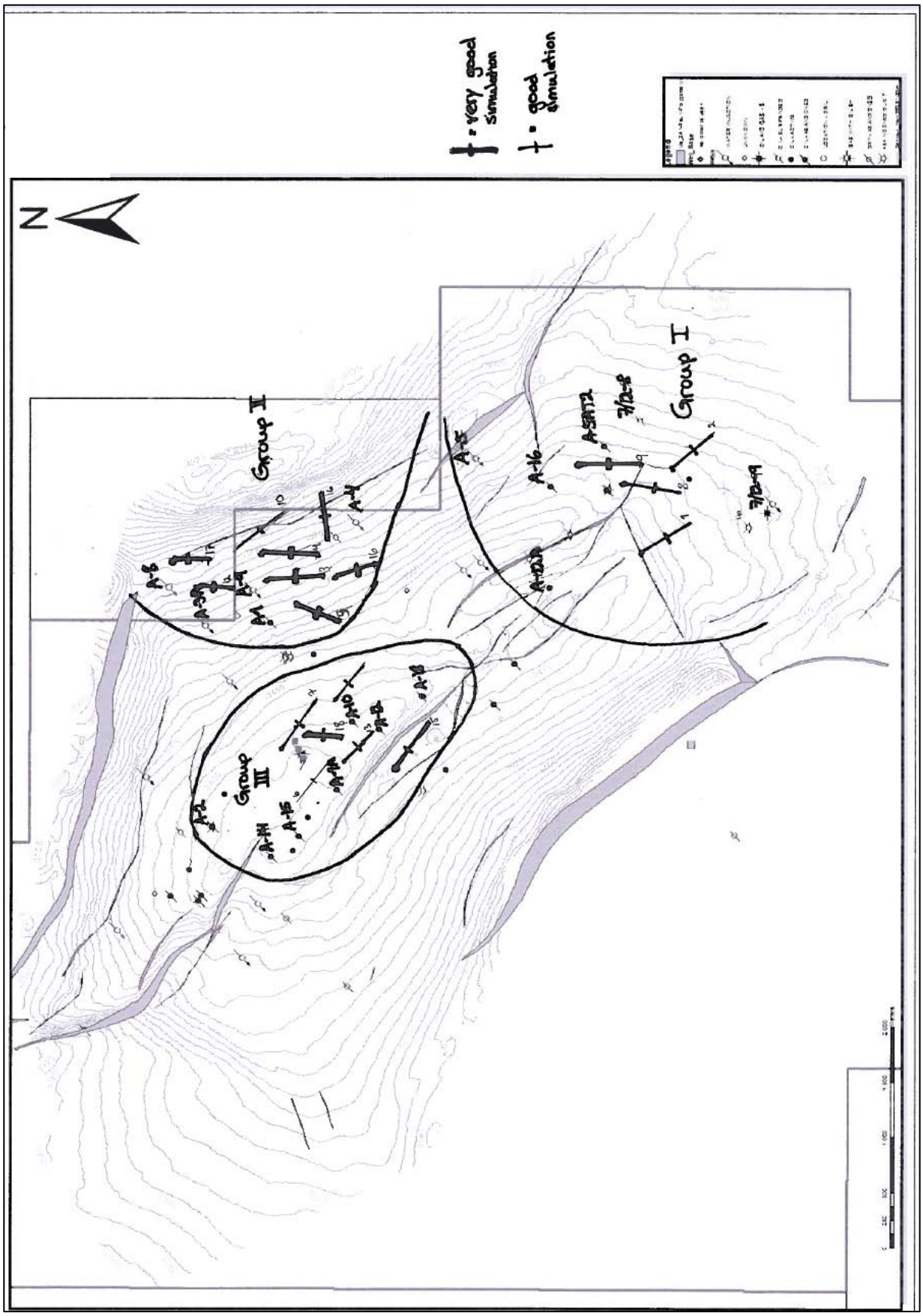

Figure 59: Inversion map showing the different stress fields on Ula. The long line is showing the direction of the maximum horizontal stress and the short line is showing the minimum horizontal stress.

8.3. Future work

The last 30 years there has been a large development in the knowledge about petroleum rock mechanics. From a better understanding of how the mechanisms in the rocks are acting it has been clear that the most important parameters are the magnitude and direction of the in-situ stresses (Aadnoy et al., 2013).

Before Aadnøy (1990) made this method by using the inversion technique to estimate the horizontal stresses there were no good method to find the maximum horizontal stress. Although there were many interpretation methods available to find the minimum horizontal stress from the pressure decline curve during LOT testing (Aadnoy et al., 2013).

The results from the simulations done in the inversion technique can be used to find the strengths of the formation in the new well that is going to be drilled. The input data would then look like this:

Table 5: Input data for anisotropic field case.

Well pressure and survey data							
Well #	**Casing**	**Depth (m TVD)**	**Pwf (LOT) (s.g)**	**Po (s.g)**	**Overb (s.g)**	**Inc (deg)**	**Azim(deg)**
A 4	18 5/8" / 20"	813	1,75	0,9582	1,8208	26,9	103,73
	13 3/8"	1740	1,96	1,382	1,942	32,79	103,79
	9 5/8"	3785	1,63	1,15	2,14	35,4	110,9
A 9	18 5/8" / 20"	811	1,86	0,958	1,8205	26,47	71,1
	13 3/8"	1755	1,88	1,386	1,943	27,48	73,05
	9 5/8"	3747	1,54	1,15	2,135	12	102
A 03A	18 5/8" / 20"	846	1,75	0,96	1,83	15,89	66,04
	13 3/8"	1753	1,9	1,385	1,943	25,22	48,18
	9 5/8"	3701	1,66	1,15	2,129	25,84	54,74
New	18 5/8" / 20"	854	?	0,961	1,83294	18	108
	13 3/8"	1745	?	1,384	1,942	28	83
	9 5/8"	3760	?	1,15	2,138	35	76

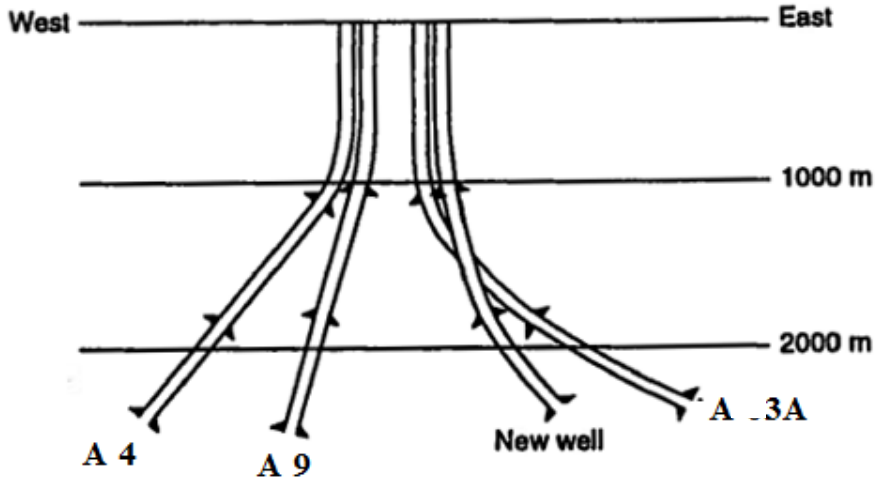

Figure 60: Example of how the field layout of the wells on a west-east projection could look like.

By running this input data through the inversion program the program will find the leak-off pressure, the two horizontal stresses and their direction for this new well. This will be a good tool when designing the well because it makes it possible to design the shape of the well such that the well can withstand the stresses in the formation as good as possible.

If the well is not designed to withstand the in-situ stresses the resulting stress concentration around the borehole wall will try to change the geometry of the borehole. This is change happens such that the hole becomes stable with minimum variation within the stresses. The hole shape will change due to deformation of the borehole or because of wellbore collapse.

9. Discussion

Writhing this thesis has been a steep learning curve. From having almost no knowledge about the field to get a good understanding of the geology and the rock mechanics aspects of the area, and understanding how this have had an inpact when drilling the wells.

To do this thesis it was important to get a good understanding of the principle of rock mechanics. Without this it would be difficult to understand and analyse the models. It has therefore been laid a good amount of work into writing about the general principles about it al. By doing this it was much easier to understand why the wells had experienced the stability poblems they had.

Much data was collected to make this thesis possible. By reading the final well reports from each of the well that were drilled on Ula it was possible to collect all the instability data and find the mud weight that was used when drilling. By reading som many reports is is notised that the content of the reports are depending on who is writing it. Some write much about the problems that has occurred and why, and some may leave some information out of the report. The extent of the problem is also collared by writer. If he/she thik it was a big problem during drilling this will be written a lot about and vise versa. After collecting all this data the data were imported together with the well trajectory and drilling logs for each well into Gocad. By doing this, it was possible to make a 3D-model of the field with all the data. By doing this it was possible to look at everything in perspective. It was then possible to see if the instability problems had occurred due to the location of the well or if there were other aspects contributing to the incidence of the problems. This also made it possible to get a good overview of the data available.

After the sampling of the instability data and the mud weight, this could be used to make models for the mud weight program for the field. By using the wells that had experienced cavings and/or mud losses this gave a good indication if the model is good or not. This is because these instability problems tells a lot about the mudweight used in that section, compared to tight spots ect. Why tights spots occur is due to many different senarios and is a definition used when experiansing overpull and high torque. This type of instability problems therefore needs to be analysed to find the real reson for the why the tight spot occurred.

By putting the formation properties and the information about the well into a program called GMI Wellcheck it was possible to get a estimated collapse curve for this well. Because of problems getting acsess to this program during the time this thesis was written, the data had to be given to another person on BP so this person could run the analysis through this program. Because of this, it was not possible to play around with the data in this program which may have given better understanding of it all. Here it would have been possible to play around with the mud weight and the different casing depth to find a perfect match for this well.

From the calculated minimum mud weight that should have been used in the example well it was possible to get an indication of the stability problem occurred due to wrong mud weight or not. The results showed a good correlation between the mudweight that was used and the problems that occurred. The model was therefore thought to be good and could be used when planning a new well on the field as the injector wells that will be drilled in near future. Although the model looks good, it could have been useful to run the model for even more wells. Looking at wells that have not experienced stability problems and see if the mud weight used in this well is in the preferred mud weight window from this model would also give a good indication if the model is correct or not.

When calculating the collapse curve to find the minimum mud weight that could be used the output will be sensitive to how the input data were collected. The model could be sensitive to which correlation were used to find the internal angle of friction and how the UCS was estimated. If there had been time there should therefore have been run a sensitivity analysis on the input parameters. There can also be big uncertainties on how a company estimates the pore pressure, fracture gradiant and the overburden of a field. It is difficult to get good data of the formation properties and the the unsertainties of these data is therefore accepted out in the industry. Aadnøy (2011) writes about the quality assurance of the wellbore stability analysis. In this paper he writes about the the inconsistencies between input data and the ouput results when evalutating many rock mechanics studies. They also pointed out the problem in some stress state models where the collapse pressure would exeed the pore pressure when lookin at the model in a three-dimensional space. This is clearly not possible, and could affect the pressure model of the field. This occurres because stress models for vertical wells is used to estimate the corresponding stress model for a horizontal well (Aadnøy, 2011).

The fracture gradient of a field is based on the leak-off test run in this area. There are large uncertainties in how the leak-off test are run and if the leak-off pressure is reached or not. A leak-off test is run after each casing is set, and the distance between each test is therefore large. A curve is therefore drawn between these point and there will therefore be some inaccuracy in the interpretation between the different casing setting depths.

This thesis also looked into the method of using the leak-off inversion technique to find the stress orientations of the Ula field. The results from this analysis corresponds to the results from the inversion technique done on the Snorre field which is represented by Aadnøy et al. (1994). The map showing the results clearly show that the stress orientations goes along the faults. This indicates that without the geological interpretation of the field, it would be possible to indicate where the fauls would be and which dicection they would have.

Because of the uncertainty in the pressure models and the leak-off test this would effect the result of this simulation. The inversion technique is very sensitive of the input data, and a small change in the data would therefore effect the results. Here there will also be a error in how the data is sampled. The input data for the pore pressure and the overburden is taken

from a pressure model made for the Ula field. This model is using some data points and are drawing a line between. Beacause of this there will not be a data point for all the depths needed for the inversion technique and the value was therefore read from the graph. This will add an human error in the uncertainty of the model. From the result of the inversion technique will find the stresses acting on the area, and giving both the minimum and maximum horizontal stresses and the overburden in the area. The inversion technique could then be used to find the stress orientation in a new well as mentioned in chapther 8.3. Although it can be discussed if the results are reliable because of the inaccuracy of the imput data, but it could be a good tool to used together with other methods used to find the formation strength before drilling a well.

10. Conclusion

After collecting all this data from the field it was possible to make a good three-dimensional overview of the field. This gave a good understanding of the field and how everything was connected to each other and how the location of the well affected the challenges they experienced during drilling.

After the PPFG plot was made for the selected wells that had experienced mud losses and cavings, it was possible to see if the model was successful or not. Since these two instability problems often show a good indication if the correct mud weight was used or not, we could see that the calculated collapse curve (minimum mud weight) gave a good indication of the margin that the mud weight should stay above in the well. From this we could conclude that the model could be used when designing the mud program for the new injector wells on the Ula field.

From the leak-off inversion technique, the simulation gave good results of the stress orientation of the field. The results were characterized as good and very good results, so none of the results was poor. After mapping the direction of the minimum and maximum horizontal stresses it could be seen that the stress direction follows the mapped faults from geological interpretations. This is a good indication that the result of the test was successful.

Bibliography

AADNOY, B. S. 1989. *Inversion technique to determine the in-situ stress field from fracturing data. Journal of Petroleum Science and Engineering,* 4.

AADNOY, B. S. & BELAYNEH, M. *A new fracture model that includes load history, temperature and poissons effects*. IADC/SPE Asia Pasific Drilling Technology Conferance and Exhibition, 25-27 August 2008 2008 Jakarta, Indonesia. 298-305.

AADNOY, B. S., BRATLI, R. & LINDHOLM, C. 1994. *In-situ stress modelling of the Snorre field. Rock Mechanics in Petroleum Engineering.* Delfi Netherlands: Society of Petroleum Engineers

AADNOY, B. S. & CHENEVERT, M. E. 1987. *Stability of Highly Inclined Boreholes (includes associated papers 18596 and 18736). SPE Drilling Engineering,* 2**,** 364-374.

AADNOY, B. S., KAARSTAD, E. & GONCALVES, C. J. D. C. 2013. *Obtaining both Horizontal Stresses from Wellbore Collapse (IADC/SPE 163563). SPE/IADC Drilling Conference and Exhibition.* Amsterdam, The Netherlands: IADC/SPE.

AADNOY, B. S. & LOOYEH, R. 2011. *Petroleum rock mechanics: drilling operations and well design*, Gulf Professional Publishing (Elsevier).

AADNOY, B. S. & ONG, S. 2003. *Introduction to special issue on borehole stability. Journal of Petroleum Science and Engineering,* 38**,** 79-82.

AADNØY, B. S. 2010. *Modern well design,* Boca Raton, CRC Press/Balkema.

AADNØY, B. S. *SPE/IADC 140205 Quality Assurance of Wellbore Stability Analyses*. 2011. New York, Curran Associates, 851-861.

ALLABY, A. & ALLABY, M. 1999a. *"Angle of internal friction", A dictionary of earth sciences* [Online]. Enclopedia.com. Available: http://www.encyclopedia.com [Accessed 5. June 2013].

ALLABY, A. & ALLABY, M. 1999b. *"unconfined compressive strength" A Dictionary of Earth Science* [Online]. Enclopedia.com. Available: http://www.encyclopedia.com [Accessed 5. June 2013].

BJØRNSETH, H. M. & GLUYAS, J. 1995. *Petroleum exploration in the Ula Trend. In:* HANSLIEN, S. (ed.) *Petroleum Exploration and Exploration in Norway.* ELSEVIER.

BP *Valhall - Distinct Permeable Zones - what they are and how to use them.*

BRADFORD, I., ALDRED, W., COOK, J., ELEWAUT, E., FULLER, J., KRISTIANSEN, T. G. & WALSGROVE, T. *When rock mechanics met drilling: effective implementation of real-time wellbore stability control.* IADC/SPE Drilling Conference, 2000. Society of Petroleum Engineers.

CHANG, C. & ZOBACK, M. D. 2003. *Unconfined Compressive Strength and Physical Property Measurements in Sedimentary Rock. Standford Rock & Borehole Geophysics Consortium.*

DAAE, V. & ULA & TAMBAR SUBSURFACE AND WELL MONITORING TEAM 2011. *Introduction Montage Ula Nov 2011*. Stavanger: BP Norway.

EVANS, D., GEOLOGICAL SOCIETY OF LONDON, NORSK PETROLEUMSFORENING & DANMARKS OG GRØNLANDS GEOLOGISKE UNDERSØGELSE 2003. *The Millennium Atlas: Petroleum Geology of the Central and Northern North Sea*, Geological Society of London.

EWY, R. T., SPE & CHEVRON PETROLEUM TECHNOLOGY CO. 1998. *Wellbore stability predictions using a modified Lade criterion. SPE/ISRM Rock Mechanics in Petroleum Engineering.* Trondheim, Norway.

FJÆR, E., HOLT, R. M., HORSRUD, P., RAAEN, A. M. & RISNES, R. 2008. *Petroleum related rock mechanics*, Elsevier Science.

FLATEBØ, R. E. 2013. *RE: From discussions with supervisor (BP).*

GRADSTEIN, F. M. 2013. *Lundin Norway at a glance (Premission from Lundin and F.M. Gadstein to use the model).* Lundin.

HEGER, A. & SPOERKER, H. F. 2011. *Understanding XLOTs. SPE/IADC Drilling Conference and Exhibition.* Amsterdam: Society of Petroleum Engineers.

HORSRUD, P., SPE & SINTEF PETROLEUM REASERCH 2001. *Estimating mechanical properties of shale from empirical correlations. SPE Drilling & Completion,* 16**,** 68-73.

KUMAR, D., ANSARI, S., WANG, S., YIMING, S., AHMED, S., POVSTYANOVA, M. & TICHELAAR, B. 2012. *Real-time wellbore stability analysis: An observation from caving at shale shakers. AAPG International Convention and Exibition.* Singapore: AAPG.

LAL, M., SPENCER, A. M., BP & AMOCO 1999. *Shale stability: drilling fluid interaction and shale strength. SPE Asia Pacific Oil and Gas Conference and Exhibition.* Jakarta, Indonesia.
MITCHELL, R. F., MISKA, S. Z. & AADNOY, B. S. 2011. *Fundamentals of drilling engineering*, Society of Petroleum Engineers.
NPD. *Ula pdf* [Online]. NPD factpage. Available: http://www.npd.no/global/norsk/3-publikasjoner/faktahefter/fakta2012/figurar/kapittel-10/ula.pdf [Accessed 22. January 2013].
NPD. 2013. *Stratigraphy* [Online]. Available: http://factpages.npd.no/factpages/Default.aspx?culture=no [Accessed 05. June 2013].
OLSEN, R. R. 2013. *RE: From discussion (BP).*
OXTOBY, N. H., MITCHELL, A. W. & GLUYAS, J. G. 1995. *The filling and emptying of the Ula Oilfield: fluid inclusion constraints. In:* CUBITT, J. M. & ENGLAND, W. A. (eds.) *The Geochemestry of reservoirs.* Geological society.
PATON, R. 2013. *RE: From discussions (BP).*
RAGAN, D. M. 2009. *Structural geology: an introduction to geometrical techniques,* New York, Cambridge University Press.
SCHLUMBERGER. *Oilfield Glossary* [Online]. [Accessed 28.05 2013].
SPENCER, A. M., HOME, P. C. & WIIK, V. 1986. *Habit of hydrocarbons in the Jurrasic Ula Trend, Central Graben, Norway. In:* SPENCER, A. M. (ed.) *Habit of hydrocarbons on the Norwegian continental shelf: proceedings of an international conference (Habitat of hydrocarbons, Norwegian oil and gas finds).* Graham & Trotman for the Norwegian Petroleum Society, 1986.
SPENCER, A. M., PETROLEUMSFORENING, N. & HOME, P. C. 1987. *Ula. Geology of the Norwegian oil and gas fields: an atlas of hydrocarbon discoveries, containing full descriptions of 37 of Norway's major oil and gas fields and finds.* Published by Graham & Trotman for the Norwegian Petroleum Society.
THOMAS, S., DUNCAN, J., HAAJIZADEH, M. & WILLIAMS, J. *ULA FIELD-LIFE AFTER THE FLOOD: CORE & LOG EXPERIENCE FROM BEHIND A MATURING WAG FRONT.* SPWLA 49th Annual Logging Symposium, May 25th-28th, 2008, 2008 Edinburgh. Society of Petrophysicists and Well Log Analysts (SPWLA).
TWISS, R. J. & MOORES, E. M. 2006. *Structural Geology,* New York, W. H. Freeman and Company.
ULA TAMBAR SUBSURFACE TEAM 2013. *Ula Hub Development.* BP.
WANG, H., SOLIMAN, M. Y., SHAN, Z., MENG, F. & TOWLER, B. F. 2011. *Understanding the Effect of Leakoff Tests on Wellbore Strength. SPE Drilling & Completion,* Volume 26, Number 4.
ZOBACK, M. D., MOOS, D., MASTIN, L. & ANDERSON, R. N. 1985. Well bore breakouts and in situ stress. *Journal of Geophysical Research: Solid Earth,* 90**,** 5523-5530.

Appendix

Appendix A: Table of instability problems on Ula
Appendix B: Table with mud weights used on Ula wells
Appendix C: Leak-off inversion technique results

Appendix A: Table of instability problems on Ula

Well name	Depth m MD	Depth m TVD	Formation	Section	Instability problem	
7-12-6	1480	1479,97	Nordland Group	17 1/2" Hole	Cavings	
7-12-6	1700	1699,96	Hordaland Group	12 1/4" Hole	Stuck pipe (Cavings)	
7-12-6	3700	3699	Skagerrak? (End of well)	8 1/2" Hole	Stuck pipe	
7-12-8	715	715	Nordland Group	20" Hole	Tight spots	
7-12-8	1045	1045	Nordland Group	17 1/2" Hole	Tight spots	
7-12-8	1695	1695	Hordaland Group	17 1/2" Hole	Pack off	
7-12-8	2145	2145	Hordaland Group	17 1/2" Hole	Tight spots	
7-12-8	1695	1695	Hordaland Group	17 1/2" Hole	Pack off	
7-12-8	2145	2145	Hordaland Group	17 1/2" Hole	Tight spots	
7-12-8	1618	1618	Nordland Group	17 1/2" Hole	Washout	
7-12-8	1930	1930	Hordaland Group	17 1/2" Hole	Washout	
7-12-8	1100	1100	Nordland Group	13 3/8"	Stuck	
7-12-8	2430	2430	Hordaland Group	12 1/2" Hole	Tight spots	
7-12-8	3164	3164	Tor	12 1/2" Hole	Tight spots	
7-12-8	3314	3314	Hod	12 1/2" Hole	Tight spots	
7-12-8	3154	3154	Tor	12 1/2" Hole	Tight spots	
7-12-8	3144	3144	Tor	12 1/2" Hole	Tight spots	
7-12-12 ST2	2148	1816,99	Hordaland Group	16" Hole	Stuck pipe	
7-12-12 ST2	1200	1176,99	Nordland Group	16" Hole	Washout	Sidetrack:
7-12-12 ST2	1946	1702,14	Hordaland Group	16" Hole	Pack off	
7-12-12 ST2	3000	2295,62	Hordaland Group	12 1/4" Hole	Tight spots	
7-12-A-1	2106	2035,97	Hordaland Group	17 1/2" Hole	Tight spots	
7-12-A-1	743	742,4	Nordland Group	17 1/2" Hole	Stuck pipe	
7-12-A-1	2233	2149,56	Hordaland Group	13 3/82 Casing	Pack off	
7-12-A-1	3207	3029,53	Tor	12 1/4" Hole	Stuck pipe	
7-12-A-1	3540	3326,83	Aasgard	12 1/4" Hole	Stuck pipe	
7-12-A-1	3561	3345,49	Aasgard	12 1/4" Hole	Cavings	
7-12-A-1	3287	3101,2	Hod	12 1/4" Hole	Stuck pipe	
7-12-A-1	3986	3723,38	Ula (end of well)	8 1/2" Hole	Stuck pipe	
7-12-A-1_B	1766	1762,87	Hordaland Group	12 1/4" Hole	Cavings	
7-12-A-1_B	1768	1764,87	Hordaland Group	12 1/4" Hole	Tight spots	
7-12-A-2	283	282,99	Nordland Group	24" Hole	Stuck pipe	
7-12-A-2_B_T2	2740	2608,38	Sele fm.	8 1/2" hole	Tight spots	
7-12-A-2_B_T2	4041	3362,53	Mandal fm.	8 1/2" hole	Tight spots	
7-12-A-2_B_T2	4497	3494,22	Ula fm.	8 1/2" hole	Tight spots	
7-12-A-2_B_T2	4143	3398,3	Farsund fm.	8 1/2" hole	Tight spots	
7-12-A-2_B_T2	4026	3356,89	Mandal fm.	8 1/2" hole	Tight spots	

7-12-A-2_B_T2	3385	3074,87	Hod fm.	8 1/2" hole	Pack off	
7-12-A-2_B_T2	3563	3156,1	Åsgard fm.	8 1/2" hole	Pack off	
7-12-A-2_B_T2	3790	3256,3	Åsgard fm.	8 1/2" hole	Pack off	
7-12-A-2_B_T2	3994	3344,11	Åsgard fm.	8 1/2" hole	Pack off	
7-12-A-2_B_T2	3950	3325,62	Åsgard fm.	8 1/2" hole	Pack off	
7-12-A-2_B_T2	4059	3369,2	Åsgard fm.	8 1/2" hole	Stuck pipe	
7-12-A-2_B_T2	3615	3178,76	Åsgard fm.	8 1/2" hole	Tight spots	
7-12-A-2_B_T2	4515	3497,24	Farsund fm.	6"	Tight spots	
7-12-A-2_B_T2	5080	3537,39	Ula fm.	6"	Pack off	
7-12-A-2_B_T2	4846	3528	Ula fm.	6"	Stuck pipe	Sidetrack
7-12-A-2_B_T2	4848	3528	Ula fm.	6"	Stuck pipe	
7-12-A-3	970	952,29	Nordland Group	17 1/2" Hole	Tight spots	
7-12-A-3	2185	2025,86	Hordaland Group	12 1/4" Hole	Tight spots	
7-12-A-3	3864	3545,32	LCM	8 1/2" Hole	Cavings	
7-12-A-3	3898	3578,42	Ula 2A1	8 1/2" Hole	Stuck pipe	
7-12-A-3	3947	3626,07	Ula_ 2B2	7" liner	Cavings	
7-12-A-3_B	4270	3656,88	Ula	6" Hole	Stuck pipe	
7-12-A-4	830	807,99	Nordland Group	24" Hole	Gumbo	
7-12-A-4	2234	1981,78	Hordaland Group	12 1/4" Hole	Tight spots	
7-12-A-4	2044	1823,53	Hordaland Group	12 1/4" Hole	Tight spots	
7-12-A-4	4407	3805,44	Ula fm.	8 1/2" Hole	Stuck pipe	
7-12-A-5	385	384,27	Nordland Group	24" Hole	Gumbo	
7-12-A-5	1770	1595,49	Nordland Group	17 1/2" Hole	Gumbo	
7-12-A-5	2044	1823,53	Hordaland Group	17 1/2" Hole	Tight spots	
7-12-A-5	4058	3516,74	Ula fm.	12 1/4" Hole	Stuck pipe	
7-12-A-5_A	3775		Vaale fm.	8 1/2" Hole	Lost circulation	
7-12-A-5_A	4038		Tor fm.	8 1/2" Hole	Stuck pipe	
7-12-A-5_A	4085		Tor fm.	8 1/2" Hole	Stuck pipe	
7-12-A-5_A	4915		Åsgard fm.	8 1/2" Hole	Tight spots	
7-12-A-5_A	4940		Åsgard fm.	8 1/2" Hole	Tight spots	
7-12-A-5_A	5001		Åsgard fm.	7" liner	Tight spots	
7-12-A-5_A	5001		Åsgard fm.	7" liner	Stuck pipe	
7-12-A-5_A	3578		Lista fm.	Plug back	Tight spots	
7-12-A-5_AT2	3633	2800,98	Lista fm.	8 1/2" Hole	Tight spots	
7-12-A-5_AT2	4060	3031,28	Tor fm.	8 1/2" Hole	Tight spots	
7-12-A-5_AT2	4367	3148,3	Tor fm.	8 1/2" Hole	Tight spots	
7-12-A-5_AT2	5354	3569,08	Åsgard fm.	8 1/2" Hole	Stuck pipe	
7-12-A-5_AT2	5366	3573,62	Åsgard fm.	8 1/2" Hole	Stuck pipe	
7-12-A-5_B	1052	995,21	Nordland Group	12 1/4" Hole	Tight spots	
7-12-A-5_B	2730	2160,01	Hordaland Group	12 1/4"	Pack off	
7-12-A-5_B	3280	2639,42	Sele fm.	12 1/4" Hole	Stuck pipe	
7-12-A-5_B	2349	1831,31	Hordaland Group	12 1/4" Hole	Tight spots	
7-12-A-5_B	4432	3520,95	Farsund fm.	12 1/4"	Tight spots	

7-12-A-5_B	3764	3112,18	Tor fm.	12 1/4" Hole	Tight spots	
7-12-A-5_B	3644	2992,68	Tor fm.	12 1/4"	Tight spots	
7-12-A-5_B	5031	3548,71	Ula fm.	8 1/2"	Stuck pipe	Sidetrack after this section
7-12-A-7	566	564,87	Nordland Group	17 1/2" Hole	Tight spots	
7-12-A-7	2167	1977,63	Hordaland Group	12 1/4" Hole	Pack off	
7-12-A-7	2276	2070,92	Hordaland Group	12 1/4" Hole	Pack off	
7-12-A-7	2163	1974,22	Hordaland Group		Stuck pipe	
7-12-A-7	3344	2988,21	Tor fm.			Sidetrack
7-12-A-7	4260	3851,97	Zechstein salt		Influx	
7-12-A-7_B	681	679,56	Nordland Group	16" Hole	Cavings	
7-12-A-7_B	691	689,53	Nordland Group	16" Hole	Cavings	
7-12-A-7_B	3635	3333,71	Åsgard fm.	9 5/8" Casing	Tight spots	
7-12-A-8	1010	983,76	Nordland Group		Tight spots	
7-12-A-8	1234	1173,24	Nordland Group		Tight spots	
7-12-A-8_A	1193	1173,38	Nordland Group	12 1/4" Hole	Mud loss	
7-12-A-8_A	1460	1411,63	Nordland Group	12 1/4" Hole	Pack off	
7-12-A-8_A	435	434,65	Nordland Group	12 1/4" Hole	Lost circulation + Pack off	
7-12-A-8_A	3323	2718,36	Ekofisk fm.	8 1/2" Hole	Tight spot	
7-12-A-8_A	3420	2795,62	Tor fm.	8 1/2" Hole	Tight spot	
7-12-A-8_A	3323	2718,36	Ekofisk fm.	8 1/2" Hole	Tight spot	
7-12-A-8_A	4278	3479,04	Mandal fm.	8 1/2" Hole	Tight spot	
7-12-A-8_A	4412	3585,77	Ula fm.	4 1/2" liner	Stuck pipe	
7_12-A-8_A T2	831	824,61	Nordland Group		Stuck pipe	
7_12-A-8_A T2	831	824,61	Nordland Group		Pack off	
7_12-A-8_A T2	831	824,61	Nordland Group		Mud loss	
7_12-A-8_A T2	2475	2097,8	Hordaland Group		Pack off	
7_12-A-8_A T2	2888	2375,11	Hordaland Group		Pack off	
7_12-A-8_A T2	2888	2375,11	Hordaland Group		Mud loss	
7_12-A-8_A T2	3323	2707,1	Lista fm.		tight spot	
7_12-A-8_A T2	4412	3585,77	Ula fm.		Stuck pipe	
7-12-A-9	430	429,82	Nordland Group	24" Hole	Gumbo	
7-12-A-9	1700	1583,2	Hordaland Group	17 1/2"	Pack off	
7-12-A-9	1376	1296,97	Nordland Group	17 1/2"	Tight spots	
7-12-A-9	1340	1265,02	Nordland Group	17 1/2"	Tight spots	
7-12-A-9	1295	1225,07	Nordland Group	17 1/2"	Tight spots	
7-12-A-9	1832	1699,98	Hordaland Group	17 1/2"	Tight spots	
7-12-A-9_A	1960	1799,36	Hordaland Group	12 1/4"	Tight spots	
7-12-A-9_A	2951	2705,07	Sele fm.	12 1/4"	Tight spots	
7-12-A-9_A	3262	3016,05	Tor fm.	12 1/4"	Tight spots	
7-12-A-9_A	3358	3112,04	Hod fm.	12 1/4"	Tight spots	
7-12-A-9_A	3107	2861,06	Ekofisk fm.	12 1/4"	Tight spots	

7-12-A-10	650	649,05	Nordland Group	17 1/2" Hole	Tight spots	
7-12-A-10	910	908,54	Nordland Group	17 1/2" Hole	Washout	
7-12-A-10	1719	1683,07	Hordaland Group	12 1/4" Hole	Tight spots	
7-12-A-10	2530	2444,67	Hordaland Group	12 1/4" Hole	Tight spots	
7-12-A-10_A	3435	2842,37	Ekofisk fm.	12 1/4"	Pack off	
7-12-A-10_A	4575	3425,82	Mandal fm.	8 1/2"	Tight spots	
7-12-A-11	930	880,69	Nordland Group	24" Hole	Washout	
7-12-A-11	1153	1044,2	Nordland Group	24" Hole	Gumbo	
7-12-A-11	1000	934,87	Nordland Group	18 5/8" Casing	Tight spots	
7-12-A-11	6168	3663,89	Ula fm.	8 1/2" Hole	Pack off	
7-12-A-11	5934	3584,83	Ula fm.	8 1/2" Hole	Tight spots	
7-12-A-11	6028	3616,35	Ula fm.	8 1/2" Hole	Pack off	
7-12-A-11	6033	3618,05	Ula fm.	8 1/2" Hole	Pack off	
7-12-A-11	5985	3601,87	Ula fm.	8 1/2" Hole	Stuck pipe	
7-12-A-11	5610	3474,11	Farsund fm.	8 1/2" Hole	Pack off	Sidetrack #2
7-12-A-11	5743	3518,79	Ula fm.	8 1/2" Hole	Pack off	
7-12-A-11	5864	3560,4	Ula fm.	8 1/2" Hole	Pack off	
7-12-A-11	5647	3486,73	Farsund fm.	8 1/2" Hole	Tight spots	
7-12-A-11	5647	3486,73	Farsund fm.	8 1/2" Hole	Pack off	
7-12-A-11	5628	3480,27	Farsund fm.	8 1/2" Hole	Pack off	Sidetrack
7-12-A-11	5992	3604,2	Ula fm.	8 1/2" Hole	Pack off	
7-12-A-11	5535	3447,63	Farsund fm.	8 1/2" Hole	Pack off	
7-12-A-11_T2	6010	3610,21	Rødby fm.	8 1/2" Hole	Stuck pipe	
7-12-A-11_T2	5381	3387,65	Rødby fm.	8 1/2" Hole	Stuck pipe	
7-12-A-11_T2	6459	3759,59	Ula fm.	6" Hole	Stuck pipe	
7-12-A-11_T2	6300	3707,3	Ula fm.	6" Hole	Stuck pipe	
7-12-A-12	1734	1569,62	Nordland Group	17 1/2" Hole	Stuck pipe	
7-12-A-12_T2	1847	1665,77	Hordaland Group	17 1/2" Hole	Pack off	
7-12-A-12_T2	2436	2156,83	Hordaland Group	12 1/4" Hole	Tight spots	
7-12-A-12_T2	3300	2880,05	Tor fm.	12 1/4" Hole	Tight spots	
7-12-A-12_T2	3700	3226,89	Åsgard fm.	12 1/4" Hole	Tight spots	
7-12-A-12_A	1022	970,33	Nordland Group	17 1/2"	Tight spots	
7-12-A-12_A	2181	1827,08	Hordaland Group	12 1/4" Hole	Tight spots	
7-12-A-12_A	4540	3511,58	Farsund fm.	8 1/2" Hole	Tight spots	
7-12-A-13	1060	1013,5	Nordland Group	17 1/2" Hole	Tight spots	
7-12-A-13	1580	1368,94	Nordland Group	17 1/2" Hole	Tight spots	
7-12-A-13	1840	1533,46	Nordland Group	17 1/2" Hole	Tight spots	
7-12-A-13	1831	1527,75	Nordland Group	17 1/2" Hole	Pack off	
7-12-A-13	3500	2618,11	Hordaland Group	12 1/4" Hole	Tight spots	
7-12-A-13	3000	2294,3	Hordaland Group	12 1/4" Hole	Tight spots	
7-12-A-13	3849	2844,05	Hordaland Group	12 1/4" Hole	Tight spots	
7-12-A-13	4753	3483,42	Åsgard fm.	12 1/4" Hole	Tight spots	

7-12-A-14	950	931,49	Nordland Group	24" Hole	Gumbo	
7-12-A-14	2060	1994,05	Hordaland Group	17 1/2"	Tight spots	
7-12-A-14	1286	1251,92	Nordland Group	17 1/2"	Pack off	
7-12-A-14	3592	3443,18	Ula fm.	8 1/2"	Influx	
7-12-A-14	3592	3443,18	Ula fm.	8 1/2"	Lost circulation + Stuck pipe	
7-12-A-14_A	3201	3062,66	Tuxen fm.	12 1/2" Hole	Tight spots	
7-12-A-14_A	3708	3370,48	Åsgard fm.	12 1/2" Hole	Mud loss	
7-12-A-14_A	3809	3386,97	Ula fm.	8 1/2" Hole	Mud loss	
7-12-A-15	400	399,97	Nordland Group	18 5/8" casing	Pack off	
7-12-A-15	1420	1418,19	Nordland Group	17 1/2"	Gumbo	
7-12-A-16	806	803,59	Nordland Group	18 5/8" casing	Gumbo	
7-12-A-16	5089	3628,97	Farsund fm.	8 1/2"	Influx	
7-12-A-16_A	2185	1778,62	Hordaland Group	12 1/4" Hole	Pack off	
7-12-A-16_A	2200	1788,83	Hordaland Group	12 1/4" Hole	Pack off	
7-12-A-17	1704	1455,08	Nordland Group	17 1/2" Hole	Pack off	
7-12-A-17	2030	1625,56	Nordland Group	12 1/4" Hole	Pack off	Sidetrack
7-12-A-17	2390	1825,05	Hordaland Group	12 1/4" Hole	Pack off	
7-12-A-17	2025	1622,88	Nordland Group	12 1/4" Hole	Pack off	Sidetrack
7-12-A-17	2000	1609,48	Nordland Group	12 1/4" Hole	Pack off	
7-12-A-17	4520	2959	Hordaland Group	12 1/4" Hole	Pack off	
7-12-A-17	4687	3051,43	Hordaland Group	12 1/4" Hole	Tight spots	
7-12-A-17	3865	2605,41	Hordaland Group	12 1/4" Hole	Stuck pipe	
7-12-A-17	3505	2414,5	Hordaland Group	12 1/4" Hole	Lost circulation + Tight spots	
7-12-A-17	4409	2898,32	Vaale fm.		Stuck pipe	
7-12-A-17	5361	3428,33	Åsgard fm.		Stuck pipe	
7-12-A-17	4665	3039,14	Tor fm.		Washout	

Appendix B: Table with mud weights used on Ula wells

Well	Deth from	depth to	MW sg	Mud type	Hole size	comment
7-12-3	0	176	1,05			
7-12-3	176	254	1,06			
7-12-3	254	977	1,1			
7-12-3	977	1098	1,34			
7-12-3	1098	1289	1,35			
7-12-3	1289	1500	1,38			
7-12-3	1500	1596	1,41			
7-12-3	1596	1676	1,42			
7-12-3	1676	1679	1,45			
7-12-3	1679	1679	1,49			
7-12-3	1679	1820	1,45			
7-12-3	1820	2069	1,46			
7-12-3	2069	2225	1,48			
7-12-3	2225	2490	1,5			
7-12-3	2490	2759	1,51			
7-12-3	2759	2904	1,53			
7-12-3	2904	3710	1,55			
7-12-4	139	330	1,02			
7-12-4	330	498	1,16			
7-12-4	498	498	1,19			
7-12-4	498	799	1,06			
7-12-4	799	1338	1,4			
7-12-4	1338	1407	1,43			
7-12-4	1407	1587	1,44			
7-12-4	1587	1590	1,4			
7-12-4	1590	1694	1,44			
7-12-4	1694	1694	1,46			
7-12-4	1694	1890	1,45			
7-12-4	1890	2300	1,43			
7-12-4	2300	3373	1,44			
7-12-4	3373	3621	1,48			
7-12-4	3621	3621	1,46			
7-12-4	3621	3621	1,48			
7-12-4	3621	3621	1,47			
7-12-4	3621	3621	1,48			
7-12-4	3621	3621	1,49			
7-12-4	3621	3621	1,48			
7-12-4	3621	3621	1,5			
7-12-4	3621	3621	1,48			
7-12-4	3621	3621	1,49			

7-12-5	188	294	1,05		36"	
7-12-5	294	467	1,08		36"	
7-12-5	467	467	1,29		36"	
7-12-5	467	467	1,1		36"	
7-12-5	467	500	1,14		36"	
7-12-5	500	840	1,15		17,5"	
7-12-5	840	1010	1,16		17,5"	
7-12-5	1010	1246	1,17		17,5"	
7-12-5	1246	1312	1,22		17,5"	
7-12-5	1312	1497	1,26		17,5"	
7-12-5	1497	1924	1,4		17,5"	
7-12-5	1924	2414	1,42		12,25"??	
7-12-5	2414	2480	1,43		12,25"	
7-12-5	2480	2542	1,46		12,25"	
7-12-5	2542	3741	1,48		12,25"	
7-12-5	3741	4440	1,5		12,25" /8,5"	
7-12-5	4440	4400	1,51		8,5"	
7-12-6	133	172	1,06			
7-12-6	172	480	1,07			
7-12-6	480	480	1,11			
7-12-6	480	480	1,26			
7-12-6	480	483	1,23			
7-12-6	483	752	1,14			
7-12-6	752	1108	1,17			
7-12-6	1108	1180	1,14			
7-12-6	1180	1433	1,17			
7-12-6	1433	1696	1,3			
7-12-6	1696	1696	1,41			
7-12-6	1696	1696	1,42			
7-12-6	1696	1696	1,43			
7-12-6	1696	1696	1,4			
7-12-6	1696	1810	1,42			
7-12-6	1810	2028	1,45			
7-12-6	2028	2631	1,44			
7-12-6	2631	1679	1,48			
7-12-6	1679	3277	1,5			
7-12-6	3277	3350	1,54			
7-12-6	3350	3133	1,5			
7-12-6	3133	3632	1,51			
7-12-6	3632	3632	1,52			
7-12-7	174	634	1,1	Q-mix	17,5"	
7-12-7	634	1008	1,22	Q-mix	17,5"	
7-12-7	1008	1120	1,3	OBM	12,25"	
7-12-7	1120	1715	1,37	OBM	12,25"	

7-12-7	1715	2657	1,5	OBM	12,25"	
7-12-7	2657	2657	1,51	OBM	12,25"	
7-12-7	2657	2657	1,53	OBM	12,25"	
7-12-7	2657	2920	1,5	OBM	8,5"	
7-12-7	2920	2992	1,51	OBM	8,5"	
7-12-7	2992	3782	1,5	OBM	8,5"	
7-12-7	3782	3797	1,52	OBM	8,5"	
7-12-7	3797	3801	1,56	OBM	6"	
7-12-7	3801	3802	0,9	OBM	6"	
7-12-7	3802	3852	0,91	OBM	6"	
7-12-7	3852	3852	0,9	OBM	6"	
7-12-7	3852	3852	0,91	OBM	6"	
7-12-7	3852	3852	1,51	OBM	6"	
7-12-8	559	957	1,25	Q-mix	26"	
7-12-8	957	1026	1,3	Q-mix	26"	
7-12-8	1026	1336	1,42	KLC	17,5"	
7-12-8	1336	2031	1,52	KLC	17,5"	
7-12-8	2031	2316	1,54	KLC	17,5"	
7-12-8	2316	2350	1,55	KLC	17,5"	
7-12-8	2350	2350	1,57	KLC	17,5"	
7-12-8	2350	2350	1,6	KLC	17,5"	
7-12-8	2350	2350	1,62	KLC	17,5"	
7-12-8	2350	2350	1,63	KLC	17,5"	
7-12-8	2350	2355	1,62	KLC	12,25"	
7-12-8	2355	3030	1,58	KLC	12,25"	
7-12-8	3030	3187	1,54	KLC	12,25"	
7-12-8	3187	3629	1,56	KLC	12,25"	
7-12-8	3629	3721	1,58	KLC	12,25"	
7-12-8	3721	3724	0,95	OBM	8,5"	
7-12-8	3724	3750	0,91	OBM	8,5"	
7-12-8	3750	3765	0,92	OBM	8,5"	
7-12-8	3765	3788	0,93	OBM	8,5"	
7-12-8	3788	3788	0,94	OBM	8,5"	
7-12-8	3788	3788	0,95	OBM	8,5"	
7-12-9	122	950	1,08	WBM	24"?	
7-12-9	950	956	1,06	WBM	24"	
7-12-9	956	1147	1,2	Petrofree	17,5"	
7-12-9	1147	1416	1,41	Petrofree	17,5"	
7-12-9	1416	1812	1,5	Petrofree	17,5"	
7-12-9	1812	3677	1,55	Petrofree	17,5"	
7-12-9	3677	3721	0,93	Safemul	8,5"	
7-12-9	3721	3742	0,9	Safemul	8,5"	
7-12-9	3742	3742	0,92	Safemul	8,5"	
7-12-9	3742	3742	1,4	Safemul	6"	

7-12-9	3742	3762	1,43	Safemul	6"	
7-12-9	3762	3820	1,4	Safemul	6"	
7-12-9	3820	3820	1,41	Safemul	6"	
7-12-10	168	950	1,03	Spud mud	36" / 26"	
7-12-10	950	1024	1,4	Ancoquat	17,5"	
7-12-10	1024	1212	1,42	Ancoquat	17,5"	
7-12-10	1212	1366	1,48	Ancoquat	17,5"	
7-12-10	1366	1715	1,55	Ancoquat	17,5"	
7-12-10	1715	1903	1,58	Ancoquat	17,5"	
7-12-10	1903	2730	1,6	Ancoquat	17,5"	
7-12-10	2730	2724	1,65	Ancoquat	17,5"	
7-12-10	2724	2747	1,64	Ancoquat	17,5"	
7-12-10	2747	3667	1,55	CMHEC	12,25"	
7-12-12_S	3663	3663	1,21	WBM		
7-12-12_S	3663	3267	1,3	WBM		Plugged old well, before sidetrack
7-12-12_ST2	0	620	1,3	WBM		
7-12-12_ST2	620	737	1,4	OBM		
7-12-12_ST2	737	1085	1,42	OBM		
7-12-12_ST2	1085	1320	1,43	OBM		
7-12-12_ST2	1320	1567	1,47	OBM		
7-12-12_ST2	1567	1851	1,5	OBM		
7-12-12_ST2	1851	2498	1,506	OBM		
7-12-12_ST2	920	958	1,509	OBM		sidetrack?
7-12-12_ST2	1171	1876	1,505	OBM		
7-12-12_ST2	1876	2486	1,565	OBM		
7-12-12_ST2	2486	2486	1,56	OBM		
7-12-12_ST2	2486	2475	1,55	OBM		
7-12-12_ST2	2475	2475	1,539	OBM		
7-12-12_ST2	2475	2840	1,55	OBM		
7-12-12_ST2	2840	4005	1,601	OBM		
7-12-12_ST2	4005	4242	1,62	OBM		
7-12-12_ST2	4242	4290	1,624	OBM		
7-12-12_ST2	4290	4455	1,62	OBM		
7-12-12_ST2	4455	4490	1,63	OBM		
7-12-12_ST2	4490	4535	1,624	OBM		
7-12-12_ST2	4535	4539	1,63	OBM		
7-12-12_ST2	4539	5086	1,62	OBM		
7-12-12_ST2	5086	5126	1,624	OBM		
7-12-12_ST2	5126	5490	1,62	OBM		
7-12-12_ST2	5490	5490	1,61	OBM		
7-12-12_ST2	5490	6079	1,65	OBM		
7-12-12_ST2	6079	6079	1,66	OBM		

7-12-12_ST2	6079	5330	1,654	OBM		
7-12-12_ST2	5330	5335	1,65	OBM		
7-12-12_ST2	2605	2605	1,65	OBM		Sidetrack?
7-12-12_ST2	2314	2314	1,65	OBM		Sidetrack?
7-12-12_ST2	2314	2396	1,66	OBM		
7-12-A-1	0	577	1,1	Q-mix	24"	
7-12-A-1	577	577	1,11	Q-mix	24"	
7-12-A-1	577	577	1,13	Q-mix	24"	
7-12-A-1	577	577	1,11	Q-mix	24"	
7-12-A-1	577	793	1,15	KLC polymer	17,5"	
7-12-A-1	793	1114	1,18	KLC polymer	17,5"	
7-12-A-1	1114	1365	1,31	KLC polymer	17,5"	
7-12-A-1	1365	1698	1,39	KLC polymer	17,5"	
7-12-A-1	1698	1943	1,5	KLC polymer	17,5"	
7-12-A-1	1943	2106	1,52	KLC polymer	17,5"	
7-12-A-1	2106	2131	1,57	KLC polymer	17,5"	
7-12-A-1	2131	2253	1,59	KLC polymer	17,5"	
7-12-A-1	2253	2253	1,6	KLC polymer	17,5"	
7-12-A-1	2253	2253	1,61	KLC polymer	12,25"	
7-12-A-1	2253	2744	1,59	KLC polymer	12,25"	
7-12-A-1	2744	3127	1,6	KLC polymer	12,25"	
7-12-A-1	3127	3146	1,61	KLC polymer	12,25"	
7-12-A-1	3146	3207	1,6	KLC polymer	12,25"	
7-12-A-1	3207	3085	1,65	KLC polymer	12,25"	
7-12-A-1	3085	3584	1,55	KLC polymer	12,25"	
7-12-A-1	3584	3633	1,56	KLC polymer	12,25"	
7-12-A-1	3633	3748	1,57	KLC polymer	12,25"	
7-12-A-1	3748	3770	1,58	KLC polymer	12,25"	
7-12-A-1	3770	3770	1,59	KLC polymer	12,25"	
7-12-A-1	3770	3775	1,61	KLC polymer	12,25"	
7-12-A-1	3775	3855	1,63	KLC polymer	12,25"	
7-12-A-1	3855	3872	1,65	KLC polymer	12,25"	
7-12-A-1	3872	3875	1,64	KLC polymer	12,25"	
7-12-A-1	3875	3888	0,88	Safemul (OBM)	8,5"	Displace to OBM
7-12-A-1	3888	3930	0,87	Safemul (OBM)	8,5"	
7-12-A-1	3930	3986	0,88	Safemul (OBM)	8,5"	
7-12-A-1	3986	3986	0,89	Safemul (OBM)	8,5"	
7-12-A-1	3986	3986	0,91	Safemul (OBM)	8,5"	
7-12-A-1-A	164	630	1,39	KLC Polymer	17,5"	
7-12-A-1-A	630	924	1,41	KLC Polymer	17,5"	
7-12-A-1-A	924	1243	1,5	KLC Polymer	17,5"	
7-12-A-1-A	1243	1647	1,54	KLC Polymer	17,5"	
7-12-A-1-A	1647	1755	1,6	KLC Polymer	17,5"	
7-12-A-1-A	1755	1971	1,62	OBM	12,25"	

7-12-A-1-A	1971	2754	1,6	OBM	12,25"	
7-12-A-1-A	2754	2799	1,59	OBM	12,25"	
7-12-A-1-A	2799	2838	1,55	OBM	12,25"	
7-12-A-1-A	2838	2864	1,54	OBM	12,25"	
7-12-A-1-A	2864	2955	1,53	OBM	12,25"	
7-12-A-1-A	2955	3261	1,57	OBM	12,25"	
7-12-A-1-A	3261	3397	1,59	OBM	12,25"	
7-12-A-1-A	3397	3497	1,62	OBM	12,25"	
7-12-A-1-A	3497	3639	0,95	OBM	8,5"	
7-12-A-1-A	3639	3646	0,93	OBM	8,5"	
7-12-A-1-A	3646	3646	0,94	OBM	8,5"	
7-12-A-1-A	3646	3646	0,82	Base oil	8,5"	
7-12-A-2	283	283	1,09	KLC Polymer	17,5"	
7-12-A-2	283	342	1,06	KLC Polymer	17,5"	
7-12-A-2	342	44	1,09	KLC Polymer	17,5"	
7-12-A-2	44	362	1,11	KLC Polymer	17,5"	
7-12-A-2	362	555	1,12	KLC Polymer	17,5"	
7-12-A-2	555	560	1,13	KLC Polymer	17,5"	
7-12-A-2	560	800	1,16	KLC Polymer	17,5"	
7-12-A-2	800	1010	1,18	KLC Polymer	17,5"	
7-12-A-2	1010	1199	1,24	KLC Polymer	17,5"	
7-12-A-2	1199	1457	1,37	KLC Polymer	17,5"	
7-12-A-2	1457	1593	1,44	KLC Polymer	17,5"	
7-12-A-2	1593	1707	1,45	KLC Polymer	17,5"	
7-12-A-2	1707	1788	1,47	KLC Polymer	12,25"	
7-12-A-2	1788	3345	1,5	KLC Polymer	12,25"	
7-12-A-2	3345	3464	1,52	KLC Polymer	12,25"	
7-12-A-2	3464	3526	1,53	KLC Polymer	12,25"	
7-12-A-2	3526	3526	1,55	KLC Polymer	12,25"	
7-12-A-2	3526	3526	1,56	KLC Polymer	12,25"	
7-12-A-2	3526	3787	1,48	Sodium chloride/ CW HEC/ XCD/ Calcium Carbonate/ Barite	8,5"	
7-12-A-2	3787	3787	1,49	Sodium chloride/ CW HEC/ XCD/ calcium Carbonate/ Barite	8,5"	
7-12-A-2	3787	3787	1,48	Sodium chloride/ CW HEC/ XCD/ calcium Carbonate/ Barite	8,5"	
7-12-A-2	3787	3787	1,37	Sodium chloride/ CW HEC/ XCD/ calcium Carbonate/ Barite	8,5"	
7-12-A-2_B	2515	3402	1,65			
7-12-A-2_B	3402	4659	1,67			
7-12-A-2_B	4659	4659	1,69			
7-12-A-2_B	4659	4659	1,71			

7-12-A-2_B	4659	4659	1,73			
7-12-A-2_B	4659	4659	1,71			
7-12-A-2_B	4659	4871	1,4			
7-12-A-2_B	4871	4909	1,35			
7-12-A-2_B	4909	5374	1,33			
7-12-A-2_B	5374	5374	1,35			
7-12-A-2_B	5374	5374	1,31			
7-12-A-2_B	5374	5374	1,36			
7-12-A-3	503	575	1,12	Q-mix	24"	
7-12-A-3	575	575	1,13	Q-mix	24"	
7-12-A-3	575	575	1,12	Q-mix	24"	
7-12-A-3	575	762	1,15	KLC/Polymer	17,5"	
7-12-A-3	762	1020	1,19	KLC/Polymer	17,5"	
7-12-A-3	1020	1200	1,34	KLC/Polymer	17,5"	
7-12-A-3	1200	1458	1,42	KLC/Polymer	17,5"	
7-12-A-3	1458	1618	1,45	KLC/Polymer	17,5"	
7-12-A-3	1618	1760	1,47	KLC/Polymer	17,5"	
7-12-A-3	1760	1820	1,5	KLC/Polymer	12,5"	
7-12-A-3	1820	2128	1,51	KLC/Polymer	12,5"	
7-12-A-3	2128	2333	1,53	KLC/Polymer	12,5"	
7-12-A-3	2333	2533	1,56	KLC/Polymer	12,5"	
7-12-A-3	2533	2563	1,58	KLC/Polymer	12,5"	
7-12-A-3	2563	2655	1,62	KLC/Polymer	12,5"	
7-12-A-3	2655	3512	1,64	KLC/Polymer	12,5"	
7-12-A-3	3512	3540	1,66	KLC/Polymer	12,5"	
7-12-A-3	3540	3640	1,67	KLC/Polymer	12,5"	
7-12-A-3	3640	3736	1,69	KLC/Polymer	12,5"	
7-12-A-3	3736	3790	1,7	KLC/Polymer	12,5"	
7-12-A-3	3790	3822	1,69	KLC/Polymer	12,5"	
7-12-A-3	3822	3847	1,7	KLC/Polymer	12,5"	
7-12-A-3	3847	3864	1,58	POT.CHLORIDE/ CM HEC/XCD/CALIUM CARBONATE/BARITE	8,5"	
7-12-A-3	3864	3896	1,06	POT.CHLORIDE/ CM HEC/XCD/CALIUM CARBONATE/BARITE	8,5"	
7-12-A-3	3896	3913	1,07	POT.CHLORIDE/ CM HEC/XCD/CALIUM CARBONATE/BARITE	8,5"	
7-12-A-3	3913	3930	1,08	POT.CHLORIDE/ CM HEC/XCD/CALIUM CARBONATE/BARITE	8,5"	
7-12-A-3	3930	3930	1	POT.CHLORIDE/ CM HEC/XCD/CALIUM CARBONATE/BARITE	8,5"	

7-12-A-3	3930	3930	1,05	POT.CHLORIDE/ CM HEC/XCD/CALIUM CARBONATE/BARITE	8,5"	
7-12-A-3	3930	3930	1,07	POT.CHLORIDE/ CM HEC/XCD/CALIUM CARBONATE/BARITE	8,5"	
7-12-A-3	3930	3946	1,06	POT.CHLORIDE/ CM HEC/XCD/CALIUM CARBONATE/BARITE	8,5"	
7-12-A-3	3946	3955	1,07	POT.CHLORIDE/ CM HEC/XCD/CALIUM CARBONATE/BARITE	8,5"	
7-12-A-3	3955	3955	1,06	POT.CHLORIDE/ CM HEC/XCD/CALIUM CARBONATE/BARITE	8,5"	
7-12-A-3	3955	3942	1,07	POT.CHLORIDE/ CM HEC/XCD/CALIUM CARBONATE/BARITE	8,5"	
7-12-A-3_A	608	856	1,4	KLC polymer	17,5"	
7-12-A-3_A	856	1160	1,45	KLC polymer	17,5"	
7-12-A-3_A	1160	1452	1,51	KLC polymer	17,5"	
7-12-A-3_A	1452	1795	1,56	KLC polymer	17,5"	
7-12-A-3_A	1795	1840	1,61	KLC polymer	17,5"	
7-12-A-3_A	1840	1840	1,62	KLC polymer	17,5"	
7-12-A-3_A	1840	1923	1,18	Safemul OBM	12,25"	
7-12-A-3_A	1923	1979	1,61	Safemul OBM	12,25"	
7-12-A-3_A	1979	2072	1,6	Safemul OBM	12,25"	
7-12-A-3_A	2072	2559	1,61	Safemul OBM	12,25"	
7-12-A-3_A	2559	2982	1,6	Safemul OBM	12,25"	
7-12-A-3_A	2982	3026	1,59	Safemul OBM	12,25"	
7-12-A-3_A	3026	3662	1,55	Safemul OBM	12,25"	
7-12-A-3_A	3662	3800	1,57	Safemul OBM	12,25"	
7-12-A-3_A	3800	3970	1,59	Safemul OBM	12,25"	
7-12-A-3_A	3970	3993	1,6	Safemul OBM	12,25"	
7-12-A-3_A	3993	4014	0,91	LT WT OBM	8,5"	
7-12-A-3_A	4014	4016	0,92	LT WT OBM	8,5"	
7-12-A-3_A	4016	4025	0,91	LT WT OBM	8,5"	
7-12-A-3_A	4025	4071	0,92	LT WT OBM	8,5"	
7-12-A-3_A	4071	4088	0,9	LT WT OBM	8,5"	
7-12-A-3_A	4088	4088	0,91	LT WT OBM	8,5"	
7-12-A-3_A	4088	4088	0,92	LT WT OBM	8,5"	
7-12-A-3_B	1422	1422	1,6			
7-12-A-3_B	1422	1623	1,61			
7-12-A-3_B	1623	3197	1,6			
7-12-A-3_B	3197	3532	1,64			
7-12-A-3_B	3532	3680	1,65			

7-12-A-3_B	3680	2767	1,33			
7-12-A-3_B	2767	4835	1,49			Sidetrack? Cleaning run
7-12-A-3_B	4835	4835	1,55			
7-12-A-4	0	399	1,11	Q-Mix	24"	
7-12-A-4	399	830	1,2	Q-Mix	24"	
7-12-A-4	830	510	1,24	Q-Mix	24"	
7-12-A-4	510	830	1,27	Q-Mix	24"	
7-12-A-4	830	830	1,27	Q-Mix	24"	
7-12-A-4	0	399	1,11		17,5"	
7-12-A-4	399	830	1,2		17,5"	
7-12-A-4	830	510	1,24		17,5"	
7-12-A-4	510	830	1,27		17,5"	
7-12-A-4	830	835	1,4		17,5"	
7-12-A-4	835	965	1,43		17,5"	
7-12-A-4	965	1340	1,51		17,5"	
7-12-A-4	1340	1607	1,59		17,5"	
7-12-A-4	1607	1774	1,61		17,5"	
7-12-A-4	1774	1827	1,62		17,5"	
7-12-A-4	1827	1941	1,61		17,5"	
7-12-A-4	1941	1995	1,6		12,25"	
7-12-A-4	1995	3373	1,56		12,25"	
7-12-A-4	3373	3398	1,55		12,25"	
7-12-A-4	3398	4283	1,57		12,25"	
7-12-A-4	4283	4276	1,56		8,5"	
7-12-A-4	4276	4377	0,89		8,5"	
7-12-A-4	4377	4407	0,9		8,5"	working stuck pip
7-12-A-4	4407	4407	0,87		8,5"	
7-12-A-4	4407	4461	0,88		8,5"	
7-12-A-4	4461	4488	0,89		8,5"	Run liner
7-12-A-4	4488	4488	1,03		8,5"	Displace to packer fluid
7-12-A-5	422	748	1,1	Q-mix	24"	
7-12-A-5	748	1004	1,17	Q-mix	24"	
7-12-A-5	1004	1004	1,25	Q-mix	24"	
7-12-A-5	1004	1174	1,4	KLC Polymer	17,5"	
7-12-A-5	1174	1510	1,43	KLC Polymer	17,5"	
7-12-A-5	1510	1769	1,49	KLC Polymer	17,5"	
7-12-A-5	1769	2044	1,55	KLC Polymer	17,5"	
7-12-A-5	2044	2044	1,6	KLC Polymer	17,5"	
7-12-A-5	2044	2044	1,62	KLC Polymer	17,5"	
7-12-A-5	2044	2907	1,55	Safemul oil mud	12,25"	
7-12-A-5	2907	3821	1,6	Safemul oil mud	12,25"	

7-12-A-5	3821	3835	1,61	Safemul oil mud	12,25"	
7-12-A-5	3835	3840	1,6	Safemul oil mud	12,25"	
7-12-A-5	3840	3877	1,61	Safemul oil mud	12,25"	
7-12-A-5	3877	3969	1,6	Safemul oil mud	12,25"	
7-12-A-5	3969	4054	1,61	Safemul oil mud	12,25"	
7-12-A-5	4054	4080	1,6	Safemul oil mud	12,25"	
7-12-A-5	4080	4327	1,55	Safemul oil mud	12,25"	
7-12-A-5	4327	4484	1,56	Safemul oil mud	12,25"	
7-12-A-5	4484	4561	1,57	Safemul oil mud	12,25"	
7-12-A-5	4561	4751	1,58	Safemul oil mud	12,25"	
7-12-A-5	4751	4963	1,59	Safemul oil mud	12,25"	
7-12-A-5	4963	4963	1,6	Safemul oil mud	8,5"	
7-12-A-5	4963	5019	1,59	Safemul oil mud	8,5"	
7-12-A-5	5019	5088	0,89	Safemul oil mud	8,5"	
7-12-A-5	5088	5088	0,9	Safemul oil mud	8,5"	
7-12-A-5	5088	5088	0,91	Safemul oil mud	8,5"	
7-12-A-5_A	3422	3698	1,55	Petrofree		
7-12-A-5_A	3698	3869	1,56	Petrofree		
7-12-A-5_A	3869	3892	1,571	Petrofree		
7-12-A-5_A	3892	3933	1,58	Petrofree		
7-12-A-5_A	3933	4021	1,59	Petrofree		
7-12-A-5_A	4021	4150	1,601	Petrofree		
7-12-A-5_A	4150	4373	1,59	Petrofree		
7-12-A-5_A	4373	4392	1,601	Petrofree		
7-12-A-5_A	4392	4425	1,61	Petrofree		
7-12-A-5_A	4425	4502	1,571	Petrofree		
7-12-A-5_A	4502	4531	1,585	Petrofree		
7-12-A-5_A	4531	4633	1,571	Petrofree		
7-12-A-5_A	4633	4689	1,675	Petrofree		
7-12-A-5_A	4689	4871	1,571	Petrofree		
7-12-A-5_A	4871	5648	1,59	Petrofree		
7-12-A-5_A	5648	5648	1,601	Petrofree		
7-12-A-5_A	5648	5648	1,595	Petrofree		
7-12-A-5_A	5648	5648	1,58	Petrofree		
7-12-A-5_A	5648	5646	1,59	Petrofree		
7-12-A-5_A	5646	5648	1,595	Petrofree		
7-12-A-5_A	5648	4860	1,605	Petrofree		
7-12-A-5_A	4860	4860	1,595	Petrofree		Sidetrack?
7-12-A-5_A	4860	4875	1,59	Petrofree		
7-12-A-5_A	4875	4904	1,62	Petrofree		
7-12-A-5_A	4904	4704	1,624	Petrofree		
7-12-A-5_A	4704	4817	1,62	Petrofree		
7-12-A-5_A	4817	4870	1,63	Petrofree		
7-12-A-5_A	4870	5637	1,62	Petrofree		

7-12-A-5_A	5637	5637	1,63	Petrofree		
7-12-A-5_A	5637	5637	1,601	Petrofree		
7-12-A-5_A	5637	5760	0,94	OBM		
7-12-A-5_A	5760	5847	0,99	OBM		
7-12-A-5_A	5847	5853	1	OBM		
7-12-A-5_A	5853	5853	1,25	OBM		
7-12-A-5_A	5853	5853	1,12	OBM		
7-12-A-5_A	5853	5852	1,125	OBM		
7-12-A-5_A	5852	5852	1,13	OBM		
7-12-A-5_B	1406	4141	1,65			
7-12-A-5_B	4141	4239	1,66			
7-12-A-5_B	4239	4534	1,65			
7-12-A-5_B	4534	4606	1,63			
7-12-A-5_B	4606	5391	1,38			End of section: T2
7-12-A-5_B	4233	4482	1,65			T3
7-12-A-5_B	4482	5137	1,29			
7-12-A-5_B	5137	5137	1,31			
7-12-A-5_B	5137	5137	1,03			Completion?
7-12-A-7	334	568	1,1	Q-mix	24"	
7-12-A-7	568	568	1,14	Q-mix	24"	
7-12-A-7	568	707	1,15	Q-mix	24"/17,5"	
7-12-A-7	707	1028	1,18	KCL polymer	17,5"	
7-12-A-7	1028	1374	1,34	KCL polymer	17,5"	
7-12-A-7	1374	1524	1,45	KCL polymer	17,5"	
7-12-A-7	1524	1786	1,46	KCL polymer	17,5"	
7-12-A-7	1786	1786	1,49	KCL polymer	17,5"	
7-12-A-7	1786	2167	1,5	KCL polymer	17,5" / 12,25"	
7-12-A-7	2167	1988	1,51	KCL polymer	12,25"	
7-12-A-7	1988	2276	1,53	KCL polymer	12,25"	
7-12-A-7	2276	2276	1,56	KCL polymer	12,25"	
7-12-A-7	2276	2276	1,58	KCL polymer	12,25"	
7-12-A-7	2276	2276	1,6	KCL polymer	12,25"	
7-12-A-7	2276	1706	1,59	KCL polymer	12,25"	
7-12-A-7	1706	1838	1,6	KCL polymer	12,25"	
7-12-A-7	1838	2001	1,63	KCL polymer	12,25"	
7-12-A-7	2001	2234	1,67	KCL polymer	12,25"	
7-12-A-7	2234	2430	1,69	KCL polymer	12,25"	
7-12-A-7	2430	2734	1,68	KCL polymer	12,25"	
7-12-A-7	2734	3345	1,7	KCL polymer	12,25"	
7-12-A-7	3345	3395	1,67	KCL polymer	12,25"	
7-12-A-7	3395	3759	1,68	KCL polymer	12,25"	
7-12-A-7	3759	3759	1,67	KCL polymer	12,25"	
7-12-A-7	3759	3911	1,18	NACL polymer	8,5"	

7-12-A-7	3911	4231	1,4	NACL polymer	6"	
7-12-A-7	4231	4262	1,42	NACL polymer	6"	
7-12-A-7	4262	4262	1,85	NACL polymer	6"	
7-12-A-7	4262	4260	1,98	NACL polymer	6"	
7-12-A-7	4260	4260	1,4	NACL polymer	6"	
7-12-A-7_B	444	625	1,054			
7-12-A-7_B	625	336	1,042			
7-12-A-7_B	336	380	1,054			???
7-12-A-7_B	380	393	1,031			
7-12-A-7_B	393	625	1,042			
7-12-A-7_B	625	625	1,054			
7-12-A-7_B	625	625	1,126			
7-12-A-7_B	625	524	1,294			
7-12-A-7_B	524	642	1,45			????
7-12-A-7_B	642	691	1,426			
7-12-A-7_B	691	1063	1,498			
7-12-A-7_B	1063	2001	1,498			
7-12-A-7_B	2001	2003	1,594			
7-12-A-7_B	2003	2419	1,498			
7-12-A-7_B	2419	3180	1,594			
7-12-A-7_B	3180	3280	1,618			
7-12-A-7_B	3280	3484	1,606			
7-12-A-7_B	3484	4003	1,654			
7-12-A-7_B	4003	4003	1,666			
7-12-A-7_B	4003	4003	1,282			
7-12-A-7_B	4003	4062	1,666			
7-12-A-7_B	4062	5852	1,294			
7-12-A-7_B	5852	5852	1,318			
7-12-A-7_B	5852	5852	1,282			
7-12-A-7_B	5852	5852	1,318			
7-12-A-7_B	5852	5600	1,342			
7-12-A-7_B	5600	5600	0,827			
7-12-A-7_B	5600	5600	1,031			
7-12-A-7_C	2173	4018	1,654			
7-12-A-7_C	4018	4429	1,678			
7-12-A-7_C	4429	4429	1,63			
7-12-A-7_C	4429	4600	1,486			
7-12-A-8	268	378	1,12	Q-mix	24"	
7-12-A-8	378	502	1,13	Q-mix	24"	
7-12-A-8	502	787	1,14	Q-mix	24"	
7-12-A-8	787	810	1,16	Q-mix	24"	
7-12-A-8	810	1203	1,4	KLC Polymer	17,5"	
7-12-A-8	1203	1524	1,51	KLC Polymer	17,5"	
7-12-A-8	1524	1871	1,62	KLC Polymer	17,5"	

7-12-A-8	1871	3284	1,6	Safemul PE/FL	12,25"	
7-12-A-8	3284	4049	1,55	Safemul PE/FL	12,25"	
7-12-A-8	4049	4181	1,56	Safemul PE/FL	12,25"	
7-12-A-8	4181	4342	1,58	Safemul PE/FL	12,25"	
7-12-A-8	4342	4344	1,59	Safemul PE/FL	12,25"	
7-12-A-8	4344	4347	0,89	Safemul OBM	8,5"	
7-12-A-8	4347	4394	0,9	Safemul OBM	8,5"	
7-12-A-8_A	827	830	1,47	WBM		
7-12-A-8_A	830	836	1,63	EBM	12,25"	
7-12-A-8_A	836	1194	1,5	EBM	12,25"	
7-12-A-8_A	1194	3343	1,57	EBM	12,25"	
7-12-A-8_A	3343	3343	1,56	EBM	12,25"	
7-12-A-8_A	3343	3343	1,57	EBM	12,25"	
7-12-A-8_A	852	801	1,57	EBM	13,38"	Sidetrack?
7-12-A-8_A	801	837	1,56	EBM	13,38"	
7-12-A-8_A	60	150	1,5	EBM	14,625"	Sidetrack?
7-12-A-8_A	150	240	1,48	EBM	14,625"	
7-12-A-8_A	240	433	1,46	EBM	14,625"	
7-12-A-8_A	433	541	1,48	EBM	14,625"	
7-12-A-8_A	541	557	1,47	EBM	14,625"	
7-12-A-8_A	557	604	1,45	EBM	14,625"	
7-12-A-8_A	604	838	1,46	EBM	14,625"	
7-12-A-8_A	838	1109	1,45	EBM	17,5"	
7-12-A-8_A	1109	1112	1,52	EBM	12,25"	
7-12-A-8_A	1112	1369	1,55	EBM	12,25"	
7-12-A-8_A	1369	1525	1,59	EBM	12,25"	
7-12-A-8_A	1525	3352	1,63	EBM	12,25"	
7-12-A-8_A	3352	3870	1,55	EBM	8,5"	
7-12-A-8_A	3870	4308	1,58	EBM	8,5"	
7-12-A-8_A	4308	4308	1,6	EBM	8,5"	
7-12-A-8_A	4308	4308	1,62	EBM	8,5"	
7-12-A-8_A	4308	4308	1,12	OBM	6"	
7-12-A-8_A	4308	4311	1,13	OBM	6"	
7-12-A-8_A	4311	4290	1,12	OBM	6"	
7-12-A-8_A	4290	4361	1,15	OBM	6"	
7-12-A-8_A	4361	4449	1,12	OBM	6"	
7-12-A-8_A	4449	4449	1,13	OBM	6"	
7-12-A-8_A	4449	4449	1,14	OBM	6"	
7-12-A-8_A	4449	4449	1,06	OBM	6"	
7-12-A-9	431	705	1,17	Q-mix	24"	
7-12-A-9	705	822	1,18	Q-mix	24"	
7-12-A-9	822	822	1,17	Q-mix	24"	
7-12-A-9	822	822	1,16	Q-mix	24"	
7-12-A-9	822	986	1,4	KLC polymer	17,5"	

7-12-A-9	986	1436	1,43	KLC polymer	17,5"	
7-12-A-9	1436	1700	1,53	KLC polymer	17,5"	
7-12-A-9	1700	1915	1,62	KLC polymer	17,5"	
7-12-A-9	1915	3114	1,6	Safemul OBM	12,25"	
7-12-A-9	3114	3218	1,55	Safemul OBM	12,25"	
7-12-A-9	3218	3227	1,56	Safemul OBM	12,25"	
7-12-A-9	3227	3861	1,55	Safemul OBM	12,25"	
7-12-A-9	3861	4049	1,59	Safemul OBM	12,25"	
7-12-A-9	4049	4083	1,6	Safemul OBM	12,25"	
7-12-A-9	4083	4078	1,62	Safemul OBM	12,25"	
7-12-A-9	4078	4136	0,93	LT. WT. OBM	8,5"	
7-12-A-9	4136	4171	0,92	LT. WT. OBM	8,5"	
7-12-A-9_A	1504	3822	1,65			
7-12-A-9_A	3822	3848	1,27			
7-12-A-9_A	3848	3848	1,29			
7-12-A-9_A	3848	3923	1,31			
7-12-A-9_A	3923	3923	1,35			
7-12-A-10	126	297	1,08	Q-mix	24"	
7-12-A-10	297	550	1,11	Q-mix	24"	
7-12-A-10	550	560	1,13	Q-mix	24"	
7-12-A-10	560	560	1,11	Q-mix	24"	
7-12-A-10	560	720	1,1	Q-mix	24"	
7-12-A-10	720	800	1,2	KCL polymer	17,5"	
7-12-A-10	800	843	1,21	KCL polymer	17,5"	
7-12-A-10	843	916	1,24	KCL polymer	17,5"	
7-12-A-10	916	1142	1,31	KCL polymer	17,5"	
7-12-A-10	1142	1167	1,35	KCL polymer	17,5"	
7-12-A-10	1167	1331	1,4	KCL polymer	17,5"	
7-12-A-10	1331	1480	1,42	KCL polymer	17,5"	
7-12-A-10	1480	1685	1,43	KCL polymer	17,5"	
7-12-A-10	1685	1686	1,45	KCL polymer	17,5"	
7-12-A-10	1686	1686	1,48	KCL polymer	17,5"	
7-12-A-10	1686	2066	1,43	KCL polymer	12,25"	
7-12-A-10	2066	2207	1,45	KCL polymer	12,25"	
7-12-A-10	2207	3043	1,5	KCL polymer	12,25"	
7-12-A-10	3043	3474	1,52	KCL polymer	12,25"	
7-12-A-10	3474	3474	1,55	KCL polymer	12,25"	
7-12-A-10	3474	3535	1,53	Drilling mud?	8,5"	
7-12-A-10	3535	3710	1,48	Drilling mud?	8,5"	
7-12-A-10_A	1	2485	1,61	OBM		
7-12-A-10_A	2485	3730	1,601	OBM		
7-12-A-10_A	3730	3820	1,62	OBM		
7-12-A-10_A	3820	4450	1,65	OBM		
7-12-A-10_A	4450	4561	1,27	OBM		

7-12-A-10_A	4561	4712	1,29	OBM		
7-12-A-10_A	4712	5690	1,27	OBM		
7-12-A-10_A	5690	5690	1,29	OBM		
7-12-A-10_A	5690	5690	1,309	OBM		
7-12-A-10_A	5690	5690	1,33	OBM		
7-12-A-10_A	5690	5690	1,341	OBM		
7-12-A-10_A	5690	5690	1,1	OBM		
7-12-A-11	457	930	1,1	Benstonite spud mud	24"	Pilot hole
7-12-A-11	930	1165	1,16	Benstonite spud mud	24"	Pilot hole
7-12-A-11	1165	668	1,19	Benstonite spud mud	24"	
7-12-A-11	668	1157	1,2	Benstonite spud mud	24"	
7-12-A-11	1157	1157	1,26	Benstonite spud mud	24"	
7-12-A-11	1157	1165	1,2	Benstonite spud mud	24"	
7-12-A-11	1165	1303	1,61	Aquamul B II Ether Base mud	16"	
7-12-A-11	1303	3034	1,6	Aquamul B II Ether Base mud	16"	
7-12-A-11	3034	3274	1,62	Aquamul B II Ether Base mud	16"	
7-12-A-11	3274	3274	1,64	Aquamul B II Ether Base mud	16"	
7-12-A-11	3274	3849	1,65	Aquamul B II Ether Base mud	16"	
7-12-A-11	3849	3849	1,67	Aquamul B II Ether Base mud	16"	
7-12-A-11	3849	3849	1,62	Aquamul B II Ether Base mud	16"	
7-12-A-11	3849	4949	1,55	Aquamul B II Ether Base mud	16"/ 12,25"	
7-12-A-11	4949	5056	1,56	Aquamul B II Ether Base mud	12,25"	
7-12-A-11	5056	5072	1,55	Aquamul B II Ether Base mud	12,25"	
7-12-A-11	5072	5163	1,57	Aquamul B II Ether Base mud	12,25"	
7-12-A-11	5163	5227	1,55	Aquamul B II Ether Base mud	12,25"	
7-12-A-11	5227	5598	1,58	Aquamul B II Ether Base mud	12,25" / 8,5"	
7-12-A-11	5598	6168	1,6	Aquamul B II Ether Base mud	8,5"	
7-12-A-11	6168	6168	1,61	Aquamul B II Ether Base mud	8,5"	
7-12-A-11	6168	5882	1,6	Aquamul B II Ether Base mud	8,5"	Pack off ->Clean run
7-12-A-11	5882	5236	1,64	Aquamul B II Ether Base mud	8,5"	
7-12-A-11	5236	5505	1,66	Aquamul B II Ether Base	8,5"	sidetrack

				mud		
7-12-A-11	5505	5623	1,67	Aquamul B II Ether Base mud	8,5"	
7-12-A-11	5623	6049	1,68	Aquamul B II Ether Base mud	8,5"	
7-12-A-11	6049	6293	1,69	Aquamul B II Ether Base mud	8,5"	
7-12-A-11	6293	6293	1,71	Aquamul B II Ether Base mud	8,5"	
7-12-A-11	6293	6293	1,05	Safemul OBM	6"	
7-12-A-11	6293	6293	1,04	Safemul OBM	6"	
7-12-A-11	6293	6293	1,05	Safemul OBM	6"	
7-12-A-11	6293	6296	1,04	Safemul OBM	6"	
7-12-A-11	6296	6065	1,05	Safemul OBM	6"	
7-12-A-11	6065	6065	1,06	Safemul OBM	6"	Sidetrack
7-12-A-11	6065	6214	1,05	Safemul OBM	6"	
7-12-A-11	6214	6285	1,06	Safemul OBM	6"	
7-12-A-11	6285	6293	1,05	Safemul OBM	6"	
7-12-A-11	6293	6480	1,2	Safemul OBM	6"	
7-12-A-12	295	748	1,11	Q-mix	24"	
7-12-A-12	748	1003	1,17	Q-mix	24"	
7-12-A-12	1003	1003	1,25	Q-mix	24"	
7-12-A-12	1003	1003	1,26	Q-mix	24"	
7-12-A-12	1003	1155	1,25	KLC polymer	17,5"	
7-12-A-12	1155	1488	1,27	KLC polymer	17,5"	
7-12-A-12	1488	1902	1,32	KLC polymer	17,5"	
7-12-A-12	1902	1984	1,38	KLC polymer	17,5"	
7-12-A-12	1984	1984	1,39	KLC polymer	17,5"	
7-12-A-12	1984	1637	1,6	KLC polymer	17,5"	Stuck pipe + fishing
7-12-A-12	1637	1847	1,63	KLC polymer	17,5"	
7-12-A-12	1847	1847	1,64	KLC polymer	17,5"	
7-12-A-12	1847	2440	1,67	KLC polymer	17,5"	
7-12-A-12	2440	2440	1,69	KLC polymer	17,5"	
7-12-A-12	2440	2480	1,67	KLC polymer	12,25"	
7-12-A-12	2480	2686	1,5	KLC polymer	12,25"	
7-12-A-12	2686	2905	1,6	KLC polymer	12,25"	
7-12-A-12	2905	3125	1,63	KLC polymer	12,25"	
7-12-A-12	3125	3495	1,64	KLC polymer	12,25"	
7-12-A-12	3495	3617	1,6	KLC polymer	12,25"	
7-12-A-12	3617	3662	1,55	KLC polymer	12,25"	
7-12-A-12	3662	3739	1,59	KLC polymer	12,25"	
7-12-A-12	3739	4001	1,6	KLC polymer	12,25"	
7-12-A-12	4001	4001	1,47	KLC polymer	8,5"	
7-12-A-12	4001	4001	1,53	KLC polymer	8,5"	

7-12-A-12	4001	4001	1,03	KLC polymer	8,5"	
7-12-A-12_A	1158	1009	1,03		17,5"	
7-12-A-12_A	1009	1198	1,4		17,5"	
7-12-A-12_A	1198	1460	1,51		17,5"	
7-12-A-12_A	1460	1850	1,6		17,5"	
7-12-A-12_A	1850	2070	1,65		17,5"	
7-12-A-12_A	2070	2070	1,66		17,5"	
7-12-A-12_A	2070	2177	1,65		17,5"	
7-12-A-12_A	2177	3660	1,6		12,24"	
7-12-A-12_A	3660	3723	1,57		12,24"	
7-12-A-12_A	3723	4314	1,55		12,24"	
7-12-A-12_A	4314	4515	1,59		12,24"	
7-12-A-12_A	4515	4532	1,63		12,24"	
7-12-A-12_A	4532	4532	0,89		12,24"	
7-12-A-12_A	4532	4549	0,92		8,5"	
7-12-A-12_A	4549	4612	0,91		8,5"	
7-12-A-12_A	4612	4655	0,9		8,5"	
7-12-A-12_A	4655	4655	0,91		8,5"	
7-12-A-13	670	827	1,16	Q-mix	24"	
7-12-A-13	827	827	1,19	Q-mix	24"	
7-12-A-13	827	827	1,17	Q-mix	24"	
7-12-A-13	827	1031	1,4	KLC polymer	17,5"	
7-12-A-13	1031	1320	1,44	KLC polymer	17,5"	
7-12-A-13	1320	1622	1,5	KLC polymer	17,5"	
7-12-A-13	1622	1840	1,58	KLC polymer	17,5"	
7-12-A-13	1840	2088	1,62	KLC polymer	17,5"	
7-12-A-13	2088	3783	1,66	KLC polymer	17,5"/12,25"	
7-12-A-13	3783	3823	1,65		12,25"	
7-12-A-13	3823	4646	1,55		12,25"	
7-12-A-13	4646	4753	1,56		12,25"	
7-12-A-13	4753	5016	1,59		12,25"	
7-12-A-13	5016	5020	1,6		12,25"/ 8,5"	
7-12-A-13	5020	5047	0,91	0,915. G. OBM	8,5"	
7-12-A-13	5047	5053	0,9	0,915. G. OBM	8,5"	
7-12-A-13	5053	5066	0,92	0,915. G. OBM	8,5"	
7-12-A-13	5066	5098	0,93	0,915. G. OBM	8,5"	
7-12-A-13	5098	5098	0,91	0,915. G. OBM	8,5"	
7-12-A-13	5098	5111	0,92	0,915. G. OBM	8,5"	
7-12-A-13	5111	5124	0,91	0,915. G. OBM	8,5"	
7-12-A-13_A	2104	3368	1,6	Safemul OBM	12,5"	
7-12-A-13_A	3368	3458	1,62	Safemul OBM	12,5"	
7-12-A-13_A	3458	3488	1,56	Safemul OBM	12,5"	
7-12-A-13_A	3488	3982	1,55	Safemul OBM	12,5"	
7-12-A-13_A	3982	4005	1,56	Safemul OBM	12,5"	

7-12-A-13_A	4005	4030	1,57	Safemul OBM	12,5"	
7-12-A-13_A	4030	4226	1,58	Safemul OBM	12,5"	
7-12-A-13_A	4226	4226	1,59	Safemul OBM	12,5"	
7-12-A-13_A	4226	4379	1,6	Safemul OBM	12,5"	
7-12-A-13_A	4379	4405	0,9	LT. WT. OBM	8,5"	
7-12-A-13_A	4405	4473	0,92	LT. WT. OBM	8,5"	
7-12-A-13_A	4473	4473	0,93	LT. WT. OBM	8,5"	
7-12-A-14	275	456	1,13	Spud	24"	
7-12-A-14	456	665	1,19	Spud	24"	
7-12-A-14	665	956	1,2	Spud	24"	
7-12-A-14	956	956	1,18	Spud	24"	
7-12-A-14	956	956	1,2	Spud	24"	
7-12-A-14	956	1510	1,4	ANCO 2000	17,5"	
7-12-A-14	1510	1859	1,59	ANCO 2000	17,5"	
7-12-A-14	1859	2593	1,63	ANCO 2000	17,5"	
7-12-A-14	2593	2630	1,64	ANCO 2000	17,5"	
7-12-A-14	2630	2630	1,65	ANCO 2000	17,5"	
7-12-A-14	2630	2630	1,64	ANCO 2000	12,25"	
7-12-A-14	2630	3307	1,55	ANCO 2000	12,25"	
7-12-A-14	3307	3366	1,54	ANCO 2000	12,25"	
7-12-A-14	3366	3388	1,55	ANCO 2000	12,25"	
7-12-A-14	3388	3460	1,54	ANCO 2000	12,25"	
7-12-A-14	3460	3508	1,57	ANCO 2000	12,25"	
7-12-A-14	3508	3552	1,58	ANCO 2000	12,25"	
7-12-A-14	3552	3552	1,59	ANCO 2000	12,25"	
7-12-A-14	3552	3552	1,6	ANCO 2000	12,25"	
7-12-A-14	3552	3552	1,59	ANCO 2000	12,25"	
7-12-A-14	3552	3552	1,58	ANCO 2000	12,25"	
7-12-A-14	3552	3552	1,59	ANCO 2000	12,25"	
7-12-A-14	3552	3552	1,68	ANCO 2000	12,25"	
7-12-A-14	3552	3552	1,78	ANCO 2000	12,25"	
7-12-A-14	3552	3583	1,3	ANCO 2000	12,25"	
7-12-A-14	3583	3592	0,95	Safemul OBM	8,5"	
7-12-A-14	3592	3691	0,96	Safemul OBM	8,5"	
7-12-A-14	3691	3691	1	Safemul OBM	8,5"	
7-12-A-14_A	2495	2495	1,618			
7-12-A-14_A	2495	2495	1,63			
7-12-A-14_A	2495	2495	1,618			
7-12-A-14_A	2495	2495	1,63			
7-12-A-14_A	2495	2495	1,618			
7-12-A-14_A	2495	2495	1,63			
7-12-A-14_A	2495	2529	1,618			
7-12-A-14_A	2529	2432	1,63			?
7-12-A-14_A	2432	2963	1,558			

7-12-A-14_A	2963	3063	1,606			
7-12-A-14_A	3063	3809	1,642			
7-12-A-14_A	3809	3802	1,594			
7-12-A-14_A	3802	4137	1,282			
7-12-A-14_A	4137	4531	1,222			
7-12-A-14_A	4531	4531	1,246			
7-12-A-14_A	4531	4531	1,21			
7-12-A-14_A	4531	4531	1,234			
7-12-A-14_A	4531	4531	1,222			
7-12-A-14_A	4531	4531	1,234			
7-12-A-14_A	4531	4531	1,222			
7-12-A-15	595	803	1,15	Q-mix	24"	
7-12-A-15	803	1047	1,17	Q-mix	24"	
7-12-A-15	1047	1445	1,45	KLC Polymer	17,5"	
7-12-A-15	1445	1832	1,6	KLC Polymer	17,5"	
7-12-A-15	1832	1891	1,65	KLC Polymer	17,5"	
7-12-A-15	1891	2787	1,62	Safemul OBM	12,5"	
7-12-A-15	2787	3172	1,55	Safemul OBM	12,5"	
7-12-A-15	3172	3237	1,56	Safemul OBM	12,5"	
7-12-A-15	3237	3390	1,57	Safemul OBM	12,5"	
7-12-A-15	3390	3501	1,59	Safemul OBM	12,5"	
7-12-A-15	3501	3503	1,61	Safemul OBM	8,5"	
7-12-A-15	3503	3555	0,95	Safemul OBM	8,5"	
7-12-A-15	3555	3596	0,91	Safemul OBM	8,5"	
7-12-A-15	3596	3665	0,9	Safemul OBM	8,5"	
7-12-A-15	3665	3668	0,94	Safemul OBM	8,5"	
7-12-A-15	3668	3882	1,42	Safemul OBM	6"	
7-12-A-15	3882	3882	1,43	Safemul OBM	6"	
7-12-A-15	3882	3882	1,42	Safemul OBM	6"	
7-12-A-15	3882	3659	1,43	Safemul OBM	6"	
7-12-A-15	3659	3659	1,435	Safemul OBM	6"	
7-12-A-15	3659	3659	0,83	Safemul OBM	6"	
7-12-A-16	274	786	1,12	Q-mix spud mud	24"	
7-12-A-16	786	809	1,16	Q-mix spud mud	24"	
7-12-A-16	809	809	1,2	Q-mix spud mud	24"	
7-12-A-16	809	1114	1,4	ANCO 2000	17,5"	
7-12-A-16	1114	1450	1,58	ANCO 2001	17,5"	
7-12-A-16	1450	1626	1,62	ANCO 2002	17,5"	
7-12-A-16	1626	1937	1,63	ANCO 2003	17,5"	
7-12-A-16	1937	2146	1,67	ANCO 2004	17,5"	
7-12-A-16	2146	2149	1,69	ANCO 2005	17,5"	
7-12-A-16	2149	3932	1,55	Aquamuk EBM	12,25"	
7-12-A-16	3932	4077	1,57	Aquamuk EBM	12,25"	
7-12-A-16	4077	4077	1,59	Aquamuk EBM	12,25"	

7-12-A-16	4077	4750	1,6	Aquamuk EBM	12,25"	
7-12-A-16	4750	4887	1,62	Aquamuk EBM	12,25"	
7-12-A-16	4887	5088	1,63	Aquamuk EBM	12,25"	
7-12-A-16	5088	5088	1,64	Aquamuk EBM	12,25"	
7-12-A-16	5088	5088	1,63	Aquamuk EBM	12,25"	
7-12-A-16	5088	5088	1,64	Aquamuk EBM	12,25"	
7-12-A-16	5088	5088	1,02	Safemul OBM	8,5"	
7-12-A-16	5088	5088	1,03	Safemul OBM	8,5"	
7-12-A-16	5088	5088	1,51	Safemul OBM	8,5"	
7-12-A-16	5088	5088	1,56	Safemul OBM	8,5"	
7-12-A-16	5088	5096	1,1	Safemul OBM	8,5"	
7-12-A-16	5096	5126	1,05	Safemul OBM	8,5"	
7-12-A-16	5126	5222	1	Safemul OBM	8,5"	
7-12-A-16	5222	5222	1,04	Safemul OBM	8,5"	
7-12-A-16_A	2142	2142	1,049	WBM		
7-12-A-16_A	2142	2212	1,601	WBM		
7-12-A-16_A	2212	2212	1,65	WBM		
7-12-A-16_A	2212	2142	1,7	WBM		
7-12-A-16_A	2142	2142	1,69	WBM		
7-12-A-16_A	2142	2285	1,601	OBM		
7-12-A-16_A	2285	3531	1,65	OBM		
7-12-A-16_A	3531	3571	1,66	OBM		
7-12-A-16_A	3571	3825	1,65	OBM		
7-12-A-16_A	3825	4386	1,601	OBM		
7-12-A-16_A	4386	4388	1,63	OBM		
7-12-A-16_A	4388	4391	1,65	OBM		
7-12-A-16_A	4391	4391	1,019	OBM		
7-12-A-16_A	4391	4521	1,081	OBM		
7-12-A-16_A	4521	4520	1,12	OBM		
7-12-A-16_A	4520	4520	1,18	OBM		
7-12-A-17	427	751	1,13	Spud	24"	
7-12-A-17	751	810	1,17	Spud	24"	
7-12-A-17	810	1165	1,14	KCL polymer	17,5"	
7-12-A-17	1165	1435	1,51	KCL polymer	17,5"	
7-12-A-17	1435	1692	1,6	KCL polymer	17,5"	
7-12-A-17	1692	1973	1,65	KCL polymer	17,5"	
7-12-A-17	1973	2216	1,7	KCL polymer	17,5"	
7-12-A-17	2216	4501	1,6	Safemul OBM	12,25"	
7-12-A-17	4501	4687	1,55	Safemul OBM	12,25"	
7-12-A-17	4687	4687	1,56	Safemul OBM	12,25"	
7-12-A-17	4687	4687	1,6	Safemul OBM	12,25"	
7-12-A-17	4687	2961	1,64	Safemul OBM	12,25"	Stuck
7-12-A-17	2961	2811	1,64	Safemul OBM	12,25"	Sidetrack
7-12-A-17	2811	4191	1,65	Safemul OBM	12,25"	

7-12-A-17	4191	2372	1,65	Safemul OBM	12,25"	Stuck + Sidetrack
7-12-A-17	2372	3956	1,65	Safemul OBM	12,25"	
7-12-A-17	3956	4381	1,68	Safemul OBM	12,25"	
7-12-A-17	4381	4408	1,56	OBM	8,5"	
7-12-A-17	4408	5205	1,55	OBM	8,5"	
7-12-A-17	5205	5361	1,57	OBM	8,5"	
7-12-A-17	5361	5361	1,7	OBM	8,5"	
7-12-A-17	5361	4250	1,72	OBM	8,5"	Shut down period + power loss
7-12-A-17	4250	5250	1,55	OBM	8,5"	Resulted in stuck and lost circulation
7-12-A-17	5250	5397	1,6	OBM	8,5"	Sidetrack
7-12-A-17	5397	5456	1,61	OBM	8,5"	
7-12-A-17	5456	5536	0,85	OBM	6"	
7-12-A-17	5536	5536	0,86	OBM	6"	
7-12-A-17	5536	5536	0,87	OBM	6"	
7-12-A-17	5536	5536	0,89	OBM	6"	
7-12-A-17	5536	5523	0,92	OBM	6"	
7-12-A-17	5523	5523	0,91	OBM	6"	
7-12-A-17_A	4037	5098	1,6			
7-12-A-17_A	5098	5207	1,62			
7-12-A-17_A	5207	5098	1,68			
7-12-A-17_A	5098	5215	1,69			
7-12-A-17_A	5215	5220	1,68			
7-12-A-17_A	5220	5474	1,72			
7-12-A-17_A	5474	5680	1,73			
7-12-A-17_A	5680	5680	1,7			
7-12-A-17_A	5680	5711	1,3			
7-12-A-17_A	5711	5711	1,47			
7-12-A-17_A	5711	5711	1,3			
7-12-A-17_A	5711	5711	1,47			
7-12-A-17_A	5711	5729	1,43			
7-12-A-17_A	5729	5729	1,44			
7-12-A-17_A	5729	5759	1,42			
7-12-A-17_A	5759	5759	1,43			
7-12-A-17_A	5759	5759	1,44			
7-12-A-17_A	5759	5803	1,43			
7-12-A-17_A	5803	5936	1,42			
7-12-A-17_A	5936	5975	1,4			
7-12-A-17_A	5975	5975	1,41			
7-12-A-17_A	5975	6042	1,4			
7-12-A-17_A	6042	6042	1,42			

7-12-A-17_A	6042	6042	1,43			
7-12-A-17_A	6042	6061	1,4			
7-12-A-17_A	6061	6180	1,41			
7-12-A-17_A	6180	6477	1,42			
7-12-A-17_A	6477	6477	1,4			
7-12-A-17_A	6477	6477	1,46			
7-12-A-17_A	6477	6477	1,45			
7-12-A-17_B	1762	3733	1,65			
7-12-A-17_B	3733	3948	1,6			
7-12-A-17_BT2	3948	4489	1,65			T2
7-12-A-17_BT2	4489	4495	1,64			
7-12-A-17_BT2	4495	4926	1,35			
7-12-A-17_BT2	4926	4926	1,34			
7-12-A-17_BT2	4926	4926	1,43			
7-12-A-17_BT2	4926	5841	1,38			

Appendix C: Leak-off inversion technique results

Simulations done in section 18 5/8":

Group I:

Simulation 1:

Well pressure and survey data					
Well #	**Pwf (s.g)**	**Po (s.g)**	**Overb (s.g)**	**Inc. (deg.)**	**Azim. (deg.)**
7/12-8	1,63	0,9685	1,861	0,09	123,1
7/12-9	1,77	0,969	1,863	0,17	174,87
A0 5A_T2	1,7	0,967	1,852	35,17	126,5
A 16	1,99	0,9578	1,818	13,36	136,12
A 12A	1,78	0,978	1,877	34,85	152,54
A 5	1,7	0,9687	1,8615	55,17	126,28

Inversion result			
σ1 (s.g.)	σ2 (s.g.)	Dirn, β (deg.)	Σerror²
1,3565323	1,412640241	328	0,030771

Analysis- Linear elastic					
Well	**σx (s.g.)**	**σy (s.g.)**	**Predicted -LOP**	**Measured-LOP**	**Difference**
7/12-8	1,364526695	1,402693919	1,875	1,630	0,245055063
7/12-9	1,357000926	1,412191647	1,910574016	1,770	0,140574016
A0 5A_T2	1,545051721	1,376384075	1,617100506	1,700	0,082899494
A 16	1,406730298	1,385682766	1,792517999	1,990	0,197482001
A 12A	1,534411495	1,400709435	1,689716811	1,780	0,090283189
A 5	1,708476208	1,376178294	1,451358674	1,700	0,248641326

Stress ratio		
Sigma1/Sigma2	Sigm1/Sigv	Sigm1/Sig v
0,9602815	0,731120029	0,761360112

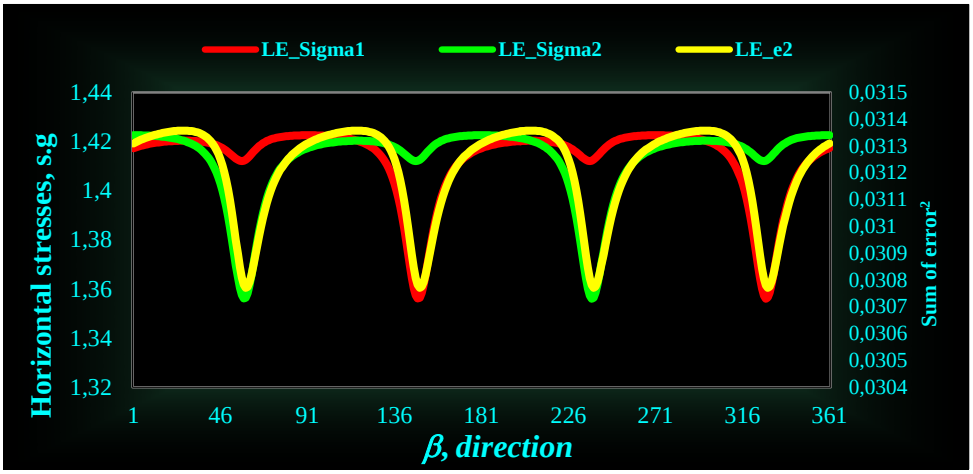

Simulation 2:

Well pressure and survey data					
Well #	**Pwf (s.g)**	**Po (s.g)**	**Overb (s.g)**	**Inc. (deg.)**	**Azim(deg.)**
7/12-8	1,63	0,9685	1,861	0,09	123,1
7/12-9	1,77	0,969	1,863	0,17	174,87
A0 5A_T2	1,7	0,967	1,852	35,17	126,5
A 16	1,99	0,9578	1,818	13,36	136,12
A 5	1,7	0,9687	1,8615	55,17	126,28

Inversion result			
σ1 (s.g.)	σ2 (s.g.)	Dirn, β (deg.)	Σerror²
1,3908	1,410703879	317	0,029662799

Analysis- Linear elastic					
Well	**σx (s.g.)**	**σy (s.g.)**	**Predicted -LOP**	**Measured-LOP**	**Difference**
7/12-8	1,391955675	1,409572423	1,868261594	1,63	-0,238261594
7/12-9	1,39834325	1,403187777	1,842220082	1,77	-0,072220082
A0 5A_T2	1,544131082	1,410055598	1,719035711	1,7	-0,019035711
A 16	1,422673556	1,401128068	1,822910649	1,99	0,167089351
A 5	1,711974713	1,397763077	1,512614517	1,7	0,187385483

Stress ratio		
Sigma1/Sigma2	Sigm1/Sigv	Sigm1/Sig v
0,9859072	0,751349501	0,762089503

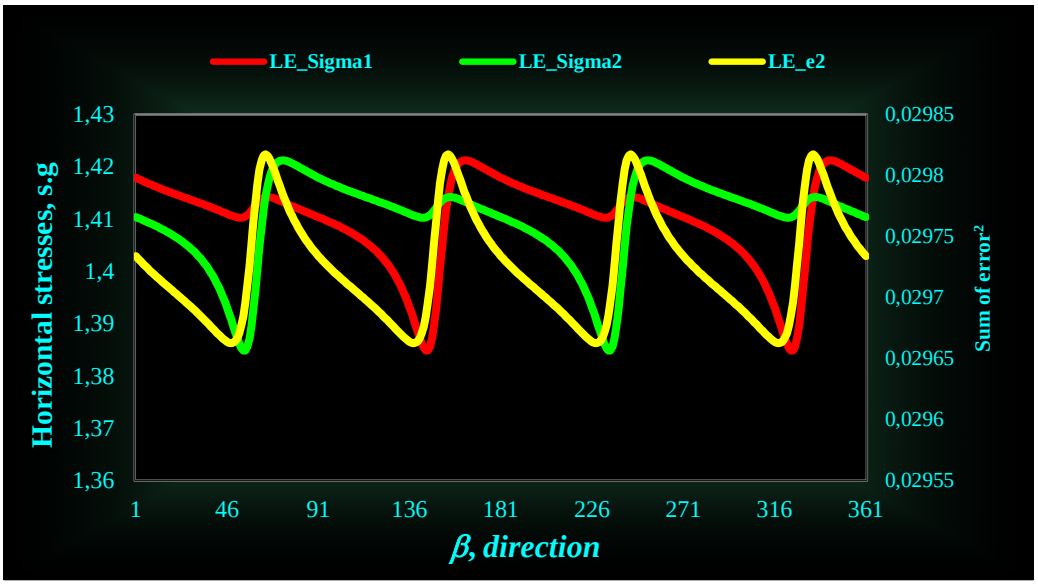

Group II:

Simulation 3:

Well pressure and survey data					
Well #	**Pwf (s.g)**	**Po (s.g)**	**Overb (s.g)**	**Inc. (deg.)**	**Azim(deg.)**
A 4	1,75	0,9582	1,8208	26,9	103,73
A 1	1,61	0,949	1,795	3,44	344,96
A 9	1,86	0,958	1,8205	26,47	71,1
A 03A	1,75	0,96	1,83	15,89	66,04
A 8	1,79	0,9573	1,817	19,81	51,05

Inversion result			
σ1 (s.g.)	σ2 (s.g.)	Dirn, β (deg.)	Σerror²
1,3982	1,317890544	356	0,003933235

Analysis- Linear elastic					
Well	**σx (s.g.)**	**σy (s.g.)**	**Predicted -LOP**	**Measured-LOP**	**Difference**
A 4	1,426748431	1,39067923	1,787089258	1,75	-0,037089258
A 1	1,396729057	1,320833818	1,616772396	1,61	-0,006772396
A 9	1,421829722	1,393022756	1,799238545	1,86	0,060761455
A 03A	1,36853127	1,384949767	1,826318032	1,75	-0,076318032
A 8	1,403299253	1,366447935	1,738744553	1,79	0,051255447

Stress ratio		
Sigma1/Sigma2	Sigm1/Sigv	Sigm1/Sig v
1,0609642	0,769673291	0,725446998

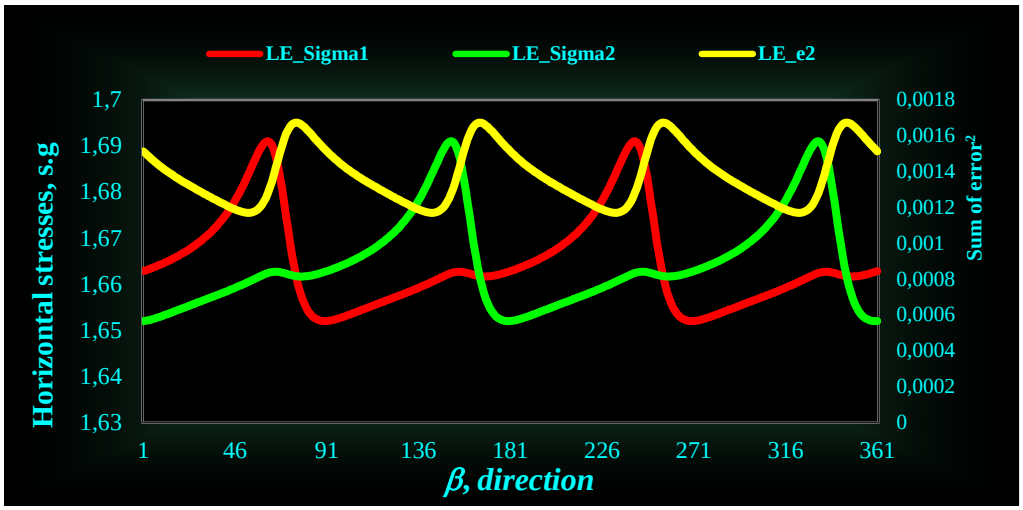

Simulation 4:

Well pressure and survey data					
Well #	**Pwf (s.g)**	**Po (s.g)**	**Overb (s.g)**	**Inc. (deg.)**	**Azim(deg.)**
A 4	1,75	0,9582	1,8208	26,9	103,73
A 1	1,61	0,949	1,795	3,44	344,96
A 9	1,86	0,958	1,8205	26,47	71,1
A 03A	1,75	0,96	1,83	15,89	66,04

Inversion result			
σ1 (s.g.)	σ2 (s.g.)	Dirn, β (deg.)	Σerror²
1,3967	1,30968387	1	0,003344192

Analysis- Linear elastic					
Well	**σx (s.g.)**	**σy (s.g.)**	**Predicted -LOP**	**Measured-LOP**	**Difference**
A 4	1,41754524	1,39254143	1,801879055	1,75	-0,051879055
A 1	1,39140391	1,316471244	1,609009824	1,61	0,000990176
A 9	1,41918594	1,386614301	1,78265696	1,86	0,07734304
A 03A	1,36196504	1,382340592	1,82505674	1,75	-0,07505674

Stress ratio		
Sigma1/Sigma2	Sigm1/Sigv	Sigm1/Sig v
1,0664668	0,76888343	0,720963279

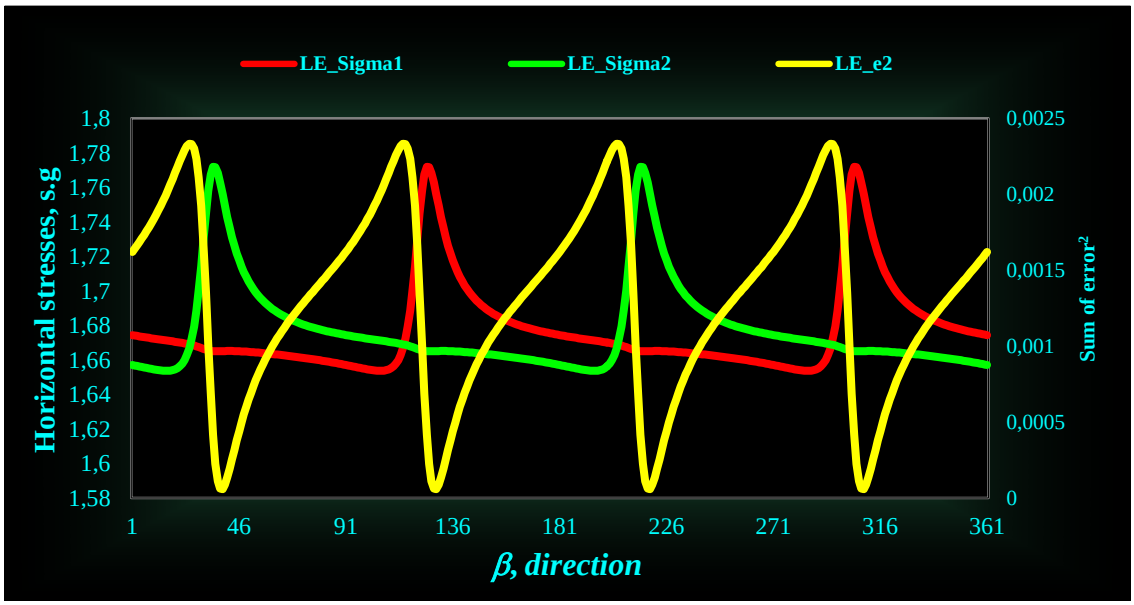

Simulation 5:

Well pressure and survey data					
Well #	**Pwf (s.g)**	**Po (s.g)**	**Overb (s.g)**	**Inc. (deg.)**	**Azim(deg.)**
A 1	1,61	0,949	1,795	3,44	344,96
A 9	1,86	0,958	1,8205	26,47	71,1
A 03A	1,75	0,96	1,83	15,89	66,04

Inversion result			
σ1 (s.g.)	σ2 (s.g.)	Dirn, β (deg.)	Σerror²
1,619481832	1,15723441	22	4,58279E-06

Analysis- Linear elastic					
Well	**σx (s.g.)**	**σy (s.g.)**	**Predicted -LOP**	**Measured-LOP**	**Difference**
A 1	1,45172205	1,326233334	1,577977956	1,61	0,03202204
A 9	1,44787046	1,421124271	1,857502352	1,86	0,00249765
A 03A	1,42876188	1,38043452	1,752541683	1,75	-0,0025417

Stress ratio		
Sigma1/Sigma2	Sigm1/Sigv	Sigm1/Sig v
1,399441479	0,89219456	0,637536172

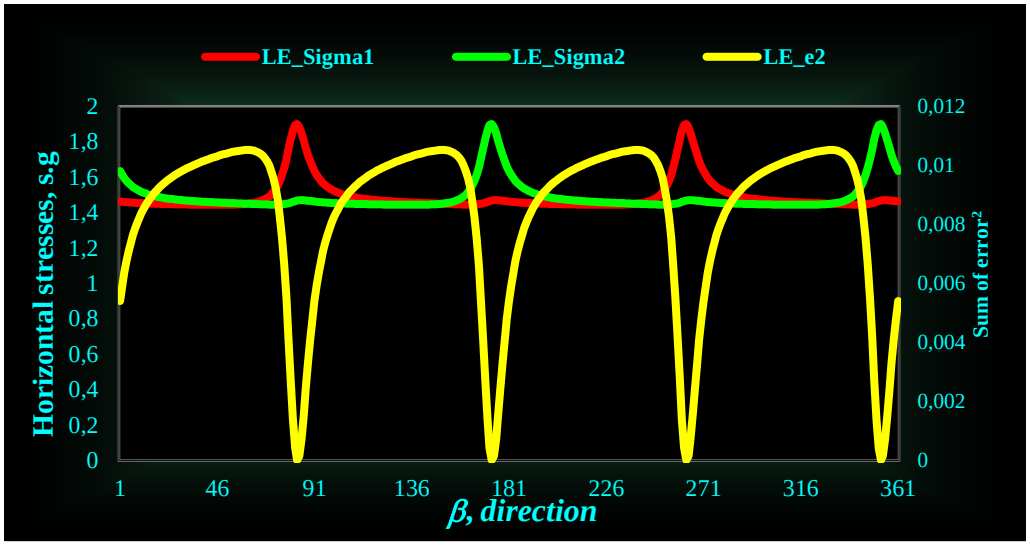

Group III:

Simulation 6:

Well pressure and survey data					
Well #	**Pwf (s.g)**	**Po (s.g)**	**Overb (s.g)**	**Inc. (deg.)**	**Azim(deg.)**
A 2	1,7	0,926	1,711	1,1	347,9
A 18	1,6	0,925	1,71	4,52	173,19
A 12	1,71	0,968	1,86	32,12	167,68
A 10	1,59	0,927	1,713	3,29	75,79
A 01A	1,75	0,93	1,72	3,88	167,14
A 15	1,91	0,9573	1,817	2,98	282,24
A 14	1,88	0,965	1,85	16,67	287,79

Inversion result			
σ1 (s.g.)	σ2 (s.g.)	Dirn, β (deg.)	$\Sigma error^2$
1,223272	1,384242	129	0,011256032

Analysis- Linear elastic					
Well	**σx (s.g.)**	**σy (s.g.)**	**Predicted -LOP**	**Measured-LOP**	**Difference**
A 2	1,284286	1,320765164	1,752	1,700	0,052009499
A 18	1,228599	1,381978309	1,992335989	1,600	0,392335989
A 12	1,408441	1,376913102	1,754297884	1,710	0,044297884
A 10	1,375604	1,232971609	1,396310691	1,590	0,193689309
A 01A	1,233585	1,376267639	1,965218347	1,750	0,215218347
A 15	1,37836	1,230506881	1,355860948	1,910	0,554139052
A 14	1,408957	1,238297988	1,340936578	1,880	0,539063422

Stress ratio		
Sigma1/Sigma2	Sigm1/Sigv	Sigm1/Sig v
0,883713	0,691616	0,782625915

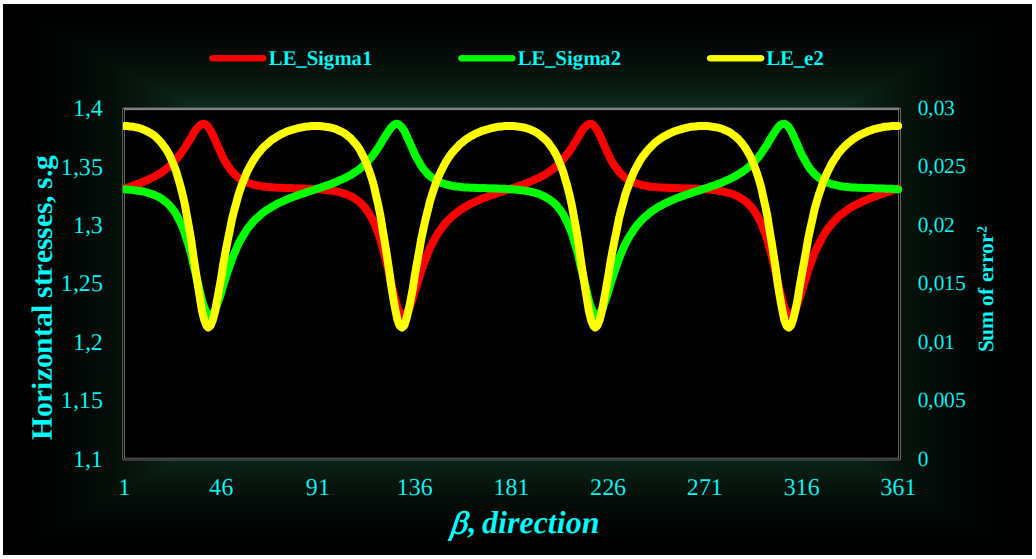

Simulation 7:

Well pressure and survey data					
Well #	**Pwf (s.g)**	**Po (s.g)**	**Overb (s.g)**	**Inc. (deg.)**	**Azim(deg.)**
A 2	1,7	0,926	1,711	1,1	347,9
A 18	1,6	0,925	1,71	4,52	173,19
A 10	1,59	0,927	1,713	3,29	75,79
A 01A	1,75	0,93	1,72	3,88	167,14

Inversion result			
σ1 (s.g.)	σ2 (s.g.)	Dirn, β (deg.)	Σerror²
1,1463	1,45563402	305	0,000272705

Analysis- Linear elastic					
Well	**σx (s.g.)**	**σy (s.g.)**	**Predicted -LOP**	**Measured-LOP**	**Difference**
A 2	1,2896575	1,312394342	1,721525531	1,7	-0,021525531
A 18	1,32092484	1,283400812	1,604277592	1,6	-0,004277592
A 10	1,32426112	1,278918806	1,585495299	1,59	0,004504701
A 01A	1,16434056	1,440109465	2,225987831	1,75	-0,475987831

Stress ratio		
Sigma1/Sigma2	Sigm1/Sigv	Sigm1/Sig v
0,7874662	0,66895981	0,849509203

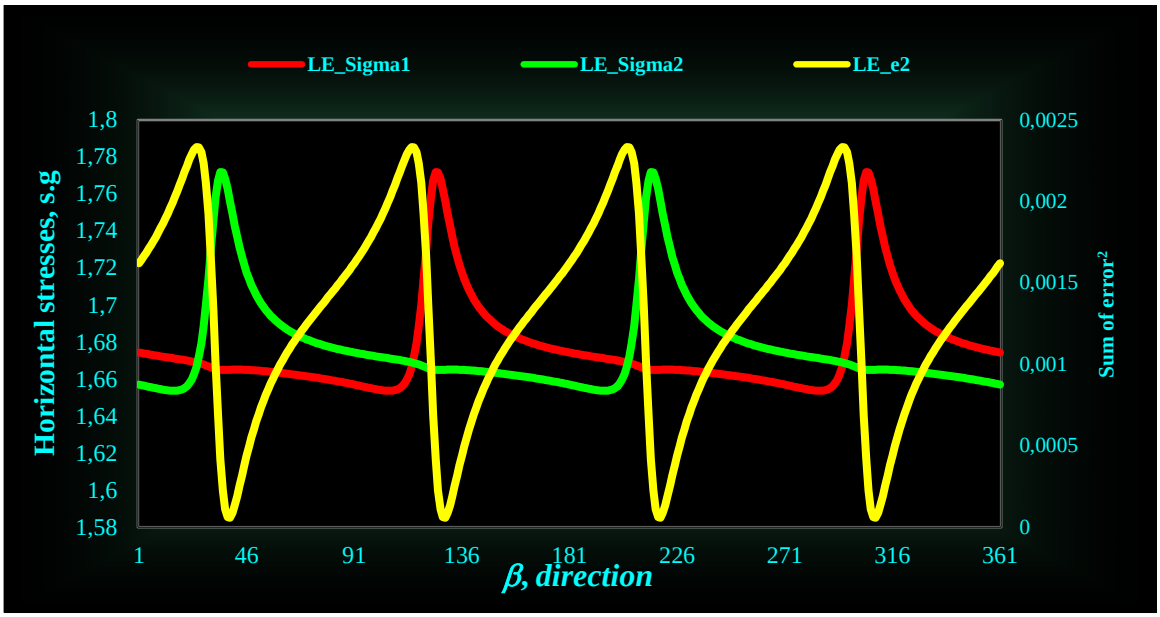

Simulations done in section 13 3/8":

Group I:

Simulation 8:

Well pressure and survey data					
Well #	**Pwf (s.g)**	**Po (s.g)**	**Overb (s.g)**	**Inc. (deg.)**	**Azim(deg.)**
7/12-8	1,97	1,432	1,981	0,53	134,49
7/12-9	2,13	1,432	1,981	1,16	36,5
A 05A_T2	1,76	1,3781	1,941	45,99	118,73
A 16	1,95	1,382	1,943	50,22	133,94
A 12A	1,82	1,385	1,943	46,68	144,65
A5	1,76	1,3783	1,941	45,9	118,73

Inversion result			
σ1 (s.g.)	σ2 (s.g.)	Dirn, β (deg.)	Σerror²
1,662323	1,763584504	10	0,006652983

Analysis- Linear elastic					
Well	**σx (s.g.)**	**σy (s.g.)**	**Predicted -LOP**	**Measured-LOP**	**Difference**
7/12-8	1,732948436	1,694792809	1,919	1,970	0,05057001
7/12-9	1,698235294	1,727756748	2,05303495	2,130	0,07696505
A 05A_T2	1,84402445	1,685720058	1,835035722	1,760	0,075035722
A 16	1,84953594	1,711080787	1,901706422	1,950	0,048293578
A 12A	1,826797507	1,729687941	1,977266316	1,820	0,157266316
A5	1,843709478	1,685720058	1,835150694	1,760	0,075150694

Stress ratio		
Sigma1/Sigma2	Sigm1/Sigv	Sigm1/Sig v
0,942582	0,85029309	0,90208926

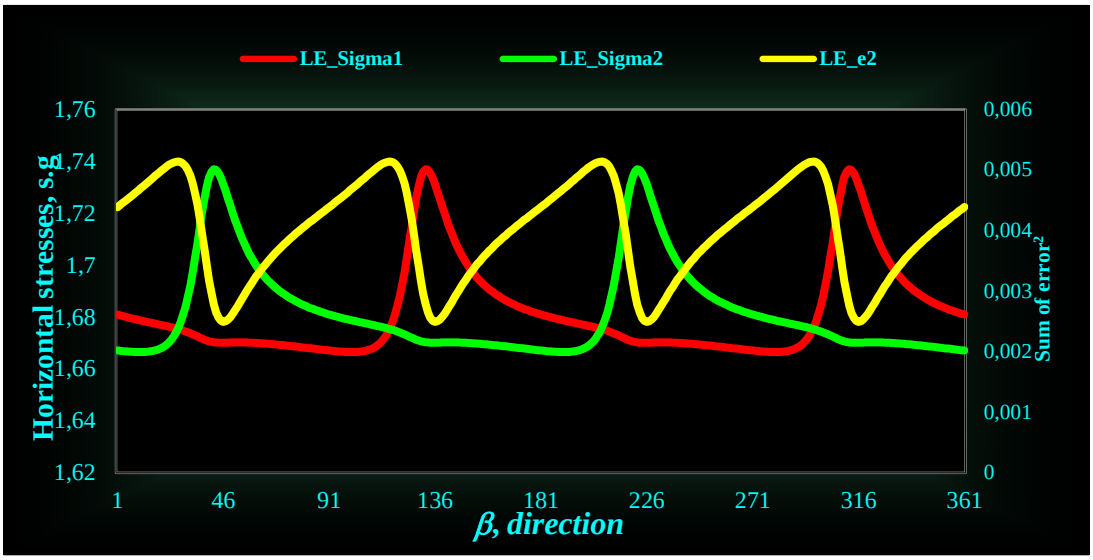

Simulation 9:

Well pressure and survey data					
Well #	**Pwf (s.g)**	**Po (s.g)**	**Overb (s.g)**	**Inc. (deg.)**	**Azim(deg.)**
7/12-8	1,97	1,432	1,981	0,53	134,49
7/12-9	2,13	1,432	1,981	1,16	36,5
A0 5A_T2	1,76	1,3781	1,941	45,99	118,73
A 16	1,95	1,382	1,943	50,22	133,94
A5	1,76	1,3783	1,941	45,9	118,73

Inversion result			
σ1 (s.g.)	σ2 (s.g.)	Dirn, β (deg.)	Σerror²
1,6197	1,825034147	0	0,000568745

Analysis- Linear elastic					
Well	**σx (s.g.)**	**σy (s.g.)**	**Predicted -LOP**	**Measured-LOP**	**Difference**
7/12-8	1,724447911	1,720281607	2,004396909	1,97	-0,034396909
7/12-9	1,692387758	1,752438041	2,132926367	2,13	-0,002926367
A0 5A_T2	1,862136583	1,666941486	1,760587875	1,76	-0,000587875
A 16	1,854228037	1,718312189	1,918708528	1,95	0,031291472
A5	1,861880439	1,666941486	1,76064402	1,76	-0,00064402

Stress ratio		
Sigma1/Sigma2	Sigm1/Sigv	Sigm1/Sig v
0,8874757	0,827461653	0,932376697

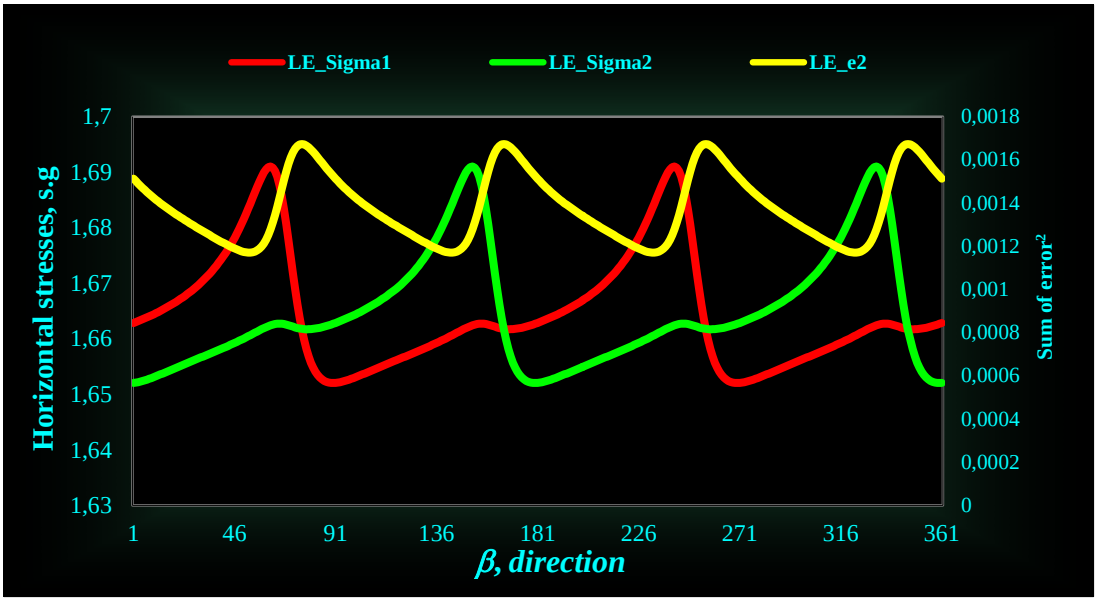

Group II:

Simulation 10:

Well pressure and survey data					
Well #	**Pwf (s.g)**	**Po (s.g)**	**Overb (s.g)**	**Inc. (deg.)**	**Azim(deg.)**
A 4	1,96	1,382	1,942	32,79	103,79
A 1	1,8	1,417	1,967	27,82	84,58
A 9	1,88	1,386	1,943	27,48	73,05
A 03A	1,9	1,385	1,943	25,22	48,18
A 8	1,83	1,381	1,942	31,82	32,73

Inversion result			
σ1 (s.g.)	σ2 (s.g.)	Dirn, β (deg.)	Σerror²
1,6607	1,684364326	322	0,001170552

Analysis- Linear elastic					
Well	**σx (s.g.)**	**σy (s.g.)**	**Predicted -LOP**	**Measured-LOP**	**Difference**
A 4	1,74948034	1,675339962	1,894539548	1,96	0,065460452
A 1	1,740453494	1,667579237	1,845284215	1,8	-0,045284215
A 9	1,736947974	1,663754175	1,868314551	1,88	0,011685449
A 03A	1,722641561	1,671209881	1,905988083	1,9	-0,005988083
A 8	1,743801197	1,677441263	1,907522591	1,83	-0,077522591

Stress ratio		
Sigma1/Sigma2	Sigm1/Sigv	Sigm1/Sig v
0,9859275	0,852758078	0,864929817

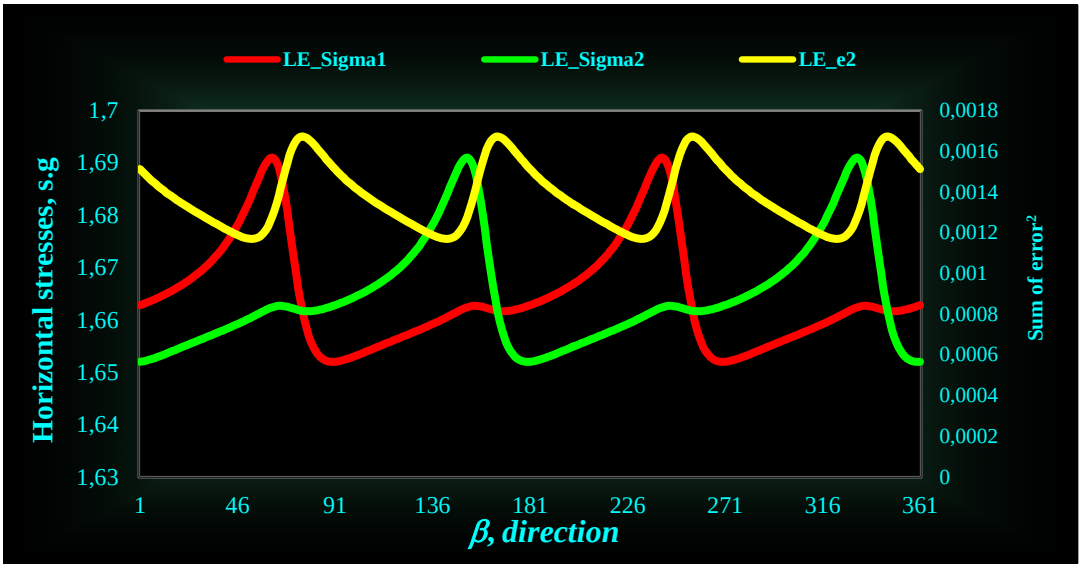

Simulation 11:

Well pressure and survey data					
Well #	**Pwf (s.g)**	**Po (s.g)**	**Overb (s.g)**	**Inc. (deg.)**	**Azim(deg.)**
A 4	1,96	1,382	1,942	32,79	103,79
A 1	1,8	1,417	1,967	27,82	84,58
A 9	1,88	1,386	1,943	27,48	73,05
A 03A	1,9	1,385	1,943	25,22	48,18

Inversion result			
σ1 (s.g.)	σ2 (s.g.)	Dirn, β (deg.)	Σerror²
1,6756	1,74408856	343	0,000405057

Analysis- Linear elastic					
Well	**σx (s.g.)**	**σy (s.g.)**	**Predicted -LOP**	**Measured-LOP**	**Difference**
A 4	1,7892987	1,693654503	1,90966481	1,96	0,05033519
A 1	1,79038589	1,678396275	1,827802938	1,8	-0,027802938
A 9	1,7864018	1,675574252	1,854320959	1,88	0,025679041
A 03A	1,75520718	1,706065191	1,977988388	1,9	-0,077988388

Stress ratio		
Sigma1/Sigma2	Sigm1/Sigv	Sigm1/Sig v
0,9607158	0,85981964	0,894978094

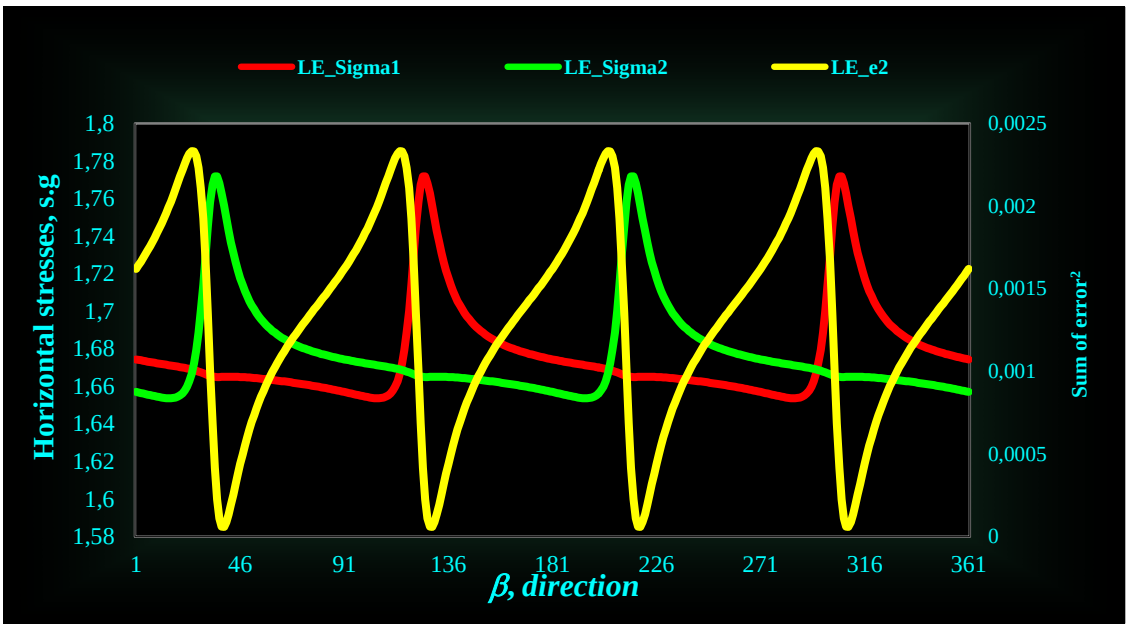

Simulation 12:

Well pressure and survey data					
Well #	**Pwf (s.g)**	**Po (s.g)**	**Overb (s.g)**	**Inc. (deg.)**	**Azim(deg.)**
A 1	1,8	1,417	1,967	27,82	84,58
A 9	1,88	1,386	1,943	27,48	73,05
A 03A	1,9	1,385	1,943	25,22	48,18

Inversion result			
σ1 (s.g.)	σ2 (s.g.)	Dirn, β (deg.)	Σerror²
1,663795645	1,67086752	4	1,86902E-13

Analysis- Linear elastic					
Well	**σx (s.g.)**	**σy (s.g.)**	**Predicted -LOP**	**Measured-LOP**	**Difference**
A 1	1,73515687	1,663986718	1,83980328	1,8	-0,0398033
A 9	1,72804337	1,664702631	1,880064526	1,88	-6,453E-05
A 03A	1,71724861	1,667435543	1,900058024	1,9	-5,802E-05

Stress ratio		
Sigma1/Sigma2	Sigm1/Sigv	Sigm1/Sig v
0,995767542	0,85279121	0,856415951

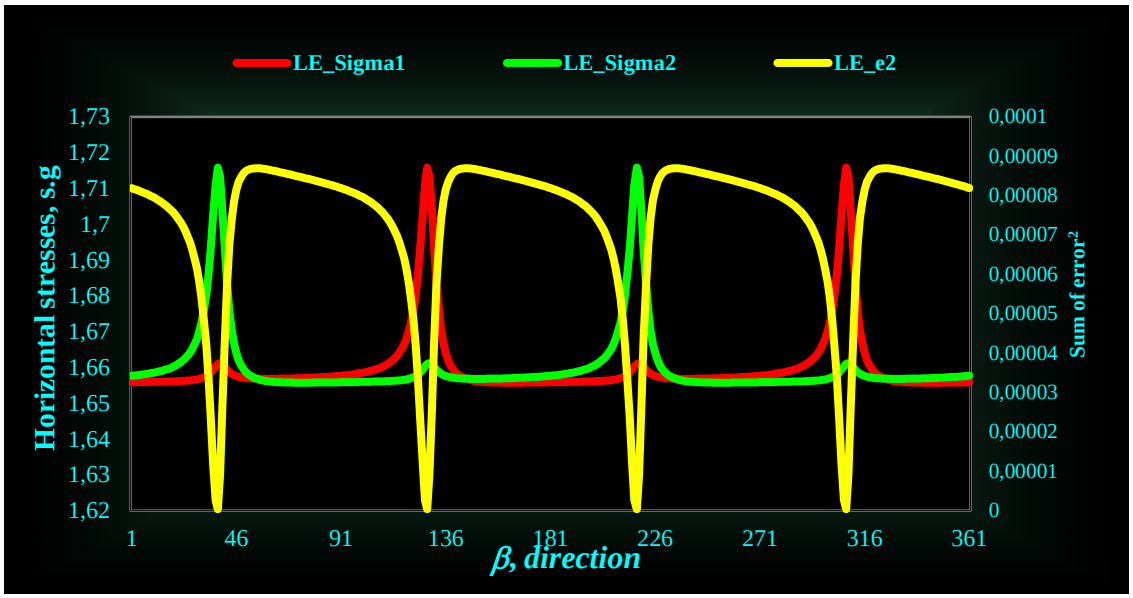

Group II:

Simulation 13:

Well pressure and survey data					
Well #	**Pwf (s.g)**	**Po (s.g)**	**Overb (s.g)**	**Inc. (deg.)**	**Azim(deg.)**
A 18	1,9	1,375	1,9385	25,7	155,73
A 12	1,89	1,417	1,967	33,76	169,09
A 10	1,88	1,377	1,939	23,45	146,96
A 01A	1,93	1,382	1,943	1,46	99,77
A 15	2,03	1,388	1,949	3,27	264
A 14(Balder)	1,93	1,448	1,992	17,67	286,25

Inversion result			
σ1 (s.g.)	σ2 (s.g.)	Dirn, β (deg.)	Σerror²
1,7309747	1,670121562	315	0,002491193

Analysis- Linear elastic					
Well	**σx (s.g.)**	**σy (s.g.)**	**Predicted -LOP**	**Measured-LOP**	**Difference**
A 18	1,765040749	1,677745908	1,893	1,900	0,006803026
A 12	1,802268005	1,672301439	1,797636312	1,890	0,092363688
A 10	1,748598021	1,688211351	1,939036032	1,880	0,059036032
A 01A	1,672031803	1,729222372	2,133635312	1,930	0,203635312
A 15	1,671720547	1,730309798	2,131208848	2,030	0,101208848
A 14	1,703999672	1,726209631	2,026629222	1,930	0,096629222

Stress ratio		
Sigma1/Sigma2	Sigm1/Sigv	Sigm1/Sig v
1,0364363	0,885522288	0,854391386

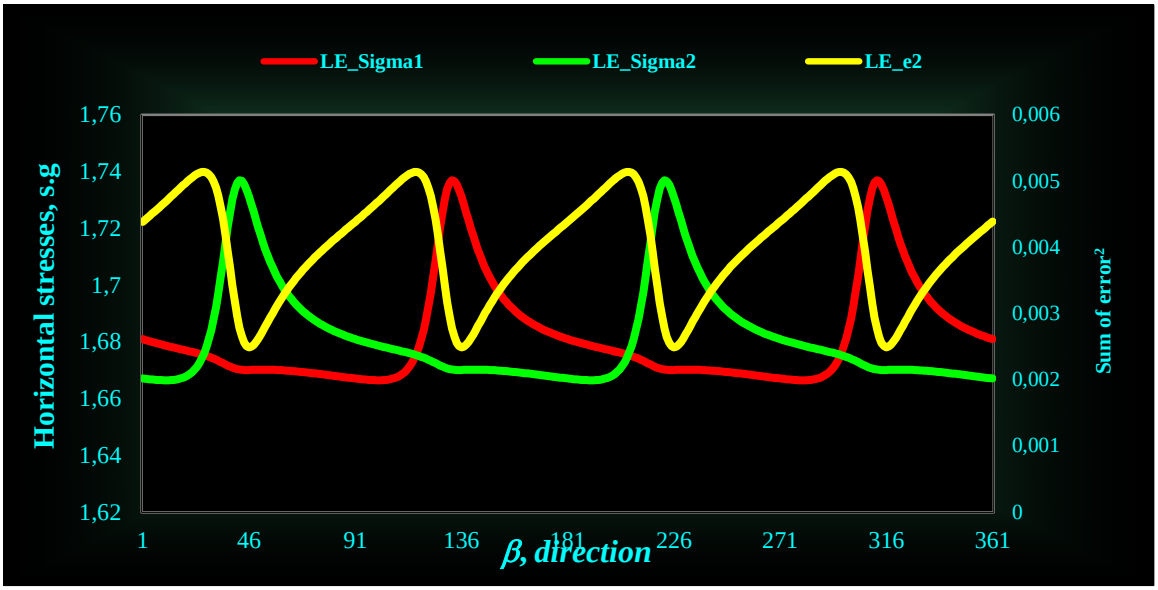

Simulation 14:

Well pressure and survey data					
Well #	**Pwf (s.g)**	**Po (s.g)**	**Overb (s.g)**	**Inc. (deg.)**	**Azim(deg.)**
A 18	1,9	1,375	1,9385	25,7	155,73
A 10	1,88	1,377	1,939	23,45	146,96
A 01A	1,93	1,382	1,943	1,46	99,77
A 15	2,03	1,388	1,949	3,27	264

Inversion result			
σ1 (s.g.)	σ2 (s.g.)	Dirn, β (deg.)	Σerror²
1,7562	1,66505408	308	5,81566E-05

Analysis- Linear elastic					
Well	**σx (s.g.)**	**σy (s.g.)**	**Predicted -LOP**	**Measured-LOP**	**Difference**
A 18	1,77434493	1,684890108	1,905325388	1,9	-0,005325388
A 10	1,77695713	1,674756291	1,870311742	1,88	0,009688258
A 01A	1,73608404	1,685308174	1,937840478	1,93	-0,007840478
A 15	1,66701432	1,755163184	2,210475235	2,03	-0,180475235

Stress ratio		
Sigma1/Sigma2	Sigm1/Sigv	Sigm1/Sig v
1,0547428	0,90415283	0,857225862

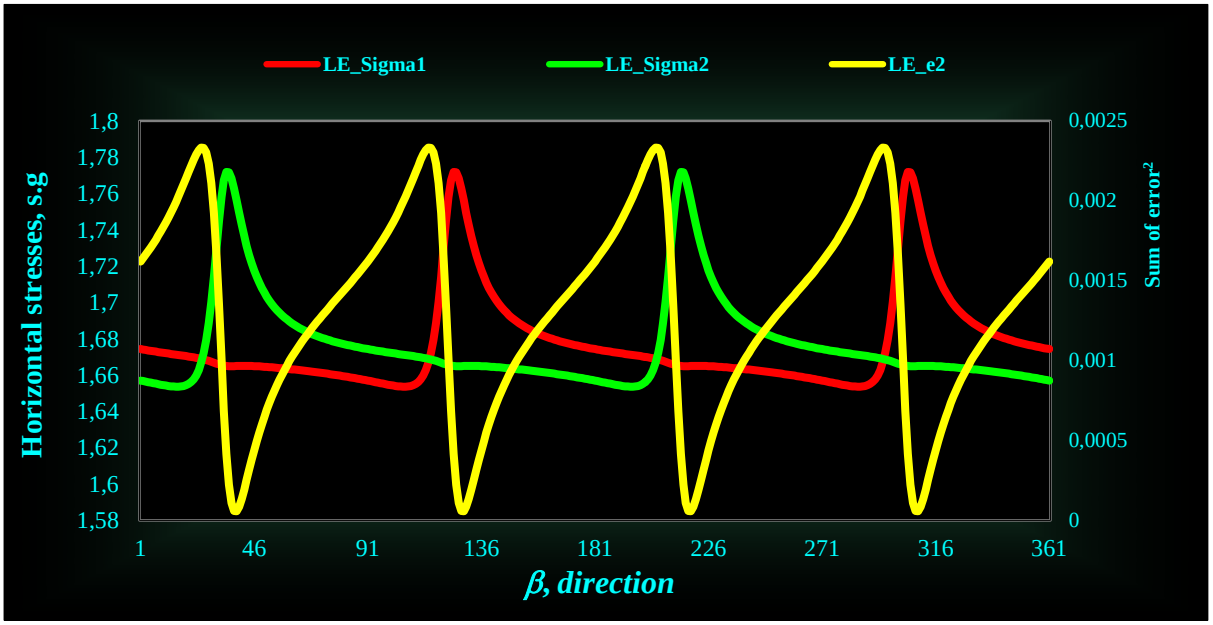

Simulation 15:

Well pressure and survey data					
Well #	**Pwf (s.g)**	**Po (s.g)**	**Overb (s.g)**	**Inc. (deg.)**	**Azim(deg.)**
A 18	1,9	1,375	1,9385	25,7	155,73
A 10	1,88	1,377	1,939	23,45	146,96
A 01A	1,93	1,382	1,943	1,46	99,77

Inversion result			
σ1 (s.g.)	σ2 (s.g.)	Dirn, β (deg.)	Σerror²
1,715874355	1,66105409	307	4,09542E-07

Analysis- Linear elastic					
Well	**σx (s.g.)**	**σy (s.g.)**	**Predicted -LOP**	**Measured-LOP**	**Difference**
A 18	1,74736482	1,673782542	1,898982803	1,9	0,0010172
A 10	1,74575594	1,667492162	1,879720552	1,88	0,00027945
A 01A	1,70463331	1,672449818	1,93071614	1,93	-0,0007161

Stress ratio		
Sigma1/Sigma2	Sigm1/Sigv	Sigm1/Sig v
1,033003299	0,88439534	0,856139897

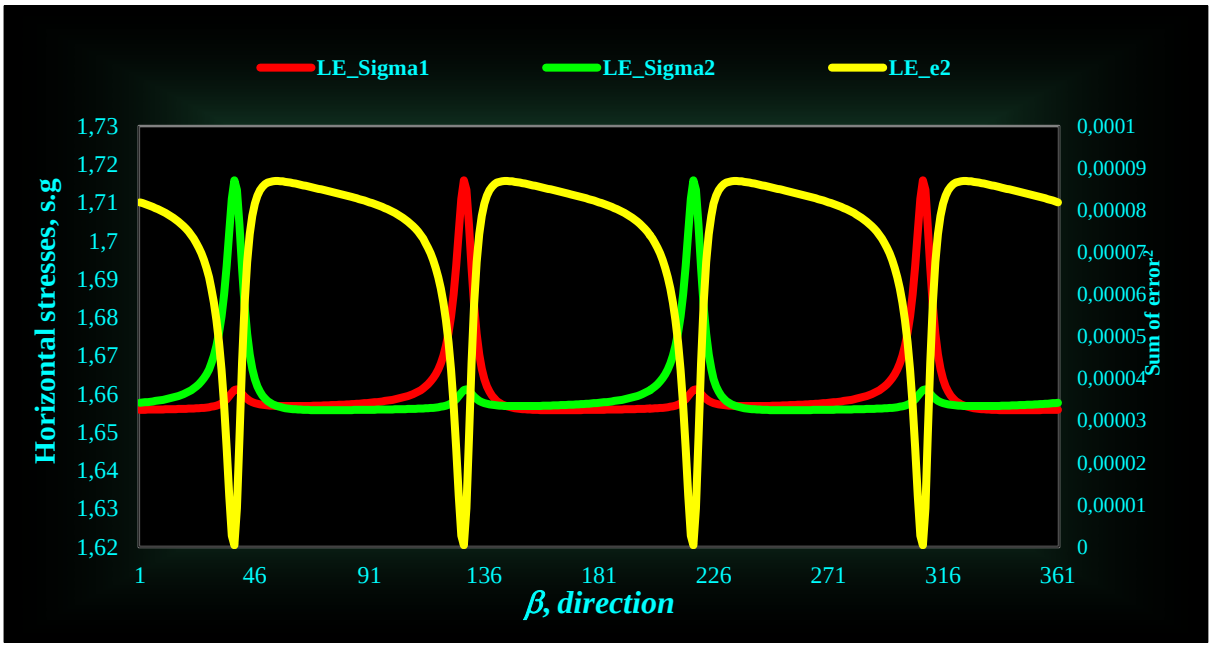

Simulations done in section 9 5/8"":

Group II:

Simulation 16:

Well pressure and survey data					
Well #	**Pwf (s.g)**	**Po (s.g)**	**Overb (s.g)**	**Inc. (deg.)**	**Azim(deg.)**
A 4	1,63	1,15	2,14	35,4	110,9
A 9	1,54	1,15	2,135	12	102
A 03A	1,66	1,15	2,129	25,84	54,74

Inversion result			
σ1 (s.g.)	σ2 (s.g.)	Dirn, β (deg.)	Σerror²
1,89895282	1,46702348	82	1,3828E-05

Analysis- Linear elastic					
Well	**σx (s.g.)**	**σy (s.g.)**	**Predicted -LOP**	**Measured-LOP**	**Difference**
A 4	1,9127717	1,567812257	1,640665074	1,63	-0,0106651
A 9	1,86084909	1,517500496	1,541652392	1,54	-0,0016524
A 03A	1,86926658	1,557553388	1,653393583	1,66	0,00660642

Stress ratio		
Sigma1/Sigma2	Sigm1/Sigv	Sigm1/Sig v
1,294425647	0,88957815	0,687237734

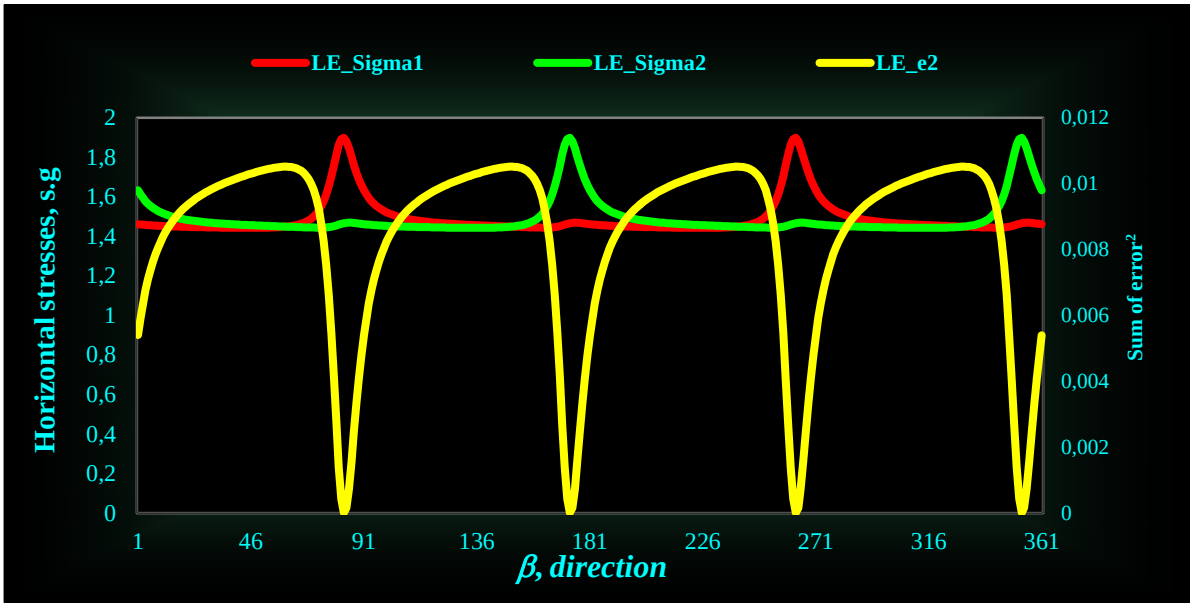

Simulation 17:

Well pressure and survey data					
Well #	**Pwf (s.g)**	**Po (s.g)**	**Overb (s.g)**	**Inc. (deg.)**	**Azim(deg.)**
A 9	1,54	1,15	2,135	12	102
A 03A	1,66	1,15	2,129	25,84	54,74

Inversion result			
σ1 (s.g.)	σ2 (s.g.)	Dirn, β (deg.)	Σerror²
1,4011136	1,48396755	20	0

Analysis- Linear elastic					
Well	**σx (s.g.)**	**σy (s.g.)**	**Predicted - LOP**	**Measured- LOP**	**0**
A 9	1,5105304	1,402735	1,54767	1,54	-0,0077
A 03A	1,56104182	1,457086	1,66022	1,66	-0,0002

Stress ratio		
Sigma1/Sigma2	Sigm1/Sigv	Sigm1/Sig v
0,9441673	0,65718276	0,696045

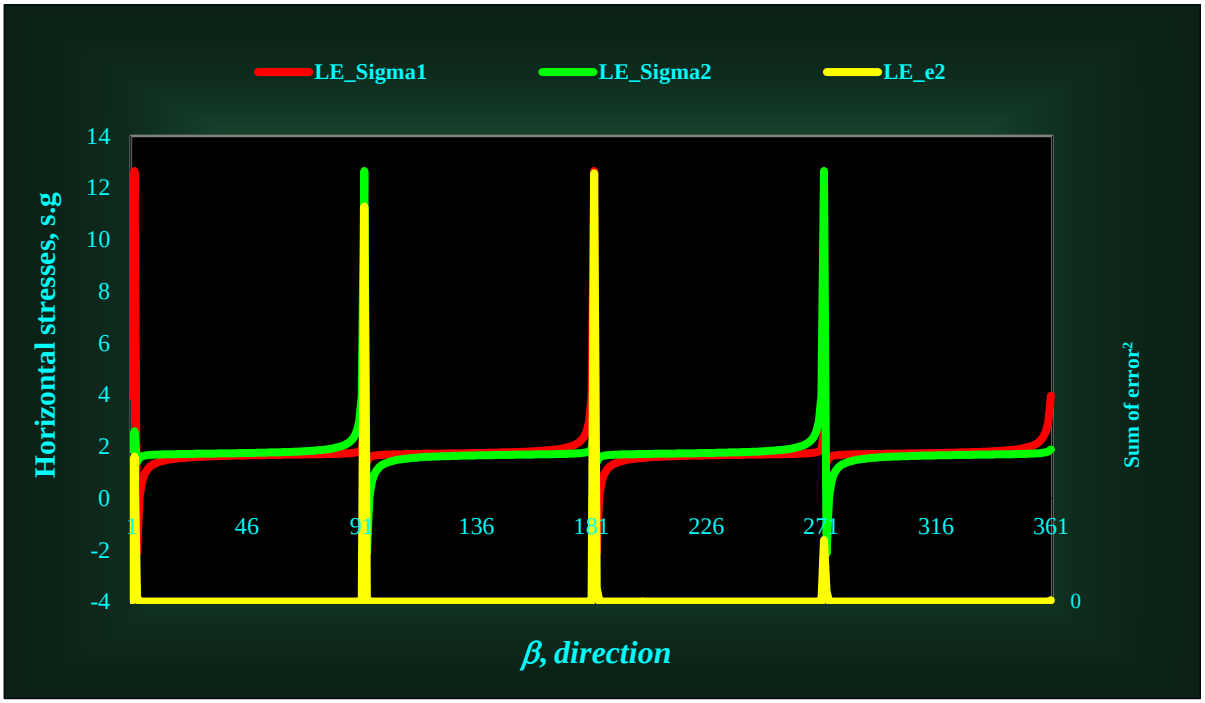

Group III:

Simulation 18:

Well pressure and survey data					
Well #	**Pwf (s.g)**	**Po (s.g)**	**Overb (s.g)**	**Inc. (deg.)**	**Azim(deg.)**
A 12	1,89	1,31	2,1	19,4	156,1
A 10	2,06	1,49	2,085	2,8	208,2

Inversion result			
σ1 (s.g.)	σ2 (s.g.)	Dirn, β (deg.)	Σerror²
1,2820017	1,67350722	8	0

Analysis- Linear elastic					
Well	**σx (s.g.)**	**σy (s.g.)**	**Predicted - LOP**	**Measured-LOP**	**0**
A 12	1,46985059	1,56372	1,91131	1,89	-0,0213
A 10	1,33003678	1,627276	2,06179	2,06	-0,0018

Stress ratio		
Sigma1/Sigma2	Sigm1/Sigv	Sigm1/Sigv
0,7660569	0,61266511	0,799765